**Enclosure 2**
**Approved Version of the Safety Analysis Methodology for the Kairos Power Fluoride Salt-Cooled High-Temperature Test Reactor Topical Report**
**(Non-Proprietary)**

# CONTENTS

# Section A

UNITED STATES
NUCLEAR REGULATORY COMMISSION
WASHINGTON, D.C. 20555-0001

January 5, 2025

Darrell Gardner
Sr. Director, Licensing
Kairos Power LLC
707 W Tower Ave
Alameda, CA 94501

SUBJECT: KAIROS POWER LLC – FINAL SAFETY EVALUATION OF TOPICAL REPORT, "SAFETY ANALYSIS METHODOLOGY FOR THE KAIROS POWER FLUORIDE SALT-COOLED HIGH-TEMPERATURE TEST REACTOR," REVISION 1 (EPID NO: L-2024-TOP-0022)

Dear Darrell Gardner:

This letter provides the final safety evaluation (SE) for the Kairos Power, LLC (Kairos) topical report (TR) "Safety Analysis Methodology for the Kairos Power Fluoride Salt-Cooled High-Temperature Test Reactor," Revision 1. By letter dated June 4, 2024, Kairos submitted for U.S. Nuclear Regulatory Commission (NRC) staff review KP-TR-020-P, "Safety Analysis Methodology for the Kairos Power Fluoride Salt-Cooled High-Temperature Test Reactor," Revision 0 (Agencywide Documents Access and Management System (ADAMS) Accession No. ML24156A162). On September 25, 2024, the NRC issued an audit plan for the purpose of gaining a better understanding of KP-TR-020-P (ML24269A202). By letter dated July 29, 2025, Kairos submitted Revision 1 of KP-TR-020-P (ML25210A576). The NRC staff issued the audit summary report in letter dated January 5, 2026 (ML25344A109).

The NRC staff's final SE for KP-TR-020-P, "Safety Analysis Methodology for the Kairos Power Fluoride Salt-Cooled High-Temperature Test Reactor," Revision 1 is enclosed. The NRC staff provided Kairos a draft of the SE for the purpose of identifying proprietary export controlled information on September 11, 2025 (ML25258A013). Kairos provided comments regarding the proprietary export controlled information in the draft SE on October 20, 2025 (ML25317A661). The NRC staff incorporated those comments, as appropriate, into the final SE.

The NRC staff requests that Kairos publish an accepted version of this TR within 3 months of receipt of this letter. The accepted version shall incorporate this letter and the enclosed SE after the title page. The accepted version shall include an "-A" (designated accepted) following the TR identification number.

The Enclosure to this letter contains Proprietary Export Controlled Information. When separated from the Enclosure this letter is DECONTROLLED

If you have any questions, please contact Brian Bettes via email at Brian.Bettes@nrc.gov.

Sincerely,

JOSHUA BORROMEO

Digitally signed by JOSHUA BORROMEO
Date: 2026.01.05 14:53:46 -05'00'

Josh Borromeo, Chief
Advanced Reactor Licensing Branch 1
Division of Advanced Reactors and Non-Power Production and Utilization Facilities
Office of Nuclear Reactor Regulation

Project No.: 99902069

Enclosure:
Safety Evaluation

SUBJECT: KAIROS POWER LLC – FINAL SAFETY EVALUATION OF TOPICAL REPORT, "SAFETY ANALYSIS METHODOLOGY FOR THE KAIROS POWER FLUORIDE SALT-COOLED HIGH-TEMPERATURE TEST REACTOR," REVISION 1 (EPID NO: L-2024-TOP-0022) DATE: JANUARY 5, 2026

**DISTRIBUTION:**
PUBLIC
RidsACRS_MailCTR Resource
RidsNrrDanu Resource
RidsNrrDanuUal1 Resource
RidsOgcMailCenter Resource
RidsOpaMailCenter Resource
JBorromeo, NRR
CdeMessieres, NRR
PSawant, NRR
ASiwy, NRR
CAdams, NRR
DGreene, NRR
BBettes, NRR
CSantos, NRR
JKaizer, NRR
MHart, NRR
ABielen, RES

**ADAMS Accession Nos.:**
**Pkg: ML25317A335**
**Letter: ML25317A472**
**Safety Evaluation (Proprietary): ML25317A469**
**Safety Evaluation (Non Proprietary): ML25317A475**

| | | | |
|---|---|---|---|
| **OFFICE** | NRR/DANU/UAL1:PM | NRR/DANU/UAL1:LA | OGC |
| **NAME** | BBettes | DGreene | Not Reviewed |
| **DATE** | 7/22/2025 | 7/29/2025 | |
| **OFFICE** | NRR/DANU/UTB2:BC | NRR/DANU/UAL1:BC | |
| **NAME** | CdeMessieres | JBorromeo | |
| **DATE** | 9/11/2025 | 1/5/2026 | |

**OFFICIAL RECORD COPY**

UNITED STATES
NUCLEAR REGULATORY COMMISSION
WASHINGTON, D.C. 20555-0001

# KAIROS POWER LLC – FINAL SAFETY EVALUATION OF TOPICAL REPORT KP-TR-020-P, "SAFETY ANALYSIS METHODOLOGY FOR THE KAIROS POWER FLUORIDE SALT-COOLED HIGH-TEMPERATURE TEST REACTOR," REVISION 1 (EPID L-2024-TOP-0022)

## SPONSOR AND SUBMITTAL INFORMATION

**Sponsor:** Kairos Power LLC (Kairos)

**Sponsor Address:** 707 W. Tower Ave, Suite A
Alameda, CA 94501

**Project No.:** 99902069

**Submittal Date:** June 4, 2024

**Submittal Agencywide Documents Access and Management System (ADAMS) Accession No.:** ML24156A162

**Revision Letter Date and ADAMS Accession No**: July 29, 2025, ML25210A574

**Brief Description of the Topical Report:** On June 4, 2024, Kairos Power LLC (Kairos) submitted topical report (TR) KP-TR-020, "Safety Analysis Methodology for the Kairos Power Fluoride Salt-Cooled High-Temperature Test Reactor," Revision 0, for the U.S. Nuclear Regulatory Commission (NRC) staff (the staff) review. On July 29, 2025, Kairos submitted Revision 1 of the TR (ML25210A576). The TR documents a safety analysis methodology for evaluating the maximum hypothetical accident (MHA) and postulated events for the Kairos Power Fluoride Salt-Cooled, High Temperature Reactor (KP-FHR) test reactor. The purpose of the safety analysis methodology is to demonstrate that the dose consequences of the postulated events are bounded by an MHA that has acceptable dose consequences. The TR identifies the computer codes used and discusses related verification and validation efforts for the postulated event analyses. The TR describes the base input model for the KP-FHR test reactor and the event-specific biases and sensitivity studies that are designed to address the uncertainties and identify the limiting postulated events.

## REGULATORY EVALUATION

Regulatory Basis

Title 10 of the *Code of Federal Regulations* (10 CFR) 50.34(b) requires that each application for an operating license (OL) include a final safety analysis report (FSAR) that provides a description and safety assessment of the plant design features intended to mitigate the radiological consequences of accidents. The FSAR must demonstrate compliance with the radiological consequence evaluation factors for offsite doses at the exclusion area boundary

(EAB) and outer boundary of the low population zone (LPZ) as required by 10 CFR Part 100, "Reactor Site Criteria."

Furthermore, 10 CFR 50.34(b)(4) requires, in part, analysis and evaluation of the design and performance of structures, systems, and components (SSCs) of the facility to assess the risk to public health and safety resulting from operation of the facility and including determination of the margins of safety during normal operations and transient conditions anticipated during the life of the facility, and the adequacy of SSCs provided for the prevention of accidents and the mitigation of the consequences of accidents.

The safety analysis methodology presented in the TR is used to evaluate the postulated event dose consequences for the KP-FHR test reactor. The safety analysis methodology follows the guidance in NUREG-1537, "Guidelines for Preparing and Reviewing Applications for the Licensing of Non-Power Reactors," (ML042430055).

Consistent with the NUREG-1537 guidance, the safety analysis methodology presented in the TR comprises two major analyses: MHA and postulated event analyses. The MHA is utilized to demonstrate that the radiological consequences from a bounding postulated event result in projected dose levels within the regulatory dose criteria.

The MHA described in TR section 2 is based on the approved KP-FHR mechanistic source term (MST) methodology described in TR KP-TR-012-NP-A, "KP-FHR Mechanistic Source Term Methodology" (ML22136A291). However, Section 2 of the TR presents deviations from the approved MST methodology as well as from the MHA analysis approved in the Hermes and Hermes 2 construction permit application reviews. The staff used guidance in NUREG-1537 to evaluate the updates to the MHA.

The postulated event analysis evaluation model (EM) described in the TR is based on the Kairos Power systems analysis code (KP-SAM). The KP-SAM EM is developed in accordance with the applicable portions of Regulatory Guide (RG) 1.203, "Transient and Accident Analysis Methods" (ML053500170). Although NUREG-1537 does not explicitly require non-power reactor applicants to follow RG 1.203 for safety analysis methodology development, the principles and expectations outlined in RG 1.203 are consistent with NUREG-1537's guidance. Specifically, NUREG-1537 requires that safety analysis models address key elements such as assumptions, approximations, validation, and uncertainty, which are also central to RG 1.203. Accordingly, the use of RG 1.203 guidance for developing and assessing the KP-SAM EM for analysis of transient and accident conditions in KP-FHR is appropriate. In particular, RG 1.203 outlines a structured 20-step process known as the Evaluation Model Development and Assessment Process (EMDAP), organized into 4 elements. Accordingly, the staff's review of the KP-SAM postulated event EM follows the applicable EMDAP guidance.

NUREG-1537, part 1, chapter 13, also describes the following objectives for the postulated event analysis:

- Ensure that enough events have been considered to include any accident with significant radiological consequences. Rejection of a potential event should be justified in the discussions.
- Categorize the initiating events and scenarios by type and likelihood of occurrence so that only the limiting cases in each group must be quantitatively analyzed.
- Develop and apply consistent, specific acceptance criteria for the consequences of each postulated event.

The staff considered these objectives for the evaluation of postulated event analysis presented in the TR.

Section 1.2 of the TR states that the safety analysis methodology is used to conform to KP-FHR principal design criteria (PDC) 19, which provides control room design criteria, including a radiological habitability accident dose criterion for control room personnel. The PDC for the KP-FHR design were reviewed and approved by the staff in TR KP-TR-003-NP-A, “Principal Design Criteria for the Kairos Power Fluoride Salt-Cooled, High Temperature Reactor,” (ML20167A174).

The staff considered the regulations, guidance, and applicable previously approved methodologies and KP-FHR PDC 19 in its review of the TR. However, evaluation of safety analysis methodology implementation will occur as part of the OL review.

## TECHNICAL EVALUATION

As described in section 1 of the TR, Kairos is requesting the staff’s approval of the safety analysis methodology as an appropriate way to determine the acceptability of postulated event dose consequences by comparing them to an MHA with acceptable dose consequences. Kairos intends to use the safety analysis methodology in a licensing application for a KP-FHR test reactor to address the requirements of 10 CFR 100.11, “Determination of exclusion area, low population zone, and population center distance,” and conformance with KP-FHR PDC 19. Section 1 of this SE summarizes the major components of the TR and clarifies the staffs evaluation of each major component.

### 1. Topical Report Overview

The TR consists of the following major sections and appendix:

Section 1 of the TR provides a brief description of KP-FHR technology and identifies key design features (i.e., SSCs) modeled by the safety analysis methodology. Limitation 5 in TR section 6.2 states that the safety analysis methodology is based on KP-FHR design features provided in section 1.1, and deviations from these design features will be justified in future applications. The staff includes this limitation through **Limitation and Condition 1** in the “Limitations and Conditions” section of this SE. The staff considered the design features described in section 1.1 of the TR throughout its technical evaluation of this TR. TR section 1 also identifies specific technical areas for which Kairos is requesting staff review and approval in this TR.

Section 2 of the TR describes the analysis approach to calculate the dose consequences of the MHA with refinements from previously approved methods and analysis (i.e., KP-TR-012-NP-A, Hermes 1 and 2 construction permit applications). This section also includes information to support disposition of the MST methodology TR safety evaluation (SE) limitations and conditions 2 and 5. The MHA in section 2 is also used to demonstrate conformance to the control room dose criterion in KP-FHR PDC 19. The staff’s evaluation of the updated MHA and its adequacy to address KP-FHR PDC 19 is in section 2 of this SE.

Section 3 of the TR addresses Element 1 of EMDAP (Establish Requirements for Evaluation Model Capability) by describing the postulated event categories addressed by the safety analysis methodology and the figures of merit (FOMs) selected for the safety analysis methodology. TR section 3 also summarizes how SSCs and associated phenomena identified

through the phenomena identification and ranking table (PIRT) process are addressed in the safety analysis methodology. The staff evaluated the adequacy of proposed postulated event categories and FOMs and reviewed the safety analysis methodology approach for addressing the PIRT phenomena in SE section 3.

Section 4 of the TR addresses, in part, Element 3 of EMDAP by describing the KP-SAM-based EM in sections 4.1 and 4.3. Section 4.2 addresses, in part, Element 2 (Develop Assessment Base) and Element 4 (Assess Evaluation Model Adequacy) of EMDAP. The staff's review of the KP-SAM code models and correlations, base input model, and proposed validations is in SE section 4.

Section 5 of the TR addresses, in part, Element 3 of EMDAP by describing event-specific biases and sensitivity studies for each postulated event category. The staff's evaluation of the proposed event-specific biases and sensitivity studies and its adequacy to account for the safety analysis methodology uncertainties is in SE section 5.

Appendix A of the TR illustrates a generic system response for selected example transients. The sample calculations in appendix A do not represent final design information and Kairos does not request NRC approval for these sample calculations. The staff considered the information in appendix A but does not make any determinations on the sample calculations in appendix A.

## 2. Maximum Hypothetical Accident

TR section 2 describes the MHA for the KP-FHR test reactor as "a hypothetical set of conditions that postulated a conservative release of radionuclides that bounds a potential release from other postulated events." TR section 2.1 states that, the MHA analysis applies assumed temperature histories to the radioactive material at risk for release (MAR) in the primary system to drive radionuclides out of the system through diffusion and evaporation.

Except for MST methodology and MHA analysis refinements evaluated below, the MHA described in the TR is fundamentally the same as was described in the preliminary safety analysis reports (PSARs) for the Hermes and Hermes 2 facilities (ML23151A745 and ML24144A092) and found acceptable by the staff in sections 13.1.1 and 13.2.1 of their respective SEs to support the issuance of the construction permits (ML23158A268 and ML24200A115). Specifically, the TR states, the MHA is a non-physical scenario with the MHA temperature conditions represented in TR figure 2-1. The temperature profile provided in TR figure 2-1 is identical to the MHA temperature profile used in the Hermes and Hermes 2 PSAR analyses. The modeling of radionuclide release and transport to develop the MHA source term is based primarily on the approved MST methodology. In the MST methodology, the development of event-specific radiological releases to the environment is accomplished by modeling the facility as a set of MAR sources, identifying the succession of barriers to release, and applying a release fraction for each barrier that contains the MAR.

TR section 2 describes MST methodology and MHA analysis refinements from the previously approved MST methodology and the MHA analysis as described in the Hermes and Hermes 2 PSARs in the following areas:

- Argon activation and release models (see SE section 2.1 and 2.3);
- Flibe radionuclide grouping structure (see SE section 2.2);

- Justification of the representative element vapor pressure correlations to address a limitation in the MST methodology TR (see SE section 2.2);
- Isotopic screening criteria (see SE section 2.4); and
- Added methods for evaluation of control room dose consequences (see SE section 2.5).

The staff's review of these refinements is presented below in the order that the MHA information is provided in TR section 2. The remainder of the information in TR section 2 describing the MHA scenario and source term methods, including information on functional containment, is unchanged from the description in the Hermes and Hermes 2 PSARs and is also consistent with the methods in the approved MST methodology. Therefore, these items, which are unchanged, are acceptable as described in the SEs for the Hermes and Hermes 2 construction permits.

2.1 Quantification of MAR

The information in TR section 2.2.1 is the same as described in the Hermes and Hermes 2 PSAR sections 13.1.1 and 13.2.1, except for the description of methods for modeling argon activation and release in TR section 2.2.1.1. Specifically, the TR adds methods for modeling argon-41 (Ar-41), which is generated from the activation of argon-40 (Ar-40) dissolved in Flibe or entrained in bubbles in Flibe.

TR section 2.2.1.1 describes the generation of Ar-41 as the product of neutron activation of argon-40 (Ar-40) in more locations than was previously modeled in the Hermes and Hermes 2 PSARs. In addition to activation of argon in the cover gas and within pores in reflector graphite and pebble carbon matrix, the TR models activation of argon dissolved in Flibe and contained in the bubbles entrained in the Flibe. This change in the Ar-41 generation model was made to support more detailed radionuclide transport modeling in the MHA analysis. Based on its review, the staff finds that the methods described in the TR to account for activation of argon exposed to a neutron flux from the core are acceptable because they use established neutron activation models based on widely used and accepted nuclear cross-section data.

The TR states in the modeling of Ar-41 release from the graphite and pebble carbon matrix that all pores are conservatively assumed to be open to the surface interface with the Flibe. This is a difference from the modeling in the Hermes and Hermes 2 PSAR, which allows for more Ar-41 release from the graphite and pebbles to the Flibe. The Ar-41 solubility-limited pore release model in the TR determines a steady state equilibrium activity distribution in the pores and Flibe. The model uses the tritium mass transfer correlations from the MST methodology to bound the mass transfer rate of argon and uses Henry's Law with the solubility of argon in Flibe. The staff confirmed the basis for the argon release model in audit discussions (ML25197A042), including data on argon solubility in Flibe. Based on its review, the staff finds that the Ar-41 model is acceptable because appropriate argon solubility data is used and the model includes conservatively biased assumptions.

There are no changes from the Hermes and Hermes 2 PSARs descriptions of the modeling of radionuclide transport in fuel (TR section 2.2.2) and transport of MAR from the Flibe to the gas space through bubble burst (TR section 2.2.3.1).

2.2 MAR Release from Flibe

TR section 2.2.3.2 provides a description of the methods to model evaporative release from Flibe. This section includes a modification of the radionuclide grouping structure for radionuclide transport in Flibe as compared to the grouping used in the approved MST methodology. The

revised radionuclide groups are listed in TR table 2-1. As stated in the TR, the modified grouping structure includes a conservative treatment of intermediate volatility noble metals (IVNM). The modified treatment is more realistic compared to the highly conservative treatment using the Flibe radionuclide grouping structure and modeling of evaporative release in the MST methodology by adding a new IVNM group.

As stated in the SE for the approved MST methodology, the staff found it acceptable to group radionuclides by their chemical behavior in Flibe because this behavior impacts how the radionuclides are retained by Flibe. The TR differs from the MST methodology by placing elements that fall into multiple groups based on the Flibe oxidation-reduction (redox) potential in the most conservative grouping (i.e., resulting in more evaporative release to the gas phase). The MHA analysis in the TR accomplishes this for each element that may fall into multiple groups by comparing the vapor pressure of the representative species for the candidate radionuclide group to the product of the vapor pressure for cesium fluoride (CsF) multiplied by the concentration of the element in Flibe. Certain salt-soluble fluorides were also re-grouped based on data collected during the operation of the Kairos engineering test unit (ETU).

TR equation 2.35 provides the relationship for natural convection mass transfer between Flibe and the cover gas. The staff confirmed during the audit that the equation is an empirical correlation that Kairos is conducting tests to validate the correlation as described in limitation and condition 11 of the MST methodology TR SE. The staff will review the test results and derivation of this correlation when the MST or safety analysis methodologies are implemented.

Based on its review, the staff finds that the Flibe radionuclide grouping structure, including the representative species and applied release fraction for each group, is acceptable because it is based on well-established sources of thermodynamic data (references 13 through 16 in the TR) to derive vapor pressure correlations and determine uncertainties for the correlations that result in conservative modeling of the release from Flibe for radionuclides other than the salt-soluble fluorides. The staff confirmed in the audit both the information supporting the new IVNM grouping, including the natural convection mass transfer relationship between Flibe and cover gas, and the assumptions that lead to conservative modeling of radionuclide transport in Flibe. The staff also finds that the IVNM group is acceptable because the grouping leads to conservative radionuclide transport in Flibe. This is because the representative transport species (indium) for the IVNM group has a higher vapor pressure than all elements in the group and the relationship between vapor pressure and temperature includes a factor to account for uncertainty which is taken from a widely-used reference.

TR section 2.2.3.3 provides information to aid in confirming that the radionuclide concentrations in Flibe are consistent with the assumption in the MST methodology of a dilute solution as an initial condition. This information will be used by an applicant using the MHA analysis. As stated in the staff's SE for the MST methodology, the MST methodology assumes dilute solutions to minimize certain chemical interactions that could increase the vaporization of Flibe and radionuclide species and allows for the use of certain simplifying assumptions related to the retention of radionuclides in the molten salt. See also limitation and condition 5 in the MST methodology TR SE. TR section 2.2.3.3 also provides a method to show that the concentration of salt soluble fluorides is below the solubility limit by comparing the total concentration of the salt soluble fluorides to the solubility limit for the least soluble trivalent fluoride.

The staff evaluated TR information, including the use of cited references, to support the confirmation of dilute solution and solubility. Through the audit, the staff also confirmed the basis of the information in TR section 2.2.3.3 and its applicability to Flibe. The selection of the

dilute solution concentration limit was based on solute-solute interaction data for a molten salt which is not Flibe but is justified as an appropriate surrogate based on the independence of the interaction from the solvent, chemical similarity of the salt to Flibe, and anticipation of a large margin between any individual impurity concentration and the limit. The staff notes that the TR information on the limit of solubility in Flibe for the salt soluble fluorides is based on solubility data for the least soluble trivalent fluoride. Therefore, based on its review, the staff finds that the information in TR section 2.2.3.3 is acceptable for use when confirming solubility and dilute solution to address limitation and condition 5 of the MST methodology TR SE.

TR section 2.2.3.4 addresses MST methodology TR SE limitation and condition 2 that the user of the MST methodology provide justification of thermodynamic data and associated vapor pressure correlations of representative species for the radionuclide groups. TR section 2.2.3.4 describes the basis for determining the vapor pressure correlations for the representative species and provides the resulting correlations for all the Flibe radionuclide transport groups used in the MHA. The staff evaluated the information in TR section 2.2.3.4 and audited information supporting the TR description.

For radionuclides other than the salt-soluble fluorides, the staff finds that the justification of the representative vapor pressure acceptable because the TR used well-established sources of thermodynamic data that can be applied to the KP-FHR operating conditions to derive vapor pressure correlations and determine uncertainties for these correlations that appear to be conservative. This includes the new IVNM grouping, which the staff still finds conservative, as previously discussed in this section of this SE.

The staff notes that confirmatory testing to validate the assumption of ideal vaporization behavior for salt-soluble fluorides as described in limitation and condition 11 in the MST methodology TR SE remains to be addressed by the user of the MST methodology, including through use of the safety analysis methodology.

## 2.3 Transport from Structural Materials

TR section 2.2.4 includes a description of the release of tritium, which is the same as in the Hermes and Hermes 2 PSARs. However, TR section 2.2.4.2 documents changes from the Ar-41 release modeling in the PSARs to include the immediate release of all Ar-41 dissolved in the Flibe, entrained in bubbles, and contained in the cover gas, and a conservative solubility-limited modeling of Ar-41 release from the reflector and fuel graphite pores to the Flibe that occurs over time. At 12 hours into the transient, any remaining Ar-41 is puff released out of the system.

The staff evaluated the updated Ar-41 release model, including an audit of an example analysis to aid in understanding the use of the solubility-limited pore release model described in TR section 2.2.1.1. The staff's evaluation of the Ar-41 pore release model finds it is acceptable, as discussed above in section 2.1 of this SE.

## 2.4 Release Pathway and Isotopic Screening Criteria

TR section 2.2.5 provides information to more succinctly address the MST methodology *de minimis* pathway screening based on the assessment of doses prior to the screening evaluation, such that a detailed computer calculation using RADTRAD is not required. Specifically, this new method involves assessment of isotopic releases for a given pathway to determine whether the pathway can be screened out of a detailed consequence modeling based on the very low offsite dose contribution from the pathway. This same process is used to identify significant dose

contributors for the pathways that are not screened out of the consequence analysis and to reduce the number of isotopes included for RADTRAD calculation. The TR screening method is based on the method approved in the MST methodology TR, simplified to use a single absolute dose criterion of a pathway dose at the EAB of 0.001 rem total effective dose equivalent (TEDE).

The staff evaluated the more succinct screening process based on the previously approved method in the MST methodology and finds that the process achieves the same goal to determine that the MAR in the pathway and potential dose contribution would not affect the offsite dose result. The staff finds that the revised *de minimis* screening described in TR section 2.3.5 is acceptable because it assures that a comprehensive list of sources of MAR and release pathways (including those that are not likely to contribute more than a small fraction of the total offsite dose results) are included in the analysis with modeling assumptions consistent with their relative importance.

2.5 Control Room Dose Consequences

TR section 2.2.6 describes the radionuclide transport within the buildings and atmospheric transport, including calculation of offsite and control room dose consequences consistent with the approved MST methodology for calculating dose consequences for design basis accidents and control room habitability. The TR provides additional information to ensure that the control room atmospheric dispersion is modeled conservatively. The conservatism in the safety analysis methodology with respect to calculating control room dose consequences also includes not crediting filtration of the control room air to reduce the radionuclide concentration and not modeling the effect of shielding for reducing direct radiation exposure. Because the safety analysis methodology does not specifically model control room shielding or a potential filtration system, the staff will evaluate the control room dose analysis performed to show that KP-FHR PDC 19 control room radiological habitability criteria are met during the review of a future licensing action that uses the safety analysis methodology. Based on the staff's experience with modeling atmospheric dispersion for control room habitability analyses, the staff agrees that the information provided in the TR will result in conservative control room atmospheric dispersion modeling and resulting control room doses. Therefore, the staff finds that the methods described for the transport in the gas space and calculation of offsite and control room dose consequences are acceptable.

## 3. Safety Analysis Methodology Requirements

Element 1 of the RG 1.203 EMDAP identifies the following steps:

1. Specify Analysis Purpose, Transient Class, and Power Plant Class
2. Specify FOMs
3. Identify Systems, Components, Phases, Geometries, Fields, and Processes That Must Be Modeled
4. Identify and Rank Key Phenomena and Processes

Consistent with the guidance in EMDAP Element 1, section 3 of the TR describes the KP-FHR test reactor postulated events modeled by the safety analysis methodology, specifies FOMs and acceptance criteria, and identifies important SSCs and associated phenomena and processes that need to be modeled to calculate the target FOMs.

Consistent with the guidance in NUREG-1537, part 1, chapter 13, section 3 of the TR identifies and categorizes the postulated events in the KP-FHR test reactor. The events are categorized based on similarity of their characteristics into the following six categories:

- Increase in heat removal
- Decrease in heat removal
- Loss of forced circulation
- Reactivity-initiated event
- Salt spills
- Pebble handling and storage system (PHSS) malfunction
- Radioactive release from a subsystem or component

The frequency of event occurrence is not considered in the categorization of events. The staff finds that this is acceptable because all the events are considered equally important and treated similarly for the conservative modeling in the safety analysis methodology.

Limitation 1 in TR section 6.2 clarifies that the safety analysis methodology presented in the TR is applicable to the postulated event categories described in TR section 3.2 and the safety analysis methodology for event categories not included in TR section 3.2 will be provided in future licensing submittals. The staff includes this limitation through **Limitation and Condition 1**, to ensure that future licensing submittals that include any new event category will address the applicable steps in EMDAP consistent with the safety analysis methodology presented in this TR. In addition, as highlighted by limitation 5 in TR section 6.2, any new design features not considered in TR section 1.1 should be addressed, consistent with the guidance in EMDAP, in a future licensing submittal; the NRC staff include this limitation through **Limitation and Condition 1** of this SE.

3.1 Postulated Event Description

TR section 3.2 describes progression of a typical event in each postulated event category and identifies the potential limiting event for each postulated event category. TR section 5 presents a deterministic approach for identification of the limiting event by performing sensitivity calculations. The staff's evaluation of this approach for determining the limiting event is presented in SE section 3.5 below.

The staff reviewed the progression of a typical event in each postulated event category and observed that the initial KP-FHR system response to a generic postulated initiating event is generally characterized by the changes in core flow and temperature and the resultant reactivity feedback that affects the core fission power. The reactivity feedback is dominated by Doppler, moderator, or coolant temperature feedback depending on the initiating event. In general, the inherent negative reactivity feedback prevents uncontrolled rise of core power and overheating fuel during this initial transient phase before the activation of the reactor protection system (RPS). The RPS response triggered by the activation safety signals results in the insertion of shutdown elements and tripping of the primary salt pump (PSP). The heat rejection blower as well as the PHSS are also tripped on activation of RPS. The safety signals that can initiate the RPS response include high coolant temperature, low coolant level, high core power, high power rate, or low PHSS pressure. The activation of RPS results in the termination of core fission power and a transition to the decay heat generation mode. The loss of primary heat transport system (PHTS) circulation due to PSP trip (or due to initiating event) causes in-vessel flow to transition to a natural circulation model. Although the decay heat removal system (DHRS) is

always active, initial core decay heat exceeds the heat removed by DHRS, leading to a slow heat up of the core and reactor system. Eventually, the DHRS heat removal exceeds the core decay heat, and the event progression transitions into the long-term continuous cooldown phase. TR section 3.2 clarifies that the analysis of Flibe freezing conditions for the long-term phase is not included in the safety analysis methodology and will be addressed in a future licensing submittal. This limitation is identified as limitation 2 in TR section 6.2. The staff includes this limitation through **Limitation and Condition 1** of this SE.

A salt spill event, as described in TR section 3.2.5, is initiated by a breach in the Flibe-carrying SSCs connected to the reactor vessel (e.g., PHTS piping such as hot and cold legs, heat rejection radiator tubing). As described in TR section 1.1.3, there are two anti-siphon break points in the PHTS: the PSP siphon break point for the hot leg and the reactor vessel siphon break point for the cold leg. These passive antisiphon features limit the amount of spilled coolant salt to the level above the elevation of natural circulation path (NCP). Since the RPS would activate either due to the low coolant level or high coolant temperature actuation signals, an adequate amount of salt is preserved in the reactor vessel to keep the NCP submerged for continuous removal of decay heat by the DHRS. Following the activation of RPS, the progression of the salt spill event is consistent with the generic event description provided in the previous paragraph of this SE.

The PHSS malfunction event, as described in TR section 3.2.6, addresses the event initiated by the break in a PHSS transfer line. This event is detected by the RPS through the PHSS low pressure actuation signal. The event progression after the activation of RPS is consistent with the generic event description provided above. TR section 3.2.6 indicates that the other PHSS malfunctions such as loss of PHSS cooling and mechanical damage to a pebble in the PHSS line are assumed to be mitigated by design and the safety analysis methodology is only applicable to the PHSS malfunction due to a transfer line break. The TR does not identify any phenomena unique to the PHSS malfunction event in TR section 3.5 or describe any unique KP-SAM modeling approach for the PHSS malfunction event in TR sections 4 and 5. The staff finds that the level of detail provided in the TR for the PHSS transfer line break event are acceptable because the event is mitigated by a dedicated RPS actuation signal that is based on the low pressure in PHSS. However, information is currently not available on design features to mitigate other PHSS malfunctions and to identify the limiting event for this event category consistent with the guidance in NUREG-1537, part 1, chapter 13. Therefore, the staff impose **Limitation and Condition 2**, to limit the applicability of the safety analysis methodology to a PHSS malfunction initiated by a break in transfer line.

TR sections 3.2.5 and 3.2.6 describe the potential for air to get entrained into the PHTS, reactor vessel, or PHSS through the break in the event of salt spill or PHSS transfer line break. The interaction of air with Flibe can generate volatile products. Furthermore, ingress of air into the reactor vessel and PHSS can lead to the generation of flammable gas due to oxidation of un-submerged structural graphite and carbon pebbles. However, limitation 4 in TR section 6.2 clarifies that the safety analysis methodology does not address the generation of flammable gas due to graphite oxidation in reactor vessel following an air ingress scenario. The staff includes this limitation through **Limitation and Condition 1**.

The postulated event category described in TR section 3.2.7 accounts for the release of radioactive material due to failure of a subsystem or component which contains radioactive material outside of the functional containment (i.e., TRISO particle and Flibe coolant). The safety analysis methodology assumes the MAR in one or multiple affected subsystems and components is fully released at the start of event. The staff finds that the assumption of release

of all the MAR at the start of the event is conservative with respect to estimating dose and is, therefore, acceptable.

Based on its review, the staff finds that the description of event progression and the expected system response described in TR section 3.2 are consistent with the example calculations presented in TR appendix A. In addition, the staff finds that postulated event description, consistent with the guidance in EMDAP element 1, provides a reasonable level of detail needed to evaluate the safety analysis methodology. Furthermore, the staff finds that the postulated event categorization presented in the TR is consistent with the requirements of NUREG-1537, part 1, chapter 13.

3.2 Figures of Merit

The important FOMs for the safety analysis methodology are related to the dose criteria for test reactor siting, as required by 10 CFR 100.11. The regulatory criteria are stated in terms of whole body and thyroid from radioiodine doses to an individual at the EAB for the initial two hours and at the LPZ for the duration of the passage of the plume from an accident. In addition, KP-FHR PDC 19 provides a control room dose criterion stated in terms of TEDE in the control room for the duration of the accident.

The MHA in the safety analysis methodology is explicitly evaluated to provide dose results that demonstrate compliance with each of these accident dose criteria for the application. In lieu of explicitly demonstrating that the doses for each of the postulated events meet the regulatory dose criteria FOMs stated above, the safety analysis methodology demonstrates that the postulated event dose pathways are bounded by the MHA. The primary dose FOM for the safety analysis methodology is the MHA 30-day TEDE at the EAB which is an aggregated dose that includes impacts from whole body, thyroid, and other organ doses. The 30-day TEDE at the EAB for each postulated event is then shown to be bounded by the MHA 30-day TEDE at the EAB. This is accomplished by evaluating the postulated events to confirm that the release pathways not considered in the dose consequence analysis for the event do not occur and demonstrating that the dose consequences of the postulated events are below those of the MHA.

To ensure that each postulated event analysis compared to the 30-day dose FOM is also relevant for all potential source term release timings and to the regulatory dose criteria exposure timing in 10 CFR 100.11, the postulated events analyses for each postulated event group also estimates the whole body and thyroid from radioiodine doses for the first two hours at the EAB and duration of the passage of the plume at the LPZ. Therefore, the staff finds that the use of 30-day TEDE at the EAB to compare to the dose FOM instead of whole body and thyroid from radioiodine doses is reasonable for the purpose of demonstrating that the MHA is bounding for other postulated event groups.

TR sections 3.3.1 through 3.3.5 describes the additional surrogate safety analysis methodology FOMs evaluated to confirm that the postulated events do not include releases not modeled in the MHA. These surrogate FOMs are summarized in table 1 of this SE. For each FOM, table 1 summarizes acceptance criteria, justification or basis, evaluation approach, and the postulated event category for which the FOM is evaluated. Table 1 also shows the 30-day TEDE dose FOM which is evaluated for each postulated event category to demonstrate that the dose consequences of the postulated events are below those of the MHA.

As shown in table 1, peak TRISO silicon carbide (SiC) layer temperature and fuel failure fraction FOMs are evaluated using the KP-BISON code, which is described in TR KP-TR-010-NP-A, "KP-FHR Fuel Performance Methodology" (ML22125A278). The peak pebble power and peak pebble surface temperature calculated using the KP-SAM hot-pebble factor (HPF) EM described in section 4.2.4 of KP-TR-020, Revision 1, and evaluated in this SE in section 4.1 are provided as input to KP-BISON. The KP-BISON methodology for calculation of the peak TRISO SiC layer temperature and fuel failure fraction FOMs is not presented in this TR; therefore, the staff impose **Limitation and Condition 3** that clarifies that the KP-BISON methodology for calculation of these FOMs is not reviewed and approved in this SE and the acceptable justification for the use of KP-BISON for the calculation of these FOMs must be provided with the licensing application referencing this TR.

TR sections 3.3.4 and 3.3.5 clarify that the acceptance criteria for the peak vessel temperature and peak structural graphite temperature FOMs are consistent with the material qualification data for the KP-FHR test reactor. The staff impose **Limitation and Condition 4(a)** to require an application referencing this TR to provide supporting material qualification data for the review. A conservative approach for the calculation of these FOMs is presented in TR section 4.2.4 and evaluated in section 4.1 of this SE.

TR section 3.3.4 clarifies that the peak vessel temperature FOM is also used as surrogate FOM for the maximum temperature of metallic materials outside of the pebble bed core (e.g., core barrel and hold-down structure). However, as identified by limitation 6 in TR section 6.2, the evaluation of peak temperature of metallic materials inside the pebble bed (e.g. shutdown elements) is not within the scope of the TR methodology. The staff includes this limitation through **Limitation and Condition 1**.

Based on its review, the staff finds that the TR, consistent with the guidance in EMDAP Element 1, provides an adequate description of the primary and surrogate FOMs and identifies appropriate acceptance criteria for the safety analysis methodology. Furthermore, the staff finds that the proposed surrogate FOMs are suitable for supporting the development of the KP-SAM EM for postulated event analysis.

**Approach for Calculation of Dose FOM**

TR section 3.3.6.1 describes the safety analysis methodology approach for evaluation of the dose FOM for three types of postulated events: primary system postulated events with MHA release pathways, non-intact postulated events with MHA and non-MHA release pathways, and releases from subsystem or component postulated events. As discussed in TR section 3.3.6.1 and summarized in table 2 of this SE, for the primary system postulated events 30-day TEDE at the EAB is calculated using the MHA release pathways (i.e., releases from the intact primary system) and bounding temperature-time and flowrate-time curves for the following parameters:

- Maximum kernel temperature (also conservatively applied to TRISO layers)
- Maximum reflector temperature
- Maximum pebble surface temperature
- Flibe-cover gas interface temperature
- Core mass flowrate
- Bypass mass flowrate

The postulated event categories considered for this approach are the events with the MHA release pathways from the primary system including the increase and decrease in heat removal events, loss of forced circulation, reactivity-initiated events, and salt spill events. The KP-SAM transient calculations for the limiting events for these event categories are used to confirm the bounding nature of the selected parameter curves. The limiting event for each category is determined using the sensitivity calculations proposed in TR section 5 and the conservative bounding values for the temperature related FOMs including peak TRISO temperature, peak vessel temperature, and peak reflector temperature calculated using the approach presented in TR section 4.2.4. However, the bounding nature for the dose analysis input parameter curves is confirmed using the nominal maximum parameter values. TR section 3.3.6.1 further describes the approach used for calculation of bounding parameter curves from the KP-SAM calculation. The staff finds that the use of KP-SAM calculated nominal maximum parameter values for confirming the bounding parameter curves for dose analysis is acceptable because the nominal maximum temperatures for kernel, reflector, and pebble surface are expected to be higher than the average temperatures for these materials during the transient.

TR section 3.3.6.2 describes the safety analysis methodology approach for the calculation of dose FOM in non-intact postulated events. For the non-intact primary system postulated event with non-MHA release pathways the sum of the 30-day TEDE at the EAB for all non-MHA release pathways for the event is added to the 30-day TEDE at the EAB from the bounding primary system postulated event (described in TR section 3.3.6.1) to give a total consequence for the event to compare against the MHA 30-day TEDE at the EAB dose FOM. The calculation of the 30-day TEDE at the EAB for non-MHA release pathways in salt spill events and PHSS malfunction postulated events is described in TR section 5 and evaluated in SE section 5.2.

For the releases of subsystem and component event category, as described in TR section 3.3.6.3, the MAR in one or more subsystem or components is assumed to be fully released to calculate the 30-day TEDE at the EAB for comparison against the MHA 30-day TEDE at the EAB dose FOM.

Based on its review, the staff finds that the approaches described in TR section 3.3.6 consider the potential radiological releases for postulated events and differences from the scenario modeled in the MHA analysis to demonstrate that the MHA consequences are bounding for the test reactor postulated events. Therefore, the staff finds that the FOMs based on these approaches also demonstrate that the MHA is bounding of the test reactor postulated events.

Table 1 Safety Analysis Methodology Figures of Merit

| **FOM** | **Acceptance Criteria** | **Basis or Justification** | **Calculation Approach** | **Applicable Event Categories** |
|---|---|---|---|---|
| Peak TRISO SiC temperature | 1600 °C | Ensures that SiC layer failures do not occur in transient conditions and transient failure fraction does not deviate from the steady state failure fraction assumed in MHA dose analysis. Ensures that the fuel remains within the qualification envelope described in TR KP-TR-011-NP-A, “Fuel Qualification Methodology for the Kairos Power Fluoride Salt- | Calculated using KP-BISON with input of peak pebble power and peak pebble surface temperature calculated using KP-SAM HPF approach. | Increase or decrease in heat removal, Loss of forced circulation, Reactivity-initiated event, and Salt spills |

| | | | | |
|---|---|---|---|---|
| | | Cooled High Temperature Reactor (KP-FHR)," (ML23089A398). | | |
| Fuel failure fraction | Steady state failure fraction assumed in MHA dose analysis | Ensures that transient failure fraction does not deviate from the steady state particle configuration fraction. Ensures that fuel performance is consistent with that assumed in the MHA dose analysis. | | |
| Peak vessel temperature | 750 °C | Consistent with material qualification for KP-FHR test reactor. Ensures that coolable geometry is maintained and vessel failure do not occur as assumed in the MHA dose analysis. | Calculated using KP-SAM peak vessel temperature and peak reflector temperature surrogate described in TR section 4.2.4 and evaluated in section this SE section 3.3. | |
| Peak structural graphite temperature | 950 °C | Consistent with material qualification for KP-FHR test reactor. Ensures that structural integrity of graphite is maintained to permit the insertion of shutdown element and to facilitate natural circulated needed to maintain the coolable geometry as assumed in the MHA dose analysis. | | |
| Energy deposition pulse width | Greater than 1 second | Ensures that fuel failures not considered in MHA do not occur in reactivity-initiated events. As the TRISO fuel constant is small, the selected acceptance criteria assures that energy deposited in TRISO fuel is dissipated without significant heat up. | Time from initiation of event to time of maximum power in KP-SAM simulation. | Reactivity-initiated event |
| 30-day TEDE dose at EAB | See table 2 of this SE for acceptance criteria and approach for calculation of this FOM. | | | All postulated event categories |

Table 2 Safety Analysis Methodology Approach for Calculation of Dose Figure of Merit

| **Postulated event** | **Acceptance criteria** | **Basis or Justification** | **Evaluation Approach** |
|---|---|---|---|
| Primary system postulated events | 30-day TEDE at EAB < (less than) MHA 30-day TEDE at EAB | TEDE is an aggregate dose FOM that includes impacts to the whole body, thyroid, and other organs | Bounding nominal parameter curves calculated using KP-SAM EM used to calculate 30-day TEDE at EAB |
| Non-intact postulated events (salt spills, PHSS malfunction) | 30-day TEDE and 30-day TEDE at EAB from all non-MHA release pathways < (less than) MHA 30-day TEDE at EAB | | Sum of 30-day TEDE doses at EAB calculated for all non-MHA pathways added to the 30-day TEDE at EAB for the bounding primary system postulated event |

| | | | |
|---|---|---|---|
| Release from subsystem and component | 30-day TEDE at EAB for bounding sequence < (less than) MHA 30-day TEDE at EAB | No releases from primary system for this event. | Only release pathways from the postulated events are directly compared to MHA dose. |

3.3 Phenomena Identification and Ranking Table

The importance rankings and knowledge levels assigned to phenomena in the PIRT guide the development of the EM (Element 3 of EMDAP), validation base (Element 2 of EMDAP), and applicability evaluation (Element 4 of EMDAP). For the KP-SAM EM presented in the TR, Kairos referenced the thermal fluids PIRT and the reactivity insertion PIRT that were developed by Kairos for the KP-FHR. The thermal fluids PIRT identified thermal-hydraulic phenomena that are relevant to all the postulated event categories except for the radioactive release from subsystem and component event category. The reactivity insertion PIRT addressed the specific phenomena in the reactivity-initiated event and the increase in heat removal events.

Kairos also identified additional PIRTs (i.e., neutronics PIRT, fuel PIRT, and structural PIRT) that have an indirect impact on the safety analysis methodology presented in the TR. The neutronics PIRT is used in the core design and analysis methodology described in TR KP-TR-024-NP, “KP-FHR Core Design and Analysis Methodology” (ML25168A340), which provides the nuclear parameter inputs to the KP-SAM point kinetics model used in the TR to calculate fission power. The fuel PIRT is used for the development of KP-BISON based fuel performance methodology in KP-TR-010-NP-A. KP-BISON is used to provide input to the source term analysis and to assess the two FOMs (i.e., peak SiC layer temperature and fuel failure fraction) of the safety analysis methodology. The structural materials PIRT is used in TR KP-TR-013-NP-A, “Metallic Materials Qualification for the Kairos Power Fluoride Salt-Cooled, High Temperature Reactor,” (ML23102A179), which has an impact on the acceptance criteria for the structural materials in the safety analysis methodology.

Table 3-1 of the TR summarizes the high and medium importance phenomena from the thermal fluids PIRT and how they are addressed by the KP-SAM EM. The thermal fluids PIRT identifies the phenomena in the following SSCs: **[[**

**]]** The staff’s evaluation of the approach used to model these PIRT phenomena and associated modeling assumptions is provided in SE section 4.3.

Although most of the thermal fluids PIRT phenomena apply to all the event categories analyzed using the KP-SAM model, some phenomena are unique to specific event categories, such as the salt spill event (e.g., **[[ ]]**). The PIRT also initially identified some phenomena as medium or high importance but later downgraded them to low importance based on insights from the sensitivity analysis, such as **[[**

**]]** The staff finds that this iterative approach for updating the PIRT is acceptable because it reduces the subjectivity in the PIRT and increases the focus on important phenomena.

The thermal fluids PIRT identifies phenomena in the **[[**

**]]** The PIRT justifies this based on the modeling approach for DHRS that involves the use of experimental data to derive the bounding high and low DHRS performance curves. Further evaluation of the DHRS modeling approach is provided in SE section 4. The thermal fluids PIRT identified some phenomena that are not represented in the KP-SAM model. These include the phenomena related to the modeling of reactor physics (e.g., **[[** **]]**) and the pebble and TRISO fuel properties and heat transfer (e.g., **[[**

**]]**). These phenomena are modeled by the other methodologies described in KP-TR-024-NP or KP-TR-010-NP-A.

Table 3-2 of the TR summarizes the high and medium ranked phenomena in the reactivity PIRT. The reactivity PIRT identifies the phenomena in the following categories: **[[**

**]]** The phenomena presented in this PIRT are either addressed in the thermal fluids PIRT or captured in the KP-TR-010-NP-A methodology used for the calculation of two FOMs as discussed in SE section 3.2 or accounted by the KP-TR-024-NP methodology used to generate conservative inputs for the point kinetics model in KP-SAM.

Table 3-3 of the TR summarizes the new high and medium importance ranked source term phenomena that were not previously identified in KP-TR-012-NP-A and the phenomena for which the importance ranking was upgraded. The staff finds that the new source term PIRT information is relevant to the more detailed radionuclide transport modeling in the primary system, for salt spills, and for releases from the PHSS as described in TR sections 2.2, 5.5.3, and 5.6.2, respectively. The staff's evaluation of the approach used to model these PIRT phenomena and associated modeling assumptions is provided in SE section 2 for the models in TR section 2.2, and in SE section 5.2 for the event-specific source term methods discussed in TR sections 5.5.3 and 5.6.2.

The PIRTs presented in the TR **[|** **]]** of the system consistent with EMDAP Step 3. The PIRTs also **[[**

**]]** as recommended by EMDAP Step 4 as the different SSCs and the associated phenomena might have a different importance level during the multiple phases of the accident or transient. For example, the phenomena that are important during the early phase of transient before the activation of RPS may have a different importance level after the RPS activation or in the long -term phase. However, the staff finds that this simplified approach is acceptable for the test reactor safety analysis methodology development. This is because the objective of the safety analysis methodology is to demonstrate that the predicted temperature-time or flow-time for the limiting events are bound by the parametric curves provided as input to the MHA analysis for the calculation of limiting dose.

## 4. KP-SAM Code, Base Model, and Validations

TR section 4 addresses EMDAP Element 2 and Element 3 for the KP-SAM EM.

EMDAP steps under Element 2 are:

- Step 5, "Specify Objectives for Assessment Base"
- Step 6, "Perform Scaling Analysis and Identify Similarity Criteria"

- Step 7, “Identify Existing Data and/or Perform Integral Effects Tests (IETs) and Separate Effects Tests (SETs) to Complete the Database”
- Step 8, “Evaluate Effects of IET Distortions and SET Scaleup Capability”
- Step 9, “Determine Experimental Uncertainties as Appropriate”

These steps are addressed, in part, in TR sections 4.2 and evaluated in SE section 4.3.

EMDAP steps under Element 3 are:

- Step 10, “Establish an Evaluation Model Development Plan”
- Step 11, “Establish Evaluation Model Structure”
- Step 12, “Develop or Incorporate Closure Models”

These steps are addressed in TR sections 4.1 and 4.2. The staff’s evaluation of KP-SAM EM documentation, quality assurance, and configuration control for EMDAP Step 10 is presented in SE section 4.4. The staff’s evaluation of KP-SAM code and base model for EMDAP steps 11 and 12 is presented in SE sections 4.1 and 4.2.

## 4.1 KP-SAM Code Description

The KP-SAM code is based upon the System Analysis Module (SAM) code, which was developed by Argonne National Laboratory (ANL) under the Department of Energy’s Nuclear Energy Advanced Modeling and Simulation (NEAMS) workbench as a generic system-level safety analysis tool for advanced non-LWRs. It is capable of modeling thermal-hydraulics and neutronics phenomena and control system behavior for integral analysis of transients and accidents in advanced reactors. The TR identifies the following major developments from SAM to KP-SAM:

- a description of the physics and system component behaviors;
- specific numerical methods such as continuous finite element method stabilizing methods; and
- addition of specific functions for the systems code.

According to section 4.1.1 of the TR, KP-SAM, like SAM, has two types of physics models: field equations and closure models. Field equations are solved to transport quantities of interest in 0-dimensional (D), 1-D, or 2-D domains. However, the KP-SAM EM presented in the TR does not use 2-D flow-field equations; it only uses 1-D single-phase flow-field equations for mass, momentum, and energy conservation along the flow direction and their primary variables are pressure, velocity and temperature. Heat structures in KP-SAM model the heat conduction inside the solids and permit the modeling of heat transfer at the interfaces between solid and fluid components. Heat structures are represented by 1-D or 2-D heat conduction in Cartesian or cylindrical coordinates. A 1-D spherical heat conduction model is also developed for pebble bed simulation. KP-SAM also includes generic closure models and correlations. Closure models and correlations specific to the KP-FHR design and their validations are discussed in TR section 4.2 and evaluated in SE section 4.1.2. These include, for example, correlations for flow and heat transfer in the pebble bed core.

The KP-SAM control system is used to perform evaluation of algebraic and other simple equations; the trip system is used to perform the evaluation of logical statements. The main execution of individual control/trip units is set at the end of each time step.

KP-SAM uses a continuous finite element method formulation for the spatial discretization of the field equations, with the code formulated such that the numerical method orders are controlled through user inputs. For fluid models, a spatial stabilization method is implemented to suppress checkerboard-type spatial oscillations that manifest when using continuous finite element methods to solve advection dominated problems.

As described below, the staff reviewed and evaluated the KP-SAM code capabilities, limitations, closure models and validations as described in this TR and the KP-SAM theory manual KP-RPT-000231, "KP-SAM Theory Manual" (ML24156A166), and user guide KP-RPT-000226, "KP-SAM Users Guide," (ML24156A167) to assess the adequacy of KP-SAM for the calculation of safety analysis methodology FOMs.

4.1.1 KP-SAM Code Limitations

TR section 4.2.4 describes the KP-SAM limitations and the safety analysis methodology approach to address these limitations. The following KP-SAM limitations are addressed by the safety analysis methodology:

- Use of 1-D fluid flow and 2-D heat transfer approach for modeling of flow and temperature distribution in reactor (core, reflector, downcomer, and vessel wall).
- Use of uniform porosity for pebble bed in core.
- Use of 1-D power distribution in core.
- Neglecting radiative heat transfer in reactor.
- No model to capture gamma and neutron heating of in-vessel heat structures (i.e., reflector and metallics). All energy from gamma and neutron heating is assumed to deposit in fuel pebbles.

These limitations, summarized in TR table 4-4, result in limited capability for KP-SAM to model 3-D temperature distributions in the core, reflector, and vessel wall. The safety analysis methodology uses conservative modeling methods or factors to account for these limitations for the calculation of key FOMs: an HPF, a peak vessel temperature surrogate, and a peak reflector temperature surrogate.

**Hot Pebble Factor**

The HPF, described in TR section 4.2.4.1, is used for the conservative calculation of pebble surface temperature which is then provided as input to KP-BISON for the calculation of the peak TRISO layer temperature FOM. It accounts for the impact of 3-D flow and power distribution in the core and uncertainties in pebble bed heat transfer correlations and pebble diameter.

The HPF is based on the hot channel factor approach used in nuclear reactor safety analysis to account for impact of different uncertainties on the calculation of safety parameters such as peak fuel temperature (References 1 and 2). It uses vertical semi-statistical methods to combine deterministic and statistical uncertainties. The HPF in the TR calculates conservative bounding factors as multipliers for the coolant temperature rise and the maximum pebble film temperature

rise (i.e., maximum temperature difference between the pebble surface temperature and the coolant temperature). The maximum pebble surface temperature is calculated using TR equation 4.8 from the bounding values of the coolant temperature rise and the maximum pebble film temperature rise.

The bounding coolant temperature rise is calculated by multiplying the KP-SAM calculated maximum coolant temperature rise by a direct subfactor that accounts for the impact of radial and azimuthal power distribution. The upper bound radial and azimuthal peaking factor value calculated from the static core design analysis is used for this subfactor. The 2-D static core design analysis is used for events with no azimuthal power variation to calculate the radial peaking factor. The 3-D static core design analysis is used if the transient induces radial as well as azimuthal power distribution perturbation (e.g., single control rod withdrawal). The axial power distribution is accounted for in the coolant temperature rise calculated by KP-SAM. The TR justifies the use of static core analysis for the calculation of peaking factors because the flux distribution in a transient spatial kinetics calculation would be flatter due to reactivity feedback effects. The staff finds that the use of 2-D or 3-D static core analysis for the calculation of upper bound radial and azimuthal peaking factor is acceptable because it results in conservative values for the peaking factor. The example calculation A.5 in appendix A of the TR estimates a value of **[[ ]]** for the radial and azimuthal peaking factor. The HPF does not account for the impact of radial flow distribution on the coolant temperature rise. Kairos clarified in audit discussions that the pebble bed induced mixing substantially reduces the impact of radial flow distribution on the coolant temperature rise. The staff finds this explanation reasonable.

The bounding maximum film temperature rise is calculated by multiplying the KP-SAM calculated maximum film temperature rise by two direct and two statistical subfactors that are combined using TR equation 4.6. The direct subfactors account for the impact of distributions in pebble power and local flow on the calculated pebble film temperature. The impact of pebble power distribution is accounted for using a pebble peaking factor which is defined as peak pebble power relative to average core power. The same approach described for the radial and azimuthal peaking factor is used for the calculation of pebble peaking factor (i.e., use of 2-D or 3-D static core analysis). The example calculation A.5 in appendix A of the TR estimates a value of **[[ ]]** for the pebble peaking factor. The direct subfactor that accounts for the impact of local flow distribution (flow penalty subfactor) is calculated using TR equation 4.12 with the support of the computational fluid dynamics (CFD) **[[ ]]** packed bed model that was described in KP-TR-024-NP. The TR states that the single flow penally subfactor for the symmetric and asymmetric events is adequate because the preliminary analysis shows that the **[[ ]]**. The TR states that the bounding value for this factor will be calculated over a range of core flow rates or Reynolds numbers. The TR further states that the uncertainties in the CFD **[[ ]]** model will be considered, and additional discretionary conservatism will be applied to account for reliance on the CFD calculation performed for **[[ ]]**.

The two statistical subfactors for the film temperature rise account for the uncertainties in pebble diameter and convective heat transfer correlation for the pebble surface heat transfer (Wakao correlation, Reference 3). TR equation 4.13 calculates the statistical subfactor for the pebble

diameter uncertainty based on the Wakao correlation. The statistical subfactor for the **[[ ]]** is calculated based on comparison of **[[ ]]** correlation to the experimental data. The example calculation A.5 in appendix A of the TR estimates values of **[[ ]]** and **[[ ]]** for the pebble diameter and **[[ ]]** correlation statistical subfactors, respectively.

The HPF does not explicitly account for the impact of uncertainties associated with calculation of total core power, core and bypass flow split, neutronics parameters and calculated power response. Kairos clarified in audit discussion that these uncertainties are separately addressed in TR section 5 as a part of event-specific event specific biases and sensitivity analysis. Additionally, the HPF does not account for the KP-SAM model limitations related to the modeling of gamma and neutron heating and radiation heat transfer. The staff finds that this modeling limitation is acceptable because it leads to the deposition of all core energy into the coolant which results in a conservative estimation of peak pebble surface temperature.

The results of the example calculation A.5 in appendix A of the TR illustrate that the contributions from the two direct subfactors that account for the impact of power distribution (i.e., radial/azimuthal peaking factor and pebble peaking factor) and the statistical subfactor that accounts for the uncertainty in pebble surface heat transfer correlation dominate the calculation of peak pebble surface temperature using the HPF. Based on the review of TR section 4.2.4.1, the staff finds that the HPF adequately addresses all the identified KP-SAM limitations. However, the HPF is dependent on the 2-D or 3-D static core design analysis for the calculation of radial/azimuthal and pebble peaking factors. Furthermore, the HPF is also dependent on the use of the CFD **[[ ]]** model for the calculation of direct subfactor that accounts for the impact of local flow distribution (flow penalty factor). KP-TR-024-NP provides a methodology for the calculation of radial/azimuthal and pebble peaking factors. Also, it appears that the CFD **[[ ]]** model presented in KP-TR-024-NP for the validation of porous media model can be used for the calculation of local flow penalty subfactor. However, neither this TR nor KP-TR-024-NP provided any calculations demonstrating the implementation of 2-D or 3-D static core design analysis or the CFD **[[ ]]** calculations for the estimation of direct subfactors in the HPF for different event categories. Therefore, the staff is imposing **Limitation and Condition 4 (b)**, that requires test reactor applications referencing this TR to provide for staff review the supporting 2-D/3-D static core analysis and the CFD **[[ ]]** model results used for the calculations of peaking factors and local flow penalty factor.

**Peak Vessel Temperature Surrogate**

The peak vessel temperature surrogate, described in TR section 4.2.4.2, accounts for the impact of the KP-SAM limitations on the calculation of peak vessel temperature. The Flibe temperature at the outlet of the NCP is used as surrogate for the peak vessel temperature. This approach is conservative because the Flibe temperature at the outlet of the NCP is maximum within the system and it neglects the loss of Flibe energy in the NCP, downcomer, and by DHRS heat removal. Furthermore, as discussed earlier, the coolant temperature calculated in KP-SAM is also maximized due to the limitations on modeling of radiation heat transfer and gamma and neutron heating. The staff finds that the approach for the calculation of peak vessel temperature FOM acceptable because it is conservative.

**Peak Reflector Temperature Surrogate**

The peak reflector temperature surrogate, described in TR section 4.2.4.3, accounts for the impact of the KP-SAM limitations on the calculation of peak reflector temperature. TR equation 4.14 is used to calculate the peak reflector temperature. Similar to the peak vessel temperature surrogate, the maximum Flibe temperature is used but with the penalty factors to account for the impact flow and power distribution in core on the local reflector temperature. The radial peaking factor is calculated using a similar approach as described for the HPF approach for uniform and asymmetric power distribution events. The flow factor that accounts for the local flow reduction is calculated from the **[[ ]]** analysis. TR table 5-1 summarizes the different direct subfactors used for the HPF and peak reflector temperature surrogate calculation and the interface with KP-TR-024-NP. The staff finds that the approach proposed for the peak reflector temperature accounts for the identified KP-SAM limitations. However, **Limitation and Condition 4 (b)** is also applicable to the 2-D/3-D static core design analysis and the CFD **[[ ]]** model analysis performed to estimate the peak reflector temperature surrogate.

The staff finds that the TR and the KP-SAM code manuals provide adequate description of the code fundamental equations and numerical methods. Furthermore, the TR adequately describes the KP-SAM limitations and EM approach to address those limitations satisfying, in part, EMDAP step 11. The KP-SAM base model described in TR section 4.3 and the event-specific biases and sensitivity described in TR section 5 address the remaining scope of EMDAP step 11.

4.1.2 KP-SAM Closure Relations

The key closure models implemented in KP-SAM include the equation of state for Flibe, material properties for solids (such as graphite and metallic materials), heat transfer correlations, and wall friction correlations. In addition to the TR, the KP-SAM theory manual provides a detailed description of the closure models available in the code.

**[[ ]]** TR section 5 indicates that the Flibe thermal-physical properties used in the KP-SAM EM are biased to bound the uncertainties described in TR KP-TR-005-NP-A, “Reactor Coolant for the Kairos Power Fluoride Salt-Cooled High Temperature Reactor,” (ML20219A591). Further evaluation of event-specific biases proposed for the Flibe properties is in SE section 5. **[[**

**]]**. Furthermore, as shown in **[[ ]]** and described in TR section 4.3.6, the thermal conductivity of the ET-10 reflector graphite material is biased in KP-SAM to a conservatively low value, corresponding to bounding irradiation temperature and fluence to maximize stored energy in reflector. **[[**

**]]** to reduce calculated margin to fuel safety limit (i.e., peak TRISO layer temperature). However, the final calculation of peak TRISO temperature FOM performed in KP-BISON uses thermal properties as function of temperature and irradiation. Therefore, based on this review,

the staff finds that the basis for the equation of state for Flibe and the material properties used in the KP-SAM EM is acceptable.

KP-SAM theory manual chapters 17 and 18 describe the closing relations for heat transfer and wall friction available in KP-SAM. TR section 4.2.2 describes the key closing relations used to model the selected high importance ranked phenomena including: **[[ ]]**. TR section 4.2.2 also describes the SETs planned to validate these correlations. The evaluation of these proposed SET validations is provided in SE section 4.3.

TR section 4.2.2.1 describes the correlations selected to model the **[[ ]]**. The staff finds that the proposed correlation for the **[[ ]]** and will be validated against applicable SET data.

TR section 4.2.2.2 describes **[[ ]]**. The staff finds the use of the **[[ ]]** acceptable because it has a well-documented basis and validation is planned against applicable SET data as described in TR section 4.2.2.2.

TR section 4.2.2.3 describes **[[ ]]**. The staff finds the use of **[[ ]]** acceptable because it has a well-documented basis and validation is planned against applicable SET data as described in TR section 4.2.2.3.

TR section 4.3.7 describes the closing relation used **[[**

**]]**.

Based on its review, the staff finds that the KP-SAM closure models are acceptable because the TR, KP-SAM user guide and theory manuals provide adequate information on the closure models to address EMDAP step 12.

4.2 KP-SAM Base Model

The KP-SAM base model described in TR section 4.3 is a best estimate model that can be adequately used for simulation of KP-FHR test reactor for postulated event analysis provided that the biases and assumptions required to perform conservative safety analysis, such as the HPFs, are applied. The vessel portion is modeled as axisymmetric around the axial direction (z-axis), with the fluid (Flibe) region modeled in 1-D and the solid regions modeled in 2-D (r-z). This modeling approximation is adequate for the test reactor since relevant flow and heat transfer conditions are expected to be axisymmetric, and power distribution asymmetries are captured by the HPF.

The core flow, including the cylindrical (CYL), converging (CON), and diverging (DIV) regions, is modeled in 1-D with nodalization only along the axial direction (i.e., with no radial or azimuthal nodalization). To allow for 1-D modeling approximation of flow in the core, the diverging and converging regions (truncated cones) of the core are modeled as equivalent cylindrical regions. The effective diameters of these cylinders are calculated such that the volumes, thus the mass and stored energy, of the converging or diverging regions are preserved. For preserving the heat transfer through the walls of the converging or diverging regions, separate effective heated perimeters are calculated and used only for that purpose. These assumptions are adequate for simulation of the KP-FHR test reactor for postulated event analysis provided that the biases and assumptions required to perform conservative safety analysis, such as the HPFs, are appropriately applied. All other fluid (Flibe) flow regions (e.g., cold leg, downcomer, hot leg, inlet flow channel, rim gap) are also modeled in 1-D, with nodalization only along the direction of the flow. Heat conduction in solid structures is modeled in 2-D.

The pebble heat structures in the reactor are modeled and nodalized in spherical 1-D as follows:

- the fuel pebbles are modeled as a three region heat structure consisting of the pebble core, the fueled core, and the pebble shell;
- the moderator pebbles are modeled as a single region heat structure; and
- the TRISO fuel particles are modeled using the KP-SAM TRISO particle model.

This nodalization and modeling is adequate for the purposes of the safety analysis methodology, provided that the output temperatures of the simulation are used as an input to the KP-BISON code for further analysis. The staff notes that the KP-SAM calculations use conservative hard-coded material properties, which reduce the calculated margin to fuel safety limits, and the final calculation of the fuel safety limits are performed using KP-BISON which explicitly captures changes in thermal properties as a function of temperature and irradiation.

The graphite reflector is composed of stacked blocks which lead to the formation of a series of both horizontally-oriented and vertically-oriented interstitial radial gaps between the reflector blocks during reactor operation, as well as a rim gap between the reflector and the core barrel to accommodate differential thermal expansion. The reflector blocks also include flow channels to accommodate instrumentation and control equipment. The paths through the pebble bed and through the annular rim gap are explicitly modeled in KP-SAM, but the paths through the gaps in the reflector are not modeled due to the uncertainty associated with their detailed geometry.

This graphite reflector configuration introduces uncertainty in modeling the bypass and core flow distribution, especially given the lack of experimental data and the use of 1-D modeling and uniform porosity in the pebble bed region. The CFD **[[ ]]** model from KP-TR-024-NP can provide some insights into the steady state bypass and core flow distribution. However, there is a lack of understanding of how that flow would develop during the initial transient phase and what its impact would be on the temperature distribution. Although the impact of uncertainty associated with dynamic flow distribution during transients may be reduced by conservative flow distribution assumptions based on each transient and by assumptions defining conservative surrogates for FOM temperatures, this is an area where the final modeling approach based on final design, sensitivity analysis results, and any applicable validation data, must be further reviewed and approved. Therefore, the staff is imposing **Limitation and Condition 4 (c)** to ensure that an application referencing this TR provides for review the justifications (e.g., bypass flow sensitivity analyses) that the transient bypass and core flow distribution as modeled results in conservative prediction of the temperature distribution.

For the salt spill event analysis, valve components in KP-SAM are used to model the anti-siphon features on the PSP and the cold leg of the PHTS. A valve component, which is added directly below the PSP component, closes and stops the flow into the PSP when the Flibe level in the upper plenum is below the axial location of the PSP anti-siphon level. A valve component, which is added on the cold leg component, closes and stops the flow into the cold leg when the Flibe level in the upper plenum is below the cold leg anti-siphon level. The pipe break in the PHTS piping is modeled using three additional valves as described in TR section 4.3.10. The staff finds this modeling approach for salt spill event analysis to be acceptable because the modeling approach provides an adequate representation of a salt spill event and system response.

In general, a typical element or node size of approximately 10 cm, with a minimum of three elements, is used in developing the mesh, which is typical and appropriate in most regions. In regions with steep gradients, a finer mesh is used to appropriately maintain mass and energy balances and to ensure that the solutions variables are appropriately captured. As stated in the TR, the adequacy of the model nodalization scheme is assessed as part of the overall EM assessment, which includes dedicated mesh sensitivity studies to confirm independence of the simulation solutions from spatial discretization. The staff did not review the specific mesh sensitivity studies for the base model since the model does not represent the final design, and the staff was not asked to review it. The staff will review these sensitivity studies for the final EMs when they are submitted. According to limitation 3 in TR section 6.2, the base model will be updated using the validation insights. This would also include confirmation of the adequacy of the nodalization selected for the base model. Specifically, the IET validation is expected to play a key role in confirming the 1-D nodalization approach selected for modeling the core. The staff includes this limitation through **Limitation and Condition 1**.

The staff notes that this SE does not approve a specific KP-SAM input model. The SE approval is limited to the general approach for the base model development. Review of the final base

model and its adequacy to represent the final geometry and the initial and boundary conditions will be addressed in a future licensing submittal.

TR sections 4.1.1 and 4.3.2 discuss the approach used to calculate the power response of the reactor core during transients simulated by KP-SAM. The fission power is calculated via KP-SAM's point kinetics approximation, accounting for changes in reactor power due to prompt and delayed neutron generation. Reactivity feedback behavior is included in the model via core-level coefficients generated with the applicant's nuclear analysis methodology described in KP-TR-024-NP. Temperature feedback coefficients are included for the fuel, moderator pebbles, coolant and reflector. **[[**

**]]** In addition to feedback coefficients, kinetics parameters (e.g., delayed neutron group fractions and lifetimes, mean generation time) and RSS trip worth are provided by nuclear design. Nuclear design calculations are also used to develop reactivity worth curves for inadvertent RCS withdrawal. Uncertainties in all these parameters are accounted for via the nuclear reliability factors (NRFs) developed as part of nuclear analysis and are biased according to the NRFs (and additional margin, if needed) on an event-specific basis. RSS trip worth is also penalized via maintaining the highest-worth control blade stuck in a fully withdrawn position. The axial power distribution used in generating the reactor trip worth is biased relative to nominal towards the bottom of the core to delay the negative reactivity of the blades entering the active core region. The power distribution used within KP-SAM simulations are biased relative to nominal towards the top of the core to penalize natural circulation flow and therefore create more challenging resultant temperature conditions. The staff finds the applicant's implementation of point kinetics to represent the reactor core power transient to be acceptable because it (1) is an implementation of a common safety analysis approach; (2) considers all relevant feedback mechanisms and external reactivity sources; and (3) appropriately considers uncertainty to produce conservative evaluations of the core and system response to an upset condition.

TR section 4.1.1 also describes that decay heat can be modeled in KP-SAM via a user-supplied decay power vs. time curve or using an internal predictive model. For an internal predictive model, core design calculations would be utilized to determine the relative fraction of fissions coming from uranium-235, uranium-238, plutonium-239 and plutonium-241 based on the core composition at the desired time in life at which the transient would be simulated. The predictive model can be further manipulated via a multiplicative factor to introduce additional conservatism in decay heat calculations as desired. The staff confirmed during its audit of Kairos' supporting documentation that the base Hermes KP-SAM model uses the nominal default decay heat model in KP-SAM, which is the same as that included in the base SAM code developed by Argonne National Laboratory. Review of the SAM theory manual (Reference 7) indicates that the default decay heat model is based on the American National Standard (ANS) standard ANSI/ANS-5.1-2005, "American National Standard Decay Heat Power in Light Water Reactors," (Reference 8). Although KP-FHRs are not light water reactors, it may be that this decay heat model is adequate for simulation purposes. However, justification for this or any other decay heat model is not included in the TR. The staff finds that the use of a decay heat model is acceptable and necessary for adequate evaluation of a KP-FHR transient. However, because no specific model has been justified at this time, the staff is imposing **Limitation and Condition 4 (d)**, that requires an applicant utilizing this safety analysis methodology to justify and submit the specific decay heat model and associated uncertainties incorporated in licensing submittals to the staff for review.

4.3 KP-SAM Validations and Applicability Evaluation

EMDAP element 2 provides guidance on development of an assessment base for the EM. The assessment base generally includes analytical (or fundamental) assessments, SET assessments, and IET assessments. The SETs are used to validate empirical correlations and closure models used in the EM (e.g., **[[ ]]**). The IETs allow validation of the EM for prediction of systems interactions and global phenomena (e.g., **[[ ]]**). The purpose of the analytical or fundamental validations is to illustrate fundamental calculational capability of the EM (e.g., conduction heat transfer). TR section 4.2 describes the analytical validations (verification), SETs, and IETs selected for the validation of the KP-SAM EM.

Table 3-1 of the TR presents a summary of the thermal fluids PIRT and describes the treatment of high and medium ranked phenomena in the KP-SAM EM. Some of the PIRT phenomena are modeled using first principal models (e.g., **[[ ]]**). The validation of KP-SAM for modeling such phenomena is performed using analytical simulations or numerical verifications and is described in TR section 4.2.1. Some phenomena in the PIRT are either conservatively neglected or modeled using a conservative bounding approach in the KP-SAM EM; therefore, the staff finds that no specific validations are needed for these types of phenomena. Examples of these phenomena include **[[**

**]]**.

TR section 4.2.2 describes the SETs planned for the validation of key empirical closing relations used in the KP-SAM model. These closing relations are summarized in SE section 4.1.2 and include **[[**

**]]**. TR section 4.2.2.1 describes the SET planned for the validation of **[[**

**]]** TR section 4.2.2.2 describes the planned SET for **[[**

**]]**.

TR section 4.2.3 describes the only IET planned for the KP-FHR test reactor. This test is planned to **[[**

**]]**. The TR states that the top-down and bottom-up scaling analysis will be performed in accordance with TR KP-TR-006-NP-A, “Scaling Methodology for the Kairos Power Testing Program,” (ML21013A430), to ensure the applicability of the IET data to the KP-FHR test reactor.

The staff finds that the TR provides an adequate description of the KP-SAM validation database consistent with EMDAP step 5. Furthermore, the scaling methodology, previously reviewed and approved by the staff in KP-TR-006-NP-A satisfies EMDAP step 6. However, EMDAP steps 7 through 9 are not addressed in the TR for the planned SETs and IET data. Limitation 3 in TR section 6.2 clarifies that the validation and code assessment results will be provided for the phenomena described in TR section 4.2. However, as indicated by EMDAP steps 7 through 9, the application of scaling methodology to evaluate the scalability of SETs and the distortions in

IET data is essential. Any limitations identified by the scalability and distortion analysis must be addressed, consistent with the applicability evaluation under EMDAP Element 4. Therefore, the staff is imposing **Limitation and Condition 4 (e)** that ensures an application referencing this TR provide for staff review scalability and distortion analysis for the SET and IET data and justifications for any limitations identified by this analysis through the applicability evaluation under EMDAP Element 4.

As discussed in SE section 3.3, **[[**

**]]**.

TR section 4.3.5 states that the DHRS in KP-SAM is modeled using the heat flux boundary conditions that are tuned to match the DHRS performance curve. Furthermore, the TR states that the DHRS performance curves are set to provide best-estimate, minimum, or maximum heat removal to bound the DHRS heat transfer rates and will be verified through testing. The TR does not provide any further information on the planned DHRS testing and the derivation of the bounding DHRS performance curves. As described in SE section 3.1, DHRS is a critical safety system that plays a key role in mitigation of many postulated events in the KP-FHR test reactor. Therefore, the staff is imposing **Limitation and Condition 4 (f)** that ensures an application referencing this TR include for staff review: (1) the DHRS test data characterizing DHRS performance and phenomena under steady-state and transient conditions used to confirm the DHRS performance curves and the applicability evaluation that describes the scaling and distortion analysis of the DHRS tests; and (2) how the DHRS performance curves bound the identified distortions.

4.4 KP-SAM Documentation, Quality Assurance and Configuration Control

The code description and supporting documentation for the safety analysis methodology described in the TR are consistent with KP-SAM code version **[[ ]]**, which is based on the SAM code developed by ANL. The SAM code was evaluated as appropriate for use as the basis for KP-SAM version **[[ ]]** through a commercial grade dedication process in accordance with the Kairos Power software quality assurance program. The KP-SAM code is maintained and its activities managed (i.e., configuration control) under the Kairos Power software quality assurance program. TR section 4.2 describes the software verification process for KP-SAM that includes verification using fast regression tests and numerical verification using analytical tests for simple models such as the fluid models, heat conduction, numerical methods, component models (e.g., pebble bed core channel, reactor power, tank, and heat structure components), and reactor core physics (e.g., decay heat and point kinetics models). The TR provided the following documentation:

- EM requirements documented in section 3 of the TR including the PIRTs
- EM documented in this TR and in other interfacing TRs including:
  - KP-TR-010-P-A
  - KP-TR-024-NP
- Code description manuals provided for SAM and KP-SAM:
  - SAM theory manual, ANL/NSE-17/4
  - KP-SAM theory manual, KP-RPT-000231
- Code user manuals and guidelines provided for SAM and KP-SAM:
  - SAM user's guide, ANL/NSE-19/18 (Reference 9)
  - KP-SAM users guide, KP-RPT-000226

- Scaling report, KP-TR-006-NP-A
- Assessment reports include numerical verifications against the analytical solutions described in TR section 4.2.1 and planned validation of KP-SAM against SET and IET data as described in TR sections 4.2.2 and 4.2.3.

The staff finds that the TR provides adequate information on the EM documentation, quality assurance, and configuration control because it is consistent with the types of information indicated by the guidance for implementing EMDAP step 10.

## 5. Event-Specific Methods

Section 5 of the TR describes the biases applied and sensitivity studies to be conducted for each event category. The event-specific biases and sensitivities account for uncertainties and are used to identify the limiting events for each event category consistent with guidance in NUREG-1537, part 1, chapter 13. The event-specific methods consider analytical limits, core design inputs, reactor physics parameters, coolant properties, treatment of non-safety and auxiliary SSCs, control systems, and operator actions. TR section 5 also describes the event-specific source-term analysis methods for the salt spill and PHSS malfunction event categories.

### 5.1 Event-Specific Biases and Sensitivities for KP-SAM Model

The biases for the following parameters are applied to the KP-SAM base model for analyzing the postulated event categories with an intact primary side (i.e., increase or decrease in heat removal, loss of forced circulation, and reactivity-initiated event) and the salt spill postulated event group:

- Reactor initial power
- Reactivity coefficients (Doppler, moderator, coolant, reflector)
- Reactor kinetics parameters (neutron mean generation time, effective neutron fractions, delayed neutron precursor decay constants)
- Power distribution
- Shutdown margin and shutdown element insertion time
- DHRS capacity
- Decay heat
- Heat rejection blower performance
- RPS actuation delays (instrument response time and actuation delays)
- Reactor coolant thermophysical properties and material properties

Additional biases considered for the salt spill event category include:

- System pressure (biased high to maximize break flow rate)
- Anti-siphon activation level (biased low to delay the onset of natural circulation cooling)
- Inventory management system recirculation flow and Flibe volume (biased high to delay the actuation of the RPS level trip)

The sensitivity calculations are proposed for KP-SAM model calculations to identify the limiting event in each event category. These calculations also include biases discussed earlier. The parameters considered for the sensitivity calculations include:

- Reactor initial power
- Reactor coolant average temperature
- Material properties
- Heat rejection radiator (HRR) outlet temperature
- Plant control systems (reactivity control and primary salt pump control)
- Bypass flow fraction
- Operation of PSP and HRR blower

In addition, for the reactivity-initiated event group, sensitivities on the magnitude of reactivity insertion are performed to simulate the range on control element withdrawals. The limiting event is defined as the scenario(s) that results in the least amount of margin to the acceptance criteria for the FOMs. The staff finds that the biases and sensitivities proposed for the KP-SAM model are appropriate for the identification of limiting events and for the conservative estimation of the safety analysis methodology FOMs including peak TRISO SiC temperature, fuel failure fraction, peak vessel temperature, peak reflector temperature, and energy deposition pulse width because they address key uncertainties in the safety analysis methodology.

TR sections 5.5.1 and 5.5.2 also list assumptions and biases used to analyze the event-specific release pathways using the source term method for the salt spill and PHSS malfunction events, respectively. The evaluation of source term methods proposed for the calculations of dose for these event categories is provided in SE section 5.2 below.

## 5.2 Event-specific Source Term Methods

Certain postulated event scenarios include radionuclide transport mechanisms or pathways that are not included in the MHA or an intact primary system event. These events are the salt spill, the PHSS malfunction, and radioactive release from subsystem or component. TR sections 5.5.3 and 5.6.2 provide source term methods for these additional transport mechanisms for the salt spill events and PHSS malfunction events, respectively. The staff's understanding of the event-specific source term methods was aided by the example calculations A.3 (salt spill) and A.4 (PHSS malfunction) provided in appendix A of the TR. Appendix A is not part of the safety analysis methodology and therefore the staff did not review appendix A and the specific assumptions used therein for acceptability.

### Salt Spill Events

As stated in TR section 5.5, for the salt spill events, the event-specific radionuclide release pathways that are additional to those modeled in the MHA are:

- Single-phase and two-phase mechanical aerosol generation through the break
- Splashing of Flibe onto the catch pan
- Release of radionuclides from the spilled Flibe pool via evaporation
- Tritium and Ar-41 releases from oxidized graphite in the reflector

The salt spill event EM uses the approved methods in the MST methodology to evaluate the single-phase mechanical aerosol generation through the break and the aerosols generated through splashing of Flibe on the catch pan, as well as the gas space transport. TR section 5.5.3 provides methods for two-phase aerosol generation, evaporative release from the spilled Flibe pool, and releases from the oxidized graphite.

For the salt spill postulated event group, the entire spectrum of break sizes and locations must be considered to identify the limiting conditions for each release pathway. The limiting event is modeled as a combination of the most limiting break conditions rather than a single break scenario. The TR describes a method using weighted release fractions for each release pathway. The TR acknowledges that the limiting break size may be different for mechanical aerosol generation than for splashing. The staff finds that this approach is acceptable because it appropriately maximizes the potential radiological releases through aerosol generation and splashing.

As described in TR section 5.5.3, the initial Flibe release through a break is modeled as single-phase flow while the Flibe-cover gas interface is above the siphon break point. After the interface falls below the siphon break point, the release is modeled as two-phase flow, which results in a change in the mechanical aerosol generation. The salt spill EM uses the aerosol release modeling for single-phase jet breakup from the approved MST methodology. The model for mechanical aerosol generation from two-phase flow uses an empirical correlation for a break in the side of a pressurized tank to determine the quality of the two-phased break flow. The Sauter Mean Diameter (SMD) is a representative diameter for the distribution of aerosol particle sizes. The method derives the SMD for two-phase flow based on an empirical correlation from a study for a liquid jet injected into a high-velocity gas stream. Then, the SMD is used in the Rosin-Rammler particle size distribution formula (described in reference 36 of the TR) to calculate the airborne release fraction from the two-phase flow jet breakup. The staff evaluated the information in TR section 5.5.3 and finds that the assumptions are appropriate because they are reasonably based on theoretical correlations to physical phenomena, use widely accepted aerosol modeling concepts such as SMD and the Rosin-Rammler distribution, and the supporting references are relevant to the modeling of aerosol formation from molten salt two-phase break flow.

TR section 5.5.3 states that the same evaporation model used for in-vessel releases in the MHA is used to calculate evaporative releases from the spilled Flibe pool. The pool surface temperature curve is calculated by the KP-SAM pool cooling model. The TR states that use of the in-vessel release model is conservative for releases from the spilled Flibe pool even though spilled Flibe could potentially form more volatile compounds through interaction with oxygen than are formed on the Flibe surface in the intact primary system such as for the MHA. This is compensated for by the model neglecting the formation of a crust on a shallow pool surface which would prevent evaporative releases. For deeper pools, the TR provides a basis that the relatively small size of the liquid-vapor interface compared to the bulk spilled Flibe would reduce the potential for interaction with oxygen and that releases are limited as the Flibe cools. The staff finds that the use of the MHA in-vessel evaporative release model is reasonably supported by the TR discussion and is acceptable for the spilled Flibe because it is based on the approved MST methodology in KP-TR-012 and subject to the limitations and conditions on the Flibe release modeling in the approval of KP-TR-012.

The salt spill event evaluation model uses the same methods as the MHA to determine the tritium and Ar-41 MAR in the graphite reflector material. The model assumes a full and instantaneous release of MAR from the exposed reflector graphite. The staff finds this modeling to be conservative and, therefore, is acceptable.

PHSS Malfunction Events

The PHSS malfunction event group source term is based on a scenario biased to ensure that the maximum amount of MAR is released. The PHSS malfunction event EM described in TR

section 5.6.2 provides source term methods for the following release pathways not modeled in the MHA:

- Releases from exposed TRISO kernels via diffusion
- Releases from dissolved TRISO particles in Flibe via evaporation and off-gassing
- Releases from graphite dust resuspension
- Tritium and Ar-41 releases from oxidized graphite in the reflector and pebble matrix material

For releases from the oxidized pebbles, the MAR in the small fraction of exposed TRISO kernels (i.e., with a failed SiC layer pre-transient) is released through diffusion driven by an assumed gas-space temperature of 650°C, which is 100°C hotter than the nominal temperature. This allows for modeling of diffusion from the pebbles without any potential retention in Flibe. Radionuclide transport modeling from the fuel and gas space is taken from the approved MST methodology and is consistent with the modeling in the MHA. The remaining TRISO particles (i.e., with an intact SiC layer) in the oxidized pebbles are assumed to fall and be dissolved into the Flibe as a conservative assumption. The SiC layer in these particles is assumed to fail instantaneously with release of MAR into the Flibe. The time-temperature curve for the hot well is used in the modeling of evaporative release from the Flibe. The release from the Flibe is modeled as evaporative releases due to prolonged temperature conditions using the approved MST methodology in KP-TR-012. The staff finds the assumptions on radioactive transport and release from the TRISO particles and Flibe to be conservative and based on previously approved methods, and, therefore, are acceptable.

TR section 5.6.1 describes the method to estimate the amount of activated graphite dust accumulated in the pebble transfer line. For the source term modeling of releases from graphite dust resuspension, the MAR in the graphite dust is assumed to puff release to the gas space at the initiation of the transient. The staff finds this modeling to result in a conservative estimation of the dose consequences from release of graphite dust and, therefore, is acceptable.

The PHSS malfunction event evaluation model uses the same methods as the MHA to determine the tritium and Ar-41 MAR in the graphite reflector and pebble matrix material prior to the transient. The model assumes a full and instantaneous release of MAR from the exposed reflector graphite and oxidized pebbles. Furthermore, the model uses the approved methods in the MST methodology in KP-TR-012 to evaluate the gas space transport. The staff finds this modeling to be acceptable because it is consistent with approved methods and the assumptions would result in a conservative estimation of the dose consequences of the release from the exposed graphite and oxidized pebbles.

Release from Subsystem or Component Events

TR section 5.7 describes the source term modeling for the radioactive release from subsystem or component events. To simplify the dose calculations for the FOM comparison, each source of MAR in the subsystem or component is modeled as an activity quantity of a representative “effective” isotope for which the amount of the isotope alone would produce the same TEDE as the combined activities of the isotopes in the MAR. The MAR is assumed to puff release at the initiation of the transient without modeling of holdup and retention in the building, radioactive decay, or delayed releases, which leads to a conservative estimate of TEDE at the EAB. The approved MST methodology in KP-TR-012 is used to determine the MAR in the subsystem or component and modeling of transport in the gas space and building. Therefore, the staff finds

that the source term modeling described for the radioactive release from subsystem or component events is acceptable because it is consistent with approved methods and the assumptions would result in a conservative estimation of the dose consequences.

## LIMITATIONS AND CONDITIONS

Kairos included six limitations on the use of this TR in section 6.2 which the staff includes through **Limitation and Condition 1**. The staff considered these limitations in the technical review presented in this SE. The staff applies the following additional limitations and conditions on the acceptance of this TR:

1. A test reactor OL application referencing this TR must demonstrate that the limitations listed in TR section 6.2 are met, subject to staff review and approval.
2. The safety analysis methodology for modeling a PHSS malfunction event is limited to modeling only events initiated by a break in the transfer line. The safety analysis methodology is not applicable to simulate any other PHSS malfunction event. A test reactor OL application referencing this TR should identify the limiting event for the PHSS malfunction event category and provide an applicable methodology for the limiting event.
3. The KP-BISON methodology for calculation of peak TRISO SiC layer temperature and fuel failure fraction FOMs is not reviewed and approved in this SE. A test reactor OL application referencing this TR must provide for staff review acceptable justification for use of KP-BISON for the calculation of these FOMs.
4. A test reactor OL application referencing this TR must provide for staff review:
    a. acceptable material qualification data that supports the acceptance criteria for the peak vessel temperature and peak structural graphite temperature FOMs;
    b. 2-D/3-D static core analysis and the CFD **[[ ]]** model results used for the calculation of peaking factors and local flow penalty factor in the HPF and the reflector temperature surrogate factor;
    c. justifications that the transient bypass and core flow distribution as modeled results in conservative prediction of the temperature distribution;
    d. specific decay heat model and relevant uncertainties;
    e. scalability and distortion analysis for the SET and IET data and justifications for any limitations identified by this analysis through the applicability evaluation under EMDAP Element 4; and
    f. DHRS test data characterizing DHRS performance and phenomena under steady-state and transient conditions used to confirm the DHRS performance curves and the applicability evaluation that describes the scaling and distortion analysis of the DHRS tests and how the DHRS performance curves bound the identified distortions.

## CONCLUSION

The staff concludes that Kairos's KP-TR-020-P, "Safety Analysis Methodology for the Kairos Power Fluoride Salt-Cooled High-Temperature Test Reactor," Revision 1, provides an acceptable safety analysis methodology for evaluating the MHA and postulated event dose consequences for the KP-FHR test reactor subject to the limitations and conditions discussed above. The evaluation of final compliance or conformance with the identified regulations and PDC will be performed during the review of a licensing application referencing this TR.

## REFERENCES


1. N. Todreas and M. Kazimi, *Nuclear Systems II: Elements of Thermal Hydraulic Design.* Hemisphere Publishing Corporation, 2001.
2. Yu et al., “Evaluation of hot channel factor for sodium-cooled fast reactors with multiphysics toolkit,” Nuclear Engineering and Design, Vol. 365, 2020.
3. K. Wakao, S. Kaguei and T. Funazkri, "Effect of Fluid Dispersion Coefficients on Particle-to-Fluid Heat Transfer Coefficients in Packed Beds," Chemical Engineering Science, Vol. 34, pp. 325-326, 1978.
4. KTA, “Reactor core design of high-temperature gas-cooled reactors, part 3: Loss of pressure through friction in pebble bed cores,” KTA 3102.3, 1981.
5. Yagi, S., Wakao, N., “Heat and Mass Transfer from Wall to Fluid in Packed Beds,” American Institute of Chemical Engineers Journal, vol. 5, pp. 79–85, 1959.
6. S. Globe and D. Dropkin, “Natural-convection heat transfer in liquids confined by two horizontal plates and heated from below,” J. Heat Transfer, vol. 81, pp. 24–28, 1959.
7. R. Hu, L. Zou, G. Hu, D. Nunez, T. Mui, and T. Fei, “SAM Theory Manual,” ANL/NSE-17/4, Revision 1. Argonne National Laboratory, 2021.
8. American National Standards Institute/American Nuclear Society (ANSI/ANS). ANSI/ANS-5.1-2005, “American National Standard Decay Heat Power in Light Water Reactors,” 2005.
9. R. Hu, L. Zou, G. Hu, “SAM User’s Guide,” ANL/NSE-19/18. Argonne National Laboratory, 2019.



Principal Contributor(s): Pravin Sawant
Michelle Hart
Tarek Zaki
Andrew Bielen
Ben Adams
Alex Siwy
Alexander Chereskin


Date: January 5, 2026

# Section B

KP-TR-020-NP-A

Kairos Power LLC
707 W. Tower Ave
Suite A
Alameda, CA 94501

# Safety Analysis Methodology for the Kairos Power Fluoride Salt-Cooled High-Temperature Test Reactor

Topical Report

Revision No. 1
Document Date: July 2025

Non-Proprietary

## COPYRIGHT NOTICE

| Rev | Description of Change | Date |
|---|---|---|
| 0 | Initial Issuance | June 2024 |
| 1 | Incorporates changes based on preliminary questions from the NRC. Due to the number of changes, they are not listed in this table but are marked with change bars in the left margin. | July 2025 |

## EXECUTIVE SUMMARY

Kairos Power is pursuing the design, licensing, and deployment of Fluoride Salt-Cooled, High Temperature Reactors (KP-FHR) including test reactors and commercial power reactors. To enable these objectives, the development of a safety analysis methodology is required. This report has been prepared to document the methodology for evaluation of the KP-FHR test reactor maximum hypothetical accident (MHA) and postulated events. The methodology can be used to demonstrate that postulated event dose consequences are acceptable by comparison with an MHA that results in dose consequences within regulatory limits.

Kairos Power is requesting NRC approval of the safety analysis methodology presented in this report as an appropriate means to determine the acceptability of postulated event dose consequences by comparing them to an MHA that has acceptable dose consequences.

The sample calculations included in this appendix do not represent final design information but are provided to illustrate a generic system response for selected transients. Kairos Power is not asking for NRC review and approval of these sample calculations in a safety evaluation report.

## TABLE OF CONTENTS

**TABLE OF TABLES**

**TABLE OF FIGURES**

## LIST OF ABBREVIATIONS

| Acronym | Definition |
|---|---|
| CFR | Code of Federal Regulations |
| C/HM | carbon to heavy metal atom ratio |
| DHRS | decay heat removal system |
| EAB | exclusion area boundary |
| EM | evaluation model |
| EMDAP | Evaluation Model Development and Assessment Process |
| FSAR | final safety analysis report |
| HPF | hot pebble factor |
| HRR | heat rejection radiator |
| KP-FHR | Kairos Power Fluoride Salt-Cooled, High Temperature Reactor |
| LPZ | low population zone |
| MAR | radioactive material at risk for release |
| MHA | maximum hypothetical accident |
| MHTGR | Modular High Temperature Gas Reactor |
| MOOSE | Multiphysics Object Oriented Simulation Environment |
| MSRE | Molten Salt Reactor Experiment |
| NRC | Nuclear Regulatory Commission |
| PDC | principal design criteria |
| PEM | pebble extraction machine |
| PHSS | pebble handling and storage system |
| PIL | pebble insertion line |
| PIRT | Phenomena Identification and Ranking Table |
| PSP | primary salt pump |
| RCSS | reactivity control and shutdown system |
| RF | release fraction |
| RG | regulatory guide |
| SiC | silicon carbide |
| SSC | structure, system, or component |
| SMD | Sauter mean diameter |
| TEDE | total effective dose equivalent |
| TRISO | tri-structural isotropic |

# 1 INTRODUCTION

Kairos Power is pursuing the design, licensing, and deployment of Fluoride Salt-Cooled, High Temperature Reactors (KP-FHR) including test reactors and commercial power reactors. To enable these objectives, the development of a safety analysis methodology is required. This report has been prepared to document the methodology for evaluation of the KP-FHR test reactor maximum hypothetical accident (MHA) and postulated events to ensure that the dose consequences of the facility remain below acceptable limits.

Kairos Power is requesting NRC approval of the safety analysis methodology presented in this report as an appropriate means to determine the acceptability of postulated event dose consequences by comparing them to an MHA that has acceptable dose consequences. The MHA methodology described in this report is based on the approved KP-FHR mechanistic source term methodology (Reference 1). Deviations from the approved methodology are presented in this report for NRC approval that the modified MHA methodology is also appropriate for evaluating bounding dose consequences for a KP-FHR test reactor.

## 1.1 DESIGN FEATURES

### 1.1.1 Design Background

This report provides transient methods applicable to a KP-FHR test reactor design. Key design features are provided in this section that are considered inherent to the KP-FHR technology. These provide the basis to support the safety review of the safety analysis methodology.

The KP-FHR is a U.S.-developed Generation IV advanced reactor technology. In the last decade, U.S. national laboratories and universities have developed pre-conceptual fluoride salt-cooled high temperature reactor (FHR) designs with different fuel geometries, core configurations, heat transport system configurations, power cycles, and power levels. More recently, University of California at Berkeley developed the Mark 1 pebble-bed FHR, incorporating lessons learned from the previous decade of FHR pre-conceptual designs (Reference 2). Kairos Power has built on the foundation laid by Department of Energy-sponsored university Integrated Research Projects (IRP) to develop the KP-FHR.

Additional design description information for KP-FHR power reactor technology is provided in the “Design Overview of the Kairos Power Fluoride Salt-Cooled, High Temperature Reactor (KP-FHR)” Technical Report (Reference 3).

### 1.1.2 KP-FHR Technology

The KP-FHR is a high temperature reactor with molten fluoride salt coolant operating at near-atmospheric pressure. The fuel in the KP-FHR is based on the Tri-Structural Isotropic (TRISO) high-temperature carbonaceous-matrix coated particle fuel in a pebble fuel element developed for high-temperature gas-cooled reactors. Coatings on the particle fuel provide retention of radionuclides. The reactor coolant is a chemically stable molten fluoride salt mixture, 2·7LiF:BeF2 (Flibe with enrichment of the 7Li isotope) which also provides retention of radionuclides that escape from fuel defects. A primary coolant loop circulates the reactor coolant using pumps and transfers the heat via a heat exchanger. The design includes decay heat removal capability for both normal conditions and accident conditions. Passive decay heat removal, along with natural circulation in the reactor vessel, is used to remove decay heat in response to a postulated event. The KP-FHR does not rely on electrical power to achieve and maintain safe shutdown for postulated events.

The KP-FHR design relies on a functional containment approach similar to the Modular High Temperature Gas-Cooled Reactor (MHTGR) instead of the typical light water reactor (LWR) low-leakage, pressure retaining containment structure. The KP-FHR functional containment safety design objective for the test reactor is to meet 10 CFR 100.11 offsite dose requirements at the plant's exclusion area boundary (EAB) with margin. A functional containment is defined in RG 1.232, “Developing Principal Design Criteria for Non-Light Water Reactors” as a "barrier, or set of barriers taken together, that effectively limit the physical transport and release of radionuclides to the environment across a full range of normal operating conditions, anticipated operational occurrences, and accident conditions.” RG 1.232 includes an example design criterion for the functional containment (MHTGR Criterion 16). As also stated in RG 1.232, the Nuclear Regulatory Commission has reviewed the functional containment concept and found it “generally acceptable,” provided that “appropriate performance requirements and criteria” are developed. The Nuclear Regulatory Commission staff has developed a proposed methodology for establishing functional containment performance criteria for non-LWRs, which is presented in SECY-18-0096, “Functional Containment Performance Criteria for Non-Light-Water-Reactors”. This SECY has been approved by the Commission.

The functional containment approach for the KP-FHR is to control radionuclides primarily at their source within the coated fuel particle under normal operations and accident conditions without requiring active design features or operator actions. The KP-FHR design relies primarily on the multiple barriers within the TRISO fuel particles to ensure that the dose at the site boundary as a consequence of postulated events meets regulatory limits. One key difference between the MHTGR and the KP-FHR design is that the molten salt coolant in the KP-FHR serves as a distinct additional barrier, providing retention of radionuclides that escape the fuel particle and fuel pebble barriers. This additional retention is a key feature of the enhanced safety and reduced source term in the KP-FHR.

### 1.1.3 KP-FHR Structures, Systems, and Components

This section describes KP-FHR structures, systems, and components (SSCs) that are modeled or drive assumptions in the safety analysis.

<u>Reactor System</u>

- Reactor
    - Fuel – TRISO coated particle fuel arranged in the annular region of graphite pebbles. The pebbles have a graphite core and outer layer surrounding the fuel region. The fuel pebbles are buoyant in the reactor coolant.
    - Reactivity Control and Shutdown – The reactor has control elements to control reactivity in the core and shutdown elements that are capable of maintaining shutdown margin without the control element worth.
    - Reactor Vessel Internals:
        - Graphite Reflector Structure – ET-10 graphite blocks form a reflector structure that forms the coolant path through the reactor core and includes penetrations for control and shutdown elements to insert. The reflector structure also includes coolant channels within the blocks.
        - Hold Down Structures – Hold down structures are provided at the top of the core that hold the buoyant graphite reflector blocks in place and keep portions of the graphite submerged at the minimum Flibe level.
        - Natural Circulation Flow Paths – Flow channels are provided through the graphite reflector structure to ensure a complete natural circulation circuit in the core.

  - Reactor Vessel – The reactor vessel is made of 316H stainless steel, and includes a cylindrical outer wall, cylindrical core barrel separating the core from the downcomer, and disc upper head. The vessel has no penetrations or attachments below the minimum coolant level required to cover the active fuel.
- Decay Heat Removal System (DHRS) – The DHRS is an ex-vessel, passive decay heat removal system that, along with natural circulation flow within the core, provides heat removal from fuel in the reactor core for postulated events via thermal radiation and convection without the need for external sources of electrical power or operator intervention. The DHRS is always operating when decay heat levels reach a certain threshold, so there is no emergency actuation necessary.
- Pebble Handling and Storage System (PHSS) – The PHSS provides for the handling and storage of fuel and other pebbles. The entire system is designed to maintain criticality-safe geometries in normal and off-normal conditions.
  - Pebble Extraction Machine – Removes buoyant pebbles that accumulate in the reactor de-fueling chute at the top of the reactor core and routes them towards the off-head conveyance.
  - Off-Head-Conveyance – This line routes pebbles from the pebble extraction machine to storage.
  - Pebble Storage – Buffer storage and spent fuel storage are designed to maintain adequate passive cooling in postulated conditions.
  - Pebble Insertion – Pebbles are inserted into the top of the reactor vessel head, then pushed through an insertion line to a fueling chute at the bottom of the reactor core.

<u>Primary Heat Transport System (PHTS)</u>

- Reactor Coolant – Flibe coolant material composition, quality requirements, impurities, and thermophysical properties are provided in the “Reactor Coolant for the Kairos Power Fluoride Salt-Cooled High Temperature Reactor” topical report, KP-TR-005-P-A (Reference 4).
- Primary Salt Pump – Variable speed, cartridge-style pump located on the reactor vessel head that controls system flow rate and pressure in the PHTS under normal operation.
- Heat Rejection Subsystem – Provides for heat transfer from the reactor coolant to the atmosphere under normal operation and includes a heat rejection blower.
- Primary Loop Piping – The primary loop piping consists of the interconnecting piping from the primary salt pump discharge to the heat rejection subsystem and from the heat rejection subsystem to the reactor vessel inlet.
- Anti-Siphon Features - There are two anti-siphon features in the PHTS – the primary salt pump (PSP) siphon break point for the hot leg side, and the reactor vessel siphon break point for the cold leg side.
  - The PSP anti-siphon break point is located at the bottom of the PSP inlet. If the Flibe level drops below the elevation of the PSP inlet during a salt spill postulated event, the PSP inlet is exposed to the surrounding gas space, which breaks the siphon.
  - The reactor vessel siphon break point is achieved through cutouts on the core barrel above the axial location of the PHTS cold leg. If the Flibe level drops below the elevation of these cutouts during a salt spill postulated event, the cutouts permit the cover gas to move into the upper downcomer region, which breaks the siphon.
- Catch Pans – Catch pans are provided to protect safety-related SSCs from spilled Flibe.

Reactor Coolant Auxiliary Systems

- Chemistry Control System (CCS) – Controls chemistry within the reactor coolant, which includes removal of oxides, particulate, tritium and fission products, and corrosion products.
- Inert Gas System (IGS) – Maintains an inert atmosphere at the free surface within reactor systems and PHTS. Within the reactor system, this inert gas is called the cover gas. The cover gas helps to remove tritium and other gases and contaminants for further downstream treatment as well as to prevent the accumulation of vapors and aerosols. The cover gas is supplied to the upper plenum by a supply tank.
- Tritium Management System – Performs the following functions:
    - Tritium separation from the IGS
    - Tritium separation from the reactor cavity
    - Treatment and storage of tritium
    - Disposition of tritium
    - Tritium monitoring
- Inventory Management System – Contains the tanks and piping required to add and remove coolant from the reactor vessel and primary heat transport system.

Instrumentation and Control System

- Plant Control System – Normal plant controls, including coolant temperature and reactivity controls.
- Reactor Protection System (RPS) – Provides protection for reactor operations by initiating signals to mitigate the consequences of postulated events and to ensure safe shutdown. Upon actuation, the RPS functions include shutdown element insertion and PSP, HRB, and PHSS trips. The RPS receives actuation signals on:
    - Coolant temperature (High Temperature)
    - Coolant level (Low Coolant Level)
    - Neutron flux (High Power and High Power-Rate)
    - PHSS (Low Pressure)

In addition to sensor input, a loss of power results in a reactor trip.

## 1.2 REGULATORY BACKGROUND

Applicants for a test reactor operating license must prepare a final safety analysis report in accordance with the applicable regulations in 10 CFR 50.34(b). The dose requirements for a non-power reactor are specified in 10 CFR 100 (referenced by 10 CFR 50.34(b)(1)). Specifically, 10 CFR 100.11 sets the dose limits for siting a test reactor. Consistent with the guidance in NUREG 1537, an MHA is used to demonstrate that the radiological consequences from a bounding event result in acceptable dose levels.

The safety analysis methodology presented in this report is consistent with the NUREG 1537 objectives for information on postulated events:

- To ensure that enough events have been considered to include any accident with significant radiological consequences. Rejection of a potential event should be justified in the discussions.
- To categorize the initiating events and scenarios by type and likelihood of occurrence so that only the limiting cases in each group must be quantitatively analyzed.
- To develop and apply consistent, specific acceptance criteria for the consequences of each postulated event.

A complete list of potential event initiators (including those prevented by design), along with the categories or groups of postulated events are provided in the final safety analysis report. The methodology in this report develops consistent, specific acceptance criteria to be applied in the final safety analysis for the consequences of postulated events.

The development of the KP-SAM modeling used in this safety analysis methodology is consistent with the applicable portions of the evaluation model development and assessment process (EMDAP) described in RG 1.203, "Transient and Accident Analysis Methods" (Reference 5). Although RG 1.203 has LWR-specific discussions and examples, the major steps of EMDAP are addressed in this report:

- Element 1: Establish Requirements for Evaluation Model Capability – Sections 1 and 3
- Element 2: Develop an Assessment Base – Section 4
- Element 3: Develop the Evaluation Model – Sections 2, 4, and 5
- Element 4: Assess Evaluation Model Adequacy – Section 4

The dose consequences of the MHA demonstrate the acceptability of the design when compared to regulatory dose limits. The dose limits in 10 CFR 100.11 require that an applicant for a test reactor evaluate dose at the exclusion area boundary (EAB) and the low population zone (LPZ) as follows:

- EAB: An individual located on the EAB for two hours immediately following onset of the postulated fission product release would not receive a total radiation dose to the whole body in excess of 25 rem or a total radiation dose in excess of 300 rem to the thyroid from iodine exposure.
- LPZ: An individual located on the outer boundary of the LPZ who is exposed to the radioactive cloud resulting from the postulated fission product release (during the entire period of its passage) would not receive a total radiation dose to the whole body in excess of 25 rem or a total radiation dose in excess of 300 rem to the thyroid from iodine exposure.

The MHA is also used to determine an accident control room dose. KP-FHR principal design criterion (PDC) 19 (Reference 6) provides an accident dose limit for control room personnel as follows:

> "Adequate radiation protection shall be provided to permit access and occupancy of the control room under accident conditions without personnel receiving radiation exposures in excess of 5 rem total effective dose equivalent as defined in § 50.2 for the duration of the accident."

The MHA results in a bounding dose consequence for a KP-FHR with design features described in Section 1.1 that meets the dose limits specified in 10 CFR 100.11 and KP-FHR PDC 19.

# 2 MAXIMUM HYPOTHETICAL ACCIDENT

## 2.1 DESCRIPTION

The MHA is a hypothetical set of conditions that postulate a conservative release of radionuclides that bounds a potential release from other postulated events. Temperature histories are applied to the radioactive material at risk for release (MAR) in the primary system to drive radionuclides out of the system through diffusion and evaporation. The MAR for the MHA includes radionuclides contained in the fuel, circulating in the Flibe, and distributed elsewhere in the primary system (i.e., steel structures and graphite). The methodology for analyzing the transport of radionuclides in the MHA is provided in Section 2.2.

The MHA is a non-physical scenario, where SSC performance is not explicitly modeled. However, the MHA conditions assume that safety functions are achieved by the nature of the transport methods described in Section 2.2. For example, decay heat removal is not explicitly modeled in the MHA (artificial temperature histories are applied to the fuel and Flibe), but the MHA models the transport of radionuclides from the fuel to the Flibe without transient-induced fuel failures. This transport condition implies that the active fuel has remained covered by Flibe, and that the decay heat removal function is achieved.

The MHA analysis is consistent with the fission product release accident analysis required for the 10 CFR 100.11 determination of exclusion area, low population zone, and population center distances. The MHA analysis is also used to demonstrate margin to the control room dose limits provided in KP-FHR PDC 19 (Reference 6). The specific dose metrics calculated for the MHA and the methodology for comparing postulated event dose consequences to the MHA are described in Section 3.3.

## 2.2 METHODOLOGY

The calculation of the dose consequences of the MHA primarily uses the approved source term methods for design basis accidents presented in Reference 1. Some of that methodology is repeated in this section for completeness. However, the following modifications are presented in this section for NRC approval:

- Argon activation and release models (Section 2.2.1.1 and 2.2.3.2)
- Modification to the Flibe radionuclide grouping structure described in Reference 1 (Section 2.2.1 and Table 2-1)
- Justification of the representative element vapor pressure correlations to address the limitation in Reference 1 (Section 2.2.4.4)
- Isotopic screening criteria (Section 2.2.5)

In addition, the methods for evaluating control room dose consequences are provided in Section 2.2.6.

The evaluation of the MHA dose consequences must identify and account for the sources of MAR and the barriers to release. Each barrier is then evaluated for a release fraction to provide dose consequences at the control room and at the exclusion area and low population zone boundaries.

The sources of MAR and associated barriers to release in the MHA:

- TRISO fuel in the reactor core

    - Barriers: TRISO layers, Flibe, and gas space
- Flibe circulating activity
    - Barriers: Flibe and gas space
- Tritium retained by graphite, carbon matrix, and in Flibe
    - Barriers: Graphite or carbon matrix grains (for non-Flibe tritium) and gas space
- Argon-41 generated from argon-40
    - Contained in graphite or carbon matrix pores
        - Barriers: Solubility at pore-Flibe interface and gas space
    - Dissolved in Flibe
        - Barriers: Gas space
    - Entrained as bubbles in Flibe
        - Barriers: Gas space
    - Flowing above Flibe free surface in vessel (cover gas)
        - Barriers: Gas space

There are several non-physical conditions that are hypothesized to ensure a bounding MHA:

- Pre-transient diffusion of radionuclides from the fuel in the reactor core is neglected. This conservatism is achieved in the evaluation by assuming that the full radionuclide inventory of the fuel is available for release at the initiation of the MHA. The circulating activity is still assumed to be at an upper bound level. Therefore, MAR originating in the fuel that contributes to the circulating activity is effectively double counted.
- Hypothetical temperature histories are applied to the transient (Figure 2-1). These temperatures set an upper limit for the figure of merit temperatures in the postulated events.
- The gas space is not credited for confinement of the radionuclides that release from the Flibe free surface. Radionuclide transport in the gas space barrier is modeled using the conservative building transport and off-site dispersion methods described in Reference 1.
- The gas space transport evaluation assumes a conservative leakage rate for the reactor building that releases the entire volume within a 2-hour window. To conservatively neglect radionuclide filtering that could occur in the HVAC system, the dispersion evaluation assumes that no radionuclides are filtered after the building transport is evaluated.
- Initial tritium inventories are conservatively specified to bound operations over the lifetime of the reactor. Lower operating powers result in a lower tritium production rate, and lower capacity factors allow for the graphite grains to experience time periods of tritium desorption instead of sorption.
- A bounding vessel void fraction of 0.1 is assumed to facilitate the release of low volatility species in the vessel via bubble burst.

### 2.2.1 Quantification of MAR Sources

The fuel MAR consists of radionuclides produced by normal operation. A Serpent2 evaluation provides the fuel inventory. The fuel MAR transport is evaluated using the radionuclide groups described in Reference 1.

A bounding value of circulating activity is assumed for Flibe MAR in the analysis. The Flibe MAR transport is evaluated using the groups described in Reference 1, which are regrouped as shown in Table 2-1 to include an intermediate volatility noble metal group, elements for atomic numbers 1-103 for completeness, clarity for grouping of elements dependent on redox, and movement of some elements (e.g., Po, Se) to a more conservative transport group.

The quantity of retained tritium is conservatively bound within graphite and structures over the operating lifetime of the reactor. The tritium speciation is simplified to fully tritium fluoride for an oxidizing salt. A fully molecular tritium case for a reducing salt is calculated, but the fully tritium fluoride case is used because it leads to a higher graphite inventory and higher total release of tritium. The tritium fluoride is assumed to be retained by the graphite, but does not permeate, and its evolution to off-gas is neglected. The steady-state tritium fluoride distribution is determined by mass transfer in Flibe, where the graphite is treated as a perfect absorber. Distribution fractions to each region are calculated by multiplying the tritium mass transfer coefficient by the associated surface area. The in-vessel mass transfer coefficients for tritium transport are calculated by the correlations in Reference 1.

#### 2.2.1.1 Argon-41

Argon-41 included in the MHA is the product of neutron activation of argon in the following locations:

- In the cover gas
- Dissolved in Flibe
- Contained in bubbles that are entrained in Flibe while circulating through regions of the reactor with significant neutron fluence
- Activated in pores in reflector graphite and pebble carbon matrix materials

The argon-41 buildup and release models predict the solubility of argon cover gas that transfers into and out of graphite and pebble carbon matrix pores in the core and reflector regions. Small entrance pore sizes prevent salt intrusion into the bulk material. The volume of the pores is conservatively assumed to be composed only of argon gas. All pores are conservatively assumed to be open (e.g., connected to the exterior surface).

A steady state equilibrium activity distribution of argon-41 contained in these pores and dissolved into the flowing Flibe is determined with a conservative application of the tritium mass transfer correlations in Reference 1 to bound the mass transfer rate of argon, and Henry's Law using the solubility of argon in Flibe.

Argon is assumed to exist in Flibe at the solubility limit. The solubility of argon in Flibe has been studied across a range of temperatures and pressures (Reference 7) to determine Henry's Law constants for gas solubility as shown in Equation 2.1:

$$K_H(T) = \frac{c_a(T,P)}{P} \tag{2.1}$$

where:

- $K_H$ is the Henry's Law gas solubility (mol/(m$^3$ atm)) (see Equation 2.2),
- $P$ is the gas pressure (atm),
- $c_a(T,P)$ is the concentration of argon in Flibe evaluated [[ ]] (mol/m$^3$) and,
- $T$ is the Flibe temperature (K).

A linear regression analysis is performed using this data. A conservative bias of [[ ]] is applied to the results of the regression analysis to bias the results towards higher values of argon solubility. This is conservative because higher argon solubilities result in both a larger argon inventory in the vessel, and higher transport rates of argon from the lower portion of the vessel to the Flibe free-surface. The resulting correlation for gas solubility is provided in Equation 2.2: [[

]]

The rate of change in number density of argon-41 gas in any given location is obtained by subtracting the production (i.e., activation of argon-40) and removal (i.e., radioactive decay, release out of the volume) rates (Equation 2.3):

$$\frac{dN_{Ar_{41}}}{dt} = \dot{P} - \dot{R} \tag{2.3}$$

where:

- $\frac{dN_{Ar_{40}}}{dt}$ is change in argon-41 number density (atoms of argon-41/second),
- $\dot{P}$ is the production rate of argon-41 (atoms of argon-41/second), and
- $\dot{R}$ is the removal rate of argon-41 (atoms of argon-41/second).

Argon-41 is produced from neutron activation of argon-40 as shown in Equation 2.4. The ideal gas law is used to determine the number density of argon-40 in pores or in the cover gas. Henry's Law is used to determine the density of argon-40 dissolved in Flibe.

$$\dot{P} = \phi N_{Ar_{40}} \sigma_{n,\gamma} \tag{2.4}$$

where:

- $\phi$ is the neutron flux (n/cm$^2$s),
- $N_{Ar_{40}}$ is the argon-40 atomic number density calculated using either Henry's Law for dissolved argon (Equation 2.8) or the ideal gas law (Equation 2.10) (atoms of argon-40/cm$^3$), and
- $\sigma_{n,\gamma}$ is the argon-41 production cross section (cm$^2$).

Argon-41 is removed through either neutron decay or argon release as shown in Equation 2.5:

$$\dot{R} = \lambda_{Ar_{41}}^{\text{Decay}} N_{Ar_{41}} + \lambda_{Ar_{41}}^{\text{Removal}} N_{Ar_{41}} \tag{2.5}$$

where:

- $\lambda_{Ar_{41}}^{\text{Decay}}$ is the argon-41 decay constant of (1.05E-4 [s$^{-1}$]) and
- $\lambda_{Ar_{41}}^{\text{Removal}}$ is the barrier removal rate (s$^{-1}$).

Balancing production with decay of argon-41 yields Equation 2.6:

$$N_{Ar_{41}} = \frac{\phi N_{Ar_{40}} \sigma_{n,\gamma}}{\lambda_{Ar_{41}}^{\text{Decay}} + \lambda_{Ar_{41}}^{\text{Removal}}} \tag{2.6}$$

The argon-41 production and decay terms equilibrate as $\lambda_{Ar_{41}}^{\text{Removal}}$ approaches zero. The activity of argon-41 can then be calculated through Equation 2.7:

$$A_{Ar_{41}}^{\text{equilibrium}} = V N_{Ar_{41}} \lambda_{Ar_{41}}^{Decay} \tag{2.7}$$

where:

- $A_{Ar_{41}}^{\text{equilibrium}}$ is the equilibrium activity of argon-41 (in Bq or Ci) and
- $V$ is the analysis volume ($cm^3$).

Direct Activation of Dissolved Argon

Dissolved argon circulating in the Flibe is activated when exposed to a neutron flux. Argon solubility in Flibe increases with increasing temperature, thus solubility of argon in Flibe increases as the Flibe is heated as it flows through the vessel. The formulation for Henry's Law argon solubility coefficients in Flibe are provided in Equation 2.2. Using Henry's Law (Equation 2.1) the concentration of argon gas ($c_a$) in Flibe can be calculated for each region. The inventory of argon dissolved in a given region is calculated using Equation 2.8:

$$I_{\text{argon-40}} = A_v \times c_a(T, P) \times V_{\text{Flibe}} \tag{2.8}$$

where:

- $A_v$ is Avogadro's number, $6.022 \times 10^{23}$ atoms/mol and
- $V_{\text{Flibe}}$ is the volume of Flibe in a region ($cm^3$).

Once the argon-40 number density is calculated for a region, the argon-41 production rate and equilibrium inventory can be calculated using Equations 2.4 and 2.7.

Pore Activation

Argon trapped in graphite pores can be exposed to a neutron flux to produce argon-41. The following methods are used to model the holdup and release of argon-41 from graphite pores.

The porosity ($\alpha$) of graphite and carbon matrix materials is calculated as a ratio based on the difference between the theoretical and measured density of the material. The total volume of argon trapped in the pores is calculated by Equation 2.9:

$$V_{\text{pores}} = \alpha \times V_{\text{graphite or carbon matrix}} \tag{2.9}$$

where:

- $V_{\text{graphite or carbon matrix}}$ is the volume of the graphite or carbon matrix ($cm^3$) and
- $V_{\text{pores}}$ is the volume of pores in that graphite or carbon matrix that may contain argon ($cm^3$).

The number density of argon in pores is calculated by the ideal gas law [[
]] in Equation 2.10:

$$N_{\text{argon-40}} = \frac{P}{A_v RT} \tag{2.10}$$

Combining the pore volume and the argon number density yields the number of argon-40 atoms available for activation (Equation 11):

$$I_{\text{argon-40}} = N_{\text{argon-40}} V_{\text{pores}} \tag{2.11}$$

Once the argon-40 inventory is calculated for a region, the argon-41 production rate and equilibrium inventory can be calculated using Equations 2.4 and 2.7.

Activated argon may either decay in the pores or leave the pores during steady state. In order for activated argon to transport from the pores, the argon must first dissolve into the Flibe and then be physically transported to the cover gas. This process is limited by the following:

1. Diffusion of argon through the open and closed pores to the edge of the reflector or pebble (not modeled, assigned release fraction of unity),
2. The solubility of argon and subsequent transport in the Flibe to the Flibe-cover gas interface (modeled), and
3. Evolution (or degassing) of dissolved gas into the cover gas (not modeled, assigned release fraction of unity).

Due to the argon cover gas, the circulating Flibe is saturated with argon. Thus, the solubility of argon in Flibe provides a resistance to argon transport from the pebbles and reflector to the cover gas. The argon solubility transport resistance model is conceptually structured as a lumped parameter model as follows:

1. Flibe is conservatively assumed to enter the downcomer without any dissolved argon-41 (e.g., the Flibe only contains argon-40).
2. Flibe either flows through the side core reflector (at bypass fraction $X_B$) or through the bottom reflector, core, and top reflector (at fraction 1-$X_B$). Flow between these two regions do not mix at significant quantities during each pass of Flibe through the vessel.
3. The exchange of argon from the Flibe (assumed clean) to the pores (activated) is limited by convective mass transfer resistance for dissolved gases. The solubility limit is evaluated at [[

]]
4. All of the argon-41 is assumed to transition to the cover gas prior to recirculation.

The only removal mechanism for argon-41 trapped in the pores is by being dissolved in the Flibe coolant. Thus, the rate at which argon-41 leaves the pores equals the rate at which argon-41 is dissolved

in the Flibe as shown in Equation 2.12. The left side of this equation describes the increase in argon-41 partial pressure in the flowing Flibe:

$$V_{\text{Pore}} \frac{dC_{\text{Ar-41}}}{dt} = -K_H P_{\text{Ar-41}} A_{Pore} k \tag{2.12}$$

where the pore-specific terms are:

- $V_{\text{Pore}}$ is the volume of pores inside the flow region of interest and
- $C_{\text{Ar-41}}$ is the concentration of argon-41 in pores (calculated),

and the Flibe-specific terms are:

- $K_H$ is the Henry coefficient [[ ]],
- $P_{\text{Ar-41}}$ is the partial pressure of argon-41 in the Flibe,
- $A_{Pore}$ is the mass transfer surface area for argon exchange (i.e., $\alpha A$ where $\alpha$ is the porosity), and
- $k$ is the mass transfer coefficient of argon in flowing Flibe (m/s).

It is more convenient in calculating release fractions to express argon-41 in terms of concentrations, so both sides of Equation 2.12 are divided by the universal gas constant ($R$) and pore temperature ($T_{\text{pore}}$) to convert the argon-41 partial pressure within the pores to a concentration using the ideal gas law, thus producing Equation 2.13 for the core and the bypass flows. Note that this equation uses total volume and surface area because the porosity terms in each side of the equation cancel out.

$$\frac{V_{\text{i}}}{RT_{\text{Pore, i}}} \frac{dC_{\text{Ar41, i}}}{dt} = -K_H\left(T_{\text{F,i}}\right) C_{\text{Ar41, i}} \text{A}_{\text{i}} k_i \tag{2.13}$$

where:

- $V_{\text{i}}$ is the graphite and pebble carbon matrix volume either in the core or bypass region ($m^3$),
- $R$ is the universal gas constant ($Jmol^{-1}K^{-1}$),
- $T_{\text{Pore,i}}$ is the [[ ]] pore temperature in either the core or bypass region,
- $T_{F,i}$ is the [[ ]] Flibe temperature in either the core or bypass region,
- $C_{\text{Ar41,i}}$ is the argon-41 concentration within pores in either the core or bypass region respectively ($mol\ m^{-3}$),
- $k_i$ is the maximum mass transfer coefficient in either the core or bypass region [[ ]] $\dot{V}_i$, which is used to calculate $k_i$, is the Flibe volumetric flow rate ($m^3 s^{-1}$) in either the core or bypass region as calculated in Equation 2.14 or 2.15, respectively:

$$\dot{V}_i = \dot{V}(1 - X_B), \text{ if i = core} \tag{2.14}$$

$$\dot{V}_i = \dot{V} X_B, \text{ if i = bypass} \tag{2.15}$$

where:

- $X_B$ , is the bypass flow fraction between the core pebbles and the reflectors (unitless).

The production of argon-41 stops, consistent with a reactor trip, so the integration of Equation 2.13 leads to:

$$C_{Ar41,i}(t) = C_{o,i}\exp\left(-\lambda_{P,i}^{PF}t\right) \tag{2.16}$$

where:

- $C_{Ar41,i}(t)$ is the argon-41 pore concentration at time $t$ in either the core or bypass region ($mol\ m^{-3}$),
- $C_{o,i}$ is the initial argon-41 concentration either in either the core or bypass region ($mol\ m^{-3}$),
- $\lambda_i^{PF}(T_F, T_P) = \frac{K_H(T_{F,i})\mathrm{A_i}k_i R T_{P,i}}{V_\mathrm{i}}$ is the normalized decay rate ($s^{-1}$) for argon from the pore to the Flibe (i.e., $PF$) at:
  - pore temperature $T_{P,i}$,
  - Flibe temperature $T_{F,i}$,
  - mass transfer coefficient $k_i$,
  - mass transfer area $A_i$, and
  - graphite and pebble carbon matrix volume ($V_i$).

Over the course of a time step starting at $t'$ and ending at $t$, Equation 2.16 is reformulated as Equation 2.17:

$$C_{Ar41,i}(t - t') = C_{Ar41,i}(t')\exp\left(-\lambda_i^{PF}(T_F, T_P)(t - t')\right) \tag{2.17}$$

The release fraction for a given time step $t - t'$ is computed by Equation 2.18:

$$d\mathrm{RF}_i(t - t') = 1 - \frac{C_{Ar41,o,i}(t - t')}{C_{o,i}(t')} \tag{2.18}$$

where:

- $d\mathrm{RF}_i(t - t')$ is the release fraction of argon-41 concentration over the time step $t - t'$ from argon pores as limited by Flibe solubility (unitless).

The release fraction over any time step $\Delta t = t - t'$ is memoryless (i.e., it only depends on the current state parameters and not the prior state or the history of prior states) as shown by combining Equation 2.17 with Equation 2.18. $\lambda_i^{PF}$ should be evaluated at the hottest Flibe and pore temperature over $t$ and $t'$ to ensure a conservative evaluation of $\lambda_i^{PF}$.

$$d\mathrm{RF}_i(\Delta t) = 1 - \exp\left(-\lambda_i^{PF}(T_F, T_P)(\Delta t)\right) \tag{2.19}$$

The cumulative release fraction ($RF$) is then computed by multiplying the individual time step release fractions.

$$\mathrm{RF}_i = 1 - \prod_{j=1}^{J}(1 - d\mathrm{RF}_j(\Delta t_j)) \tag{2.20}$$

The argon-41 solubility release model estimates the steady state release from pores, which conservatively bounds the fraction of pore inventory that escapes to the cover gas. The production rate of argon-41 in pores for each flow channel ($\dot{P}_i$) is calculated using Equation 2.21, accounting for the fact that the flow channels may combine multiple production zones:

$$\dot{P}_i = \sum_{j=1}^{J} V_j \, \phi_j N_{Ar_{40},j}^{\text{pores}} \sigma_{n,\gamma,j} \tag{2.21}$$

where:

- $j$ is an individual analyzed zone within flow channel $i$,
- $J$ is the total number of analyzed zones within flow channel $i$,
- $V_j$ is the volume of graphite pores in zone $j$,
- $N_{Ar_{40},j}^{\text{pores}}$ is the number density argon-41 in graphite pores calculated using the ideal gas law [[ ]] in zone $j$, and
- $\phi_j$ and $\sigma_{n,\gamma,j}$ are the neutron flux and argon-41 production cross sections in zone $j$.

This production rate of argon-41 in graphite pores is balanced by removal terms. The steady state removal (i.e., loss) rate of argon-41 from pores in Flibe, accounting for both radioactive decay and removal due to the solubility model, is shown in Equation 2.22. At steady state, this loss quantity is always balanced by the production ($\dot{P}_i$) of new argon-41 through pore activation, thus keeping the initial concentration of pore inventory constant $C_{o,i}$.

$$\frac{dC_{o,i}}{dt}^{\text{Loss}} = -C_{o,i}\left(\lambda^{\text{decay}} + \lambda_i^{PF}\right) \tag{2.22}$$

where:

- $\lambda^{\text{decay}}$ is the argon-41 decay constant, 1.05E-4 ($s^{-1}$), and
- $\lambda_i^{PF}$ is the calculated steady state normalized removal rate from pores to Flibe ($s^{-1}$).

This equation can be converted to a normalized argon-41 release rate ($\dot{R}_i^{\text{loss}}$) that can apply to any argon-41 quantity (e.g., activity, number of moles, concentration) by dividing each side by the initial concentration, $C_{o,i}$.

$$\dot{R}_i^{\text{loss}} = \lambda^{\text{decay}} + \lambda_i^{PF} \tag{2.23}$$

The loss of argon-41 atoms from pores to Flibe is the source of dissolved argon-41 atoms in the Flibe. Holdup of activated argon in the Flibe is not modeled and thus the Flibe is conservatively assumed to have a release fraction of 1.0.

Entrained Bubble Activation

Argon bubbles may be entrained by the primary salt pump and subsequent flow through the primary heat transport system and into the core and reflector region. Argon that enters the active core region becomes activated by the neutron flux, generating argon-41. For a given region, the argon gas volume is simply the product of the Flibe volume in that region multiplied by the void fraction as shown in Equation 2.24:

$$V_{\text{bubbles}}^{\text{argon-40}} = V_{\text{Flibe}} \times f_{\text{Voids}}^{\text{argon}} \tag{2.24}$$

where:

- $V_{\text{bubbles}}^{\text{argon-40}}$ is the volume of bubbles entrained in the Flibe and
- $V_{\text{Flibe}}$ is the volume of Flibe in a region.

The number density of argon is calculated using the ideal gas law in Equation 2.10 [[ ]]. Multiplying the number density of argon by the volume results in the total number of argon-40 atoms ($N_{\text{argon-40}}$) available for activation.

$$I_{\text{argon-40}} = N_{\text{argon-40}} V_{\text{bubbles}}^{\text{argon}} \tag{2.25}$$

Once the argon-40 inventory is calculated for a region, the argon-41 production rate and equilibrium inventory can be calculated using Equations 2.4 and 2.7.

Flowing Cover Gas Activation

The number density of argon-40 in the cover gas is determined using Equation 2.10 for a specified cover gas pressure and temperature. The equilibrium activity of argon-41 is then determined by Equation 2.7 for a specified cover gas volume.

### 2.2.2 Radionuclide Transport in Fuel

The grouped fuel MAR diffuses through the TRISO layers, driven by the hypothetical temperature history in Figure 2-1. As discussed in Reference 1, the transport of mobile fission products through the TRISO fuel particle is modeled by Fick's laws of diffusion.

No further generation of radionuclides occurs after the reactor trip. Additionally, no radioactive decay is modeled in the mass diffusion equations. The short-time approximation of the Booth solution is used to determine the fractional release of fission product from the kernel for conditions where $\tau \leq 0.155$ (no power, no further generation of nuclides) (Reference 8):

$$RF(t = T) = 6\sqrt{\frac{\tau}{\pi}} - 3\tau \tag{2.26}$$

where:

- $RF(T)$ = release fraction of fission product up to time *t=T*
- $\tau$ = reduced diffusion coefficient = $\frac{DT}{a^2}$ (unit-less)

  where:

  - $a$ = radius of equivalent sphere (m)
  - $D$ = diffusivity coefficient of the representative radionuclide ($m^2/s$) (consistent with the values from Reference 1)
  - $t$ = time (s)

For conditions where $\tau \geq 0.155$ and radioactive decay are ignored, the long-time approximation for release fraction for the kernel is modeled as (Reference 9):

$$RF(t = T) = 1 - \frac{6}{\pi^2} e^{-\pi^2 \tau} \tag{2.27}$$

The short time approximation for fractional release of a coating layer is (Reference 10):

$$RF(T) \approx \frac{24\gamma(1+\gamma)}{\sqrt{\pi}} e^{-\frac{1}{4\tau}} \tau^{1.5} [1 - 6\tau(1+\gamma) + 12\tau^2(5 + 6\gamma + 6\gamma^2)] \tag{2.28}$$

where:

- $RF(T)$ = release fraction of fission product up to time $t = T$
- $\gamma$ = ratio of layer thickness $d$ to the inner radius $r_i$ of the layer = $\frac{d}{r_i}$ (unit-less)
- $\tau$ = reduced diffusion coefficient = $\frac{DT}{d^2}$ (unit-less)

  where:

  - $D$ = diffusivity of the diffusing species in the diffusing medium ($m^2/s$) (consistent with the values from Reference 1)
  - $t$ = time (s)
  - $d$ = thickness of the coating layer (m)

This short time approximation is applied to conditions where $\tau \leq 0.2$. When $\tau > 0.2$, the following long time approximation equation is used to calculate the fractional release for a coating layer (Reference 10):

$$RF(t) \cong 1 - \left(1 + \frac{\gamma}{2}\right) e^{-3\gamma\tau} \tag{2.29}$$

Radionuclide diffusion through TRISO layers is employed for fuel release with no depletion of the radionuclide inventory due to operation time (Equation 2.30). In this bounding model, radionuclides are

assumed to continuously challenge each barrier independent of the actual quantity of radionuclides challenging a barrier at any given time. For example, radionuclides that reach the outer pyrolytic carbon (OPyC) layer at day five of the simulation would instantly be released from the OPyC layer with a fraction equivalent to radionuclides that have been diffusing through the barrier since the initiation of the transient. The release fraction (RF) of compromised layers is conservatively set to 1.0.

$$RF_{fuel}^{i}(t=T) = \prod_{j=kernel}^{OPyC} RF_{j}^{i}(t=T) \tag{2.30}$$

### 2.2.3 Transport of MAR from Flibe to the Gas Space

The two release mechanisms for MAR in the circulating Flibe are bubble burst from entrained cover gas in the vessel coolant and evaporation driven by the MHA temperature curve. Bubble burst occurs before transient diffusion can occur from the fuel into the Flibe, but evaporation mobilizes both circulating activity and MAR that has diffused from the fuel into the Flibe.

#### 2.2.3.1 Bubble Burst

For a two-phase flow, the void fraction of the flow is designated by $\alpha$. The volumetric flow rate of gas $Q_{g,2p}$ is related to the two-phase mass flow rate of Flibe $W_{f,2p}$ by the following expression:

$$Q_{g,2p} = \frac{W_{f,2p}}{\rho_f}\frac{\alpha}{1-\alpha} \tag{2.31}$$

where $\rho_f$ is the density of the fluid. The aerosol generation rate $W_{a,2p}$ is obtained through the volumetric ratio $E_a$(the ratio of the volume of particles generated by a single bubble bursting to the volume of the bubble) as the following:

$$W_{a,2p} = \rho_f E_a Q_{g,2p} = W_{f,2p} E_a \frac{\alpha}{1-\alpha} \tag{2.32}$$

The bounding value of $E_a$ = 2.1 x $10^{-6}$ is chosen for the Flibe-argon system, consistent with Reference 1.

For conservatism, no deposition is assumed during the aerosol generation process. The total mass of aerosol is given by Equation 2.33:

$$m_{a,2p} = \int_0^t W_{a,2p}\,dt = m_{f,2p} E_a \frac{\alpha}{1-\alpha} \tag{2.33}$$

where $m_{f,2p}$ is the mass of two-phase Flibe. Thus, the aerosol release fraction from bubble burst is calculated using:

$$ARF_{2p} = E_a \frac{\alpha}{1-\alpha} \tag{2.34}$$

#### 2.2.3.2 Evaporative Release

The release rates for gases and high volatility noble metals in the circulating activity are conservatively bounded by instantaneous (or “puff”) releases at the beginning of the transient.

Other radionuclides are released from the Flibe at a rate determined by the general evaporation law, as described in Reference 1. Liquid side mass transfer resistance is conservatively neglected.

The natural convection mass transfer relationship between Flibe and cover gas is defined as follows:

$$h_m = 0.15 \times \left(\frac{g\beta D_{AB}^2}{\nu}\right)^{\frac{1}{3}} \times \Delta T^{\frac{1}{3}} \tag{2.35}$$

The radionuclide grouping structure for transport analysis in Flibe has been modified from Reference 1. The elements are grouped as shown in Table 2-1. The grouping in Reference 1 was overly conservative for intermediate volatility noble metals. Therefore, an intermediate volatility noble metal group is added that still provides a conservative treatment of this subset of elements that were previously released at bounding rates with the high volatility noble metal group. Consistent with Reference 1, the noble metal grouping (low, intermediate, or high) is determined by comparing the equilibrium vapor pressure of each element in its stable condensed state.

Elements that fall into multiple groups depending on the Flibe redox potential are placed in the most conservative grouping. In a departure from Reference 1, vapor pressure is used to determine the most conservative group. The grouping is selected by analyzing the vapor pressure of the representative species in the phase separated category (i.e., Noble Metals) compared to the product of the activity ($a$) of the element in question, in solution with Flibe, and the vapor pressure of CsF. The categorization that yields the highest vapor pressure is selected. For example, in the case of Fe, the vapor pressure of Pd is compared to the vapor pressure of CsF multiplied by the concentration ($x$) of Fe in Flibe. This simplification (that is, using $x$ in place of $a$) is justified since an activity coefficient ($\gamma$) of unity is conservative and $a = \gamma \cdot x$.

The radionuclides evaporated from the Flibe free-surface are separated into the following release inventories corresponding to the MHA time temperature curve:

1. “Puff” release of dissolved noble gases and bubble burst Flibe aerosols at the beginning of the transient
2. One linear release for evaporation of radionuclides over the first 10 min temperature interval corresponding to pre-scrammed fuel temperature
3. One linear release for evaporation of radionuclides over the next 110 min temperature interval
4. One linear release for evaporation of radionuclides over the next 70-hour release interval
5. One linear release per day for the next seven days for the reactor cool down period
6. One final linear release over the remaining 20 days.

#### 2.2.3.3 Confirmation of Solubility and Dilute Solution

Confirmation of Dilute Solution

Interactions for species in solution are concentration dependent. It is standard to use a Redlich-Kister (Reference 11) polynomial or similar formalism that well represents the physics for a wide variety of systems. The leading and most impactful term of the expression is the product of constituent concentrations. For solute-solute interactions, it is bounding to use two-body interactions. Therefore, the figure of merit for the dilute solution regime is the product of binary solute mole fractions. When two species have very low concentrations (i.e., are very dilute), the product of mole fractions renders the interaction term negligible. Newton et al. (Reference 12) show solute-solute interactions for

impurities in LiC-KCl eutectic are not measurable until the product of both solutes is greater than 0.00004 mole fraction. This is equivalent to two solutes at a concentration of 6,325 ppm by mole. The molten salt used in Reference 12 is an appropriate surrogate for Flibe because solute-solute interactions are independent of the solvent, fluoride and chloride salts are chemically similar, and there is expected to be a large margin between any individual impurity and the 6,325 ppm limit.

Native impurities, notably Na, Mg, and Ca, are a fundamental constituent of Flibe. All current measurements and legacy data include native impurities. These solutes are an indivisible part of the Flibe. Their effect is already accounted for. Therefore, these are not to be considered when assessing the dilute solution limit applicability.

Salt soluble fluoride (SSF) inventories are evaluated to ensure that elemental mole fractions for non-native impurities are less than 6,325 ppm and thus dilute and.

Confirmation of Solubility

The limit for the solubility of trivalent fluorides in Flibe is conservatively low and bounding for all other salt soluble fluorides (SSFs). Therefore, the concentration of the SSFs is shown to be below the solubility limit by comparing the total concentration of SSFs to the solubility limit for the least soluble trivalent fluoride (i.e., $PuF_3$).

An exponential regression was performed on the solubility data for $PuF_3$ from Reference 40. The resulting solubility limit of $PuF_3$ ($S^0_{PuF_3}$) is given by Equation 2.36 (in units of mole %).

$$S_{SSF} = S^0_{PuF_3} = 1033.57e^{\frac{-6800.811}{T/K}} \quad (2.36)$$

where $S_{SSF}$ is the solubility of the elements grouped as SSFs and $T$ is the absolute temperature in Kelvin.

The sum of the concentration of all SSFs (except for native impurities and O) is compared to the solubility limit of $PuF_3$ for a given temperature to confirm that the concentration of salt soluble fluorides is below the solubility limit.

#### 2.2.3.4 Justification of Representative Species Vapor Pressures

A limitation of Reference 1 is to provide justification of thermodynamic data and associated vapor pressure correlations of representative species. Justification for the Flibe thermophysical properties, including vapor pressure, is outside the scope of this report. This section describes the thermodynamic basis for determining vapor pressure correlations for the remaining representative species (CsF, Pd, In, and Cd), and provides the resulting correlations used in the MHA.

Vapor pressure correlations for representative species are developed using existing data that meet the following criteria:

1. Data are from a quality-assured source or information accepted as established fact.
2. Data demonstrate acceptable agreement with existing experimental measurements of accepted, peer-reviewed quality.
3. Data are accompanied by uncertainties or allow for uncertainty quantification.
4. Data can be justifiably applied to the KP-FHR operating conditions.

Primary data are taken from the MELCOR code reference manuals (References **Error! Reference source not found.** and 14), the CRC Handbook of Physics (Reference 15), and the NIST-JANAF Thermochemical Tables (Reference 16), which are compared to peer-reviewed corroborating data to demonstrate reasonable agreement with direct experimental vapor pressure measurements.

Equilibrium partial pressures (i.e., vapor pressures) are calculated using differences in Gibbs energies, combined with the ideal gas assumption. This method is illustrated for cesium fluoride (CsF) but is applicable to the other pure matter vapor correlations (i.e., Pd, In, and Cd).

The evaporative reaction for CsF liquid into CsF gas is given by Equation 2.37:

$$CsF^{liquid} = CsF^{gas} \tag{2.37}$$

At equilibrium, the chemical potential ($\mu$) is given by Equation 2.38:

$$\mu_{CsF}^{liquid} = \mu_{CsF}^{gas} \tag{2.38}$$

The ideal gas law defines the chemical potential ($\mu$) of a gas as the Gibbs energy of species *i* ($G_i$) modified by pressure effects and/or entropy of mixing, as shown in Equation 2.39:

$$\mu_i^{gas} = G_i^{gas} + RT \ln p_i \tag{2.39}$$

where $R$ is the ideal gas constant, $T$ is temperature and $p_i$ is the partial pressure of species $i$.

The chemical potential ($\mu$) of pure, condensed CsF liquid is simply the Gibbs energy of the liquid ($G_{CsF}^{liquid}$). The partial pressure is calculated from the difference in Gibbs energy according to Equations 2.40 and 2.41:

$$\ln p_{CsF} = \frac{G_{CsF}^{liquid} - G_{CsF}^{gas}}{RT} \tag{2.40}$$

$$p_{CsF} = e^{\frac{G_{CsF}^{liquid} - G_{CsF}^{gas}}{RT}} \tag{2.41}$$

A logarithmic expression is used to describe the relationship between vapor pressure and temperature, consistent with the approach used in the CRC handbook (Reference 15). The general form is given by Equation 2.42:

$$p_i/Pa = 10^{5.006 + A_i + B_i T^{-1} + C_i log T + D_i T^{-3}} \tag{2.42}$$

where $A_i$, $B_i$, $C_i$, and $D_i$ are distinct coefficients for each species $i$.

The Gibbs energy (*G*) of a species is a continuous function of temperature. The Gibbs energy is defined as:

$$G = H - TS \tag{2.43}$$

The enthalpy (*H*) and the entropy (*S*) are related to the heat capacity ($c_i$) as follows:

$$H(T) = H° + \int_{298.15K}^{T} c_p dT \tag{2.44}$$

$$S(T) = S° + \int_{298.15K}^{T} \frac{c_p}{T} dT \tag{2.45}$$

The Dulong Petit law and the Neumann-Kopp rule show the $c_p$ of crystalline solids are not strongly dependent on $T$. For liquids, $c_p$ is nearly constant with $T$, except at reduced temperatures. The reduced temperature ($T_r$) is defined as $T/T_c$, where $T_c$ is the critical temperature (i.e., the temperature above which a gas cannot be liquified by pressurization) (Reference 17). Values of $T_c$ > 0.7 correspond to very high temperatures outside of the ranges for scenarios relevant to KP-FHR technology. Adopting a constant $c_p$ for liquids is the standard approach (References 18-20). Therefore, for $T_r$ < 0.7, extrapolating the vapor pressures of pure species from high temperatures to lower ones, even through phase transitions, is justified and defensible because $G$ is a continuous function of T and the $G$ for the condensed phase can be estimated with a high degree of accuracy.

The activity coefficients of all representative radionuclide species are conservatively bounded by a value of 1.0. The partial pressure for representative elements is the mole fraction weighted pure material vapor pressure (i.e., $P_x = \chi_x K_x$). The following pure matter vapor pressure correlations are valid for an expected transient operational range of 500°C to 816°C.

Cesium fluoride (CsF)

Cesium fluoride (CsF) represents the SSF grouping. The vapor pressure of CsF is determined using Equation 2.40 in 10 K increments from 298-1600 K using the Gibbs energies for liquid and vapor CsF given in the NIST-JANAF Thermochemical tables (Reference 16). The temperature range was selected to bound the operation and design basis range of the KP-FHR, as well as the measurements reported in the literature. The resulting correlation for CsF vapor pressure is shown in Equation 2.45. The $\chi_{CsF}$ is calculated during the transient. A factor of [[ ]] is multiplied to this vapor pressure to account for the uncertainties in the enthalpy of formation and entropy terms as reported in Reference 16.

$$P_{CsF} = \chi_{CsF} \times K_{CsF} = [[\quad ]](\text{Pa}) \tag{2.46}$$

Palladium (Pd)

Palladium (Pd) is the representative species for the low volatility noble metals. The melting point of Pd is well outside the design basis temperature range for the KP-FHR. Therefore, Pd is always a solid with no phase transitions. The relationship between vapor pressure and temperature is taken directly from the CRC handbook (Reference 15), as shown in Equation 2.47. The $\chi_{Pd}$ is set to unity because it is assumed to be phase-separated material. A factor of 1.05 is multiplied to this vapor pressure to account for uncertainty, as reported in Reference 15.

$$\mathrm{P_{Pd}} = \mathrm{K_{Pd}} = 1.05 \times 10^{5.006+9.502-\frac{1.9813\mathrm{E}+4}{\mathrm{T}}-0.9258\times\log\mathrm{T}}(\text{Pa}) \tag{2.47}$$

Indium (In)

Indium (In) is the representative species for the intermediate volatility noble metals. The relationship between vapor pressure and temperature is taken directly from the CRC handbook (Reference 15), as shown in Equation 2.48. The $\chi_{In}$ is set to unity because it is assumed to be phase-separated material. A factor of 1.05 is multiplied to this vapor pressure to account for uncertainty, as reported in Reference 15.

$$\mathrm{P_{In}} = \mathrm{K_{In}} = 1.05 \times 10^{5.006+5.374-\frac{1.2276\mathrm{E}+4}{\mathrm{T}}}(\text{Pa}) \tag{2.48}$$

Cadmium (Cd)

Cadmium (Cd) is the representative species for the high volatility noble metals. The relationship between vapor pressure and temperature is taken directly from the CRC handbook (Reference 15), as shown in Equation 2.49. The $\chi_{Cd}$ is set to unity because it is assumed to be phase-separated material. Cadmium has a low pure matter boiling point and is assumed to be a gas at temperatures greater than 367°C.

$$P_{Cd} = K_{Cd} = 1.01 \times 10^5 \text{(Pa)} \tag{2.49}$$

Flibe

Although justification is outside the scope of this report, the vapor pressure for Flibe is shown in Equation 2.50 for completeness. A factor of [[ ]] is multiplied to this vapor pressure to account for uncertainty, and the mole fraction of Flibe is set to unity because all contaminates are dilute.

$$P_{Flibe} = K_{Flibe} = [[\quad]] \times 133 \times 10^{\left(9.47 - \frac{11028}{T}\right)} \text{(Pa)} \tag{2.50}$$

### 2.2.4 Transport from Structural Materials

#### 2.2.4.1 Tritium Release

Once the transient begins, the concentration of tritium in the Flibe is reduced to zero and thus the concentration gradient reverses, moving tritium out of grains and back into the Flibe. Tritium release fractions are calculated using a numerical solution to diffusion equations. The tritium transport through graphite pores is assumed to be instantaneous, and all graphite grains are exposed to the same tritium uptake conditions. Strong tritium trapping sites are neglected to bound release fractions. The tritium is released into the gas space in the following batches, which roughly correspond to the $\chi/Q$ dispersion bins:

1. "Puff" release of all tritium in both the Flibe and pebble carbon matrix, due to the high diffusivities at the prescribed pebble carbon matrix temperatures, at the beginning of the transient.
2. A bounding diffusion model estimates the fraction of tritium that transports out of reflector graphite grains during the following intervals:
    a. 0 to 10 min
    b. 10 min to 2 hours
    c. 2 hours to 8 hours
    d. 8 hours to 14 hours
    e. 14 hours to 24 hours
3. The remaining tritium in the system transports out of the system by a puff release 24 hours into the transient.

#### 2.2.4.2 Argon-41 Release

Upon the initiation of the transient, production of argon-41 stops per Reference 1 and activated argon contained in pores during steady state continues to be transferred to the Flibe which is conservatively modeled as flowing at steady state flow rates to enhance mass transfer. Activated argon which exists in the cover gas or the Flibe is immediately passed into the gas space. The argon-41 is released into the gas

space in the following intervals, which are generally specified to reduce numerical errors due to the short half-life of argon-41:

1. "Puff" release of all argon-41 dissolved in the Flibe, entrained in bubbles, and contained in the cover gas. This is due to high evaporative releases at the prescribed Flibe-cover gas interfacial temperatures at the beginning of the transient.
2. A conservative, solubility-limited pore release model (Section 2.2.1.1) estimates the release fractions from reflector and fuel graphite pores to Flibe during the following intervals to determine activity released:
    a. 0 to 10 min
    b. 10 min to 2 hours
    c. 2 hours to 4 hours
    d. 4 hours to 6 hours
    e. 6 hours to 12 hours
3. The remaining argon-41 in the system transports out of the system by a puff release 12 hours into the transient, although this inventory is expected to be negligible due to the short half-life of argon-41.

### 2.2.5 Release Pathway and Isotopic Screening Criteria

The absolute and relative screening approaches described in Reference 1 require an assessment of doses prior to conducting the screening evaluation. This section presents an isotopic screening methodology to assess doses, which eliminates the need for a detailed RADTRAD simulation. If all isotopes are screened from a given pathway per the screening methodology, the pathway is also considered screened, as there is reasonable assurance that a more mechanistic dose assessment would result in a dose pathway less than the screening criteria of 0.001 rem 30-day TEDE dose at the EAB. The cumulative dose from screened pathways is then reported in the pathway screening evaluation, consistent with Reference 1. The process for conducting isotopic screening is as follows:

1. Sum up all releases of an isotope ($i$) from each release pathway ($k$) into the gas space (i.e., the enclosure) into a single cumulative released activity ($A_i^k$). Some release pathways are fast (effectively puff releasing isotopes into the gas space) while other pathways may release radionuclides over hours or days (e.g., evaporation from Flibe, diffusion from fuel or graphite) that may be divided over multiple intervals.
2. Calculate the undecayed TEDE dose of each isotopic activity using the first two-hour $\chi/Q$ at the EAB and breathing rate while ignoring the impacts of transient radionuclide decay and building holdup (see Equation 2.51).
3. Screen any isotope that does not produce a pathway TEDE dose at the EAB of over 0.001 rem (i.e., the absolute DBA pathway screening criteria from Reference 1).

$$D_i^k = A_i^k \times \frac{\chi}{Q}_{\text{0-2hr}} \times \left(C_i^{\text{cloudshine}} + B_{\text{0-2hr}} \times C_i^{\text{committed}}\right) \tag{2.51}$$

Equation 2.51 produces conservative estimates of isotopic TEDE doses at the EAB compared to the expected RADTRAD result because it ignores two-hour building holdup and associated radioactive decay,

and it ignores delayed releases of radionuclides (i.e., all radionuclides are released at the beginning of the transient).

This isotopic screening process is also used within unscreened pathways to identify significant dose contributors and reduce the number of isotopes for RADTRAD analysis.

### 2.2.6 Gas Space

The gas space transport evaluation is divided into two models: building transport and atmospheric dispersion. The methodology for design basis accidents in Reference 1 is used to evaluate the gas space transport.

The atmospheric dispersion characteristics in the MHA analysis are based on site-specific meteorology values. The distances to the EAB, LPZ, and control room will be specified in a license application. As described in Reference 1, the building and reactor vessel head space are not credited as confinement barriers and are modeled with artificially increased leakage rates. Henry's Correlation and conservative building leakage rates are used to conservatively model aerosol deposition for Flibe aerosols, consistent with Reference 1. The methods in Reference 1 are used to calculate conservative near field atmospheric dispersion, which results in conservative dose consequence values at the EAB and LPZ.

The methods for evaluating control room $\chi/Q$ values are consistent with the guidance in Regulatory Guide 1.194, "Atmospheric Relative Concentrations for Control Room Radiological Habitability Assessments at Nuclear Power Plants" (Reference 21), with the following exceptions:

1. All releases are conservatively set to be non-buoyant, ground-level plumes.
2. The height of the receptor is set as a ground-level receptor.
3. The distance between the control room and the release point is conservatively set to be the minimum distance between the enclosure building outer wall and the control room outer wall.
4. Building releases are assumed to be sustained long enough (greater than one minute) for Gaussian plume modeling to be applicable, consistent with the two-hour building holdup assumption in Reference 1.

The breathing rates and occupancy factors are consistent with those specified in Regulatory Guide 1.183, "Alternative Radiological Source Terms for Evaluating Design Basis Accidents at Nuclear Power Reactors" (Reference 33). Control room doses are conservatively assessed as if the control room operators are standing in an open field. This approach is conservative as it does not take credit for shielding from the control room walls or filtering of the release particulates through the HVAC system. This assessment is accomplished by modeling the control room doses with a RADTRAD "doseLocation" that is not contained within a RADTRAD "compartment."

**Table 2-1: Radionuclide Groups for Transport Analysis in Flibe**

| Common Name Chemical Group | Elements | Representative Species | Applied Release Fraction |
|---|---|---|---|
| Flibe | Li, Be, F | $Li_2BeF_4$ | Vapor properties of Flibe |
| Salt-Soluble Fluorides | Ac, Al, Am, As, At, Ba, Bi, Bk, Br, Ca, Cd†, Ce, Cf, Cl, Cm, Co†, Cr†, Cs, Dy, Er, Eu, Es, Fe†, Fm, Fr, Ga†, Ge†, Gd, Hf, Ho, I, In†, K, La, Lr, Lu, Md, Mg, Mo, Na, Nb†, Nd, Ni†, No, Np, O, P, Pa†, Pb†, Pm, Po, Pr, Pu, Ra, Rb, S, Sb, Sc, Se, Sm, Sn†, Sr, Tb, Te, Th, Ti, Tm, U, Y, Yb, Zn, Zr | CsF | Vapor properties of CsF dissolved in molten Flibe |
| Gases (Partially contained in Flibe) | Ar, H, He, Hg, Kr, N, Ne, Rn, Xe | Kr | Vapor properties of the pure substance once saturated in the Flibe |
| Low Volatility Noble Metals (Phase separated and not retained by Flibe) | B, C, Co†, Cr†, Fe†, Ir, Nb†, Ni†, Os, Pa†, Pd, Pt, Re, Rh, Ru, Si, Ta, Tc, V, W | Pd | Vapor properties of Pd |
| Intermediate Volatility Noble Metals[1] (Phase separated and not retained by Flibe) | Ag, Au, Cu, Ge†, In†, Mn, Sn† | In | Vapor properties of In |
| High Volatility Noble Metals (Phase separated and not retained by Flibe) | Cd†, Ga†, Pb†, Tl | Cd | Vapor properties of Cd |

†Elements dependent upon redox that can exist as either an SSF or in one of the noble metal groupings.

**Figure 2-1: Hypothetical Temperatures Prescribed for Maximum Hypothetical Accident**

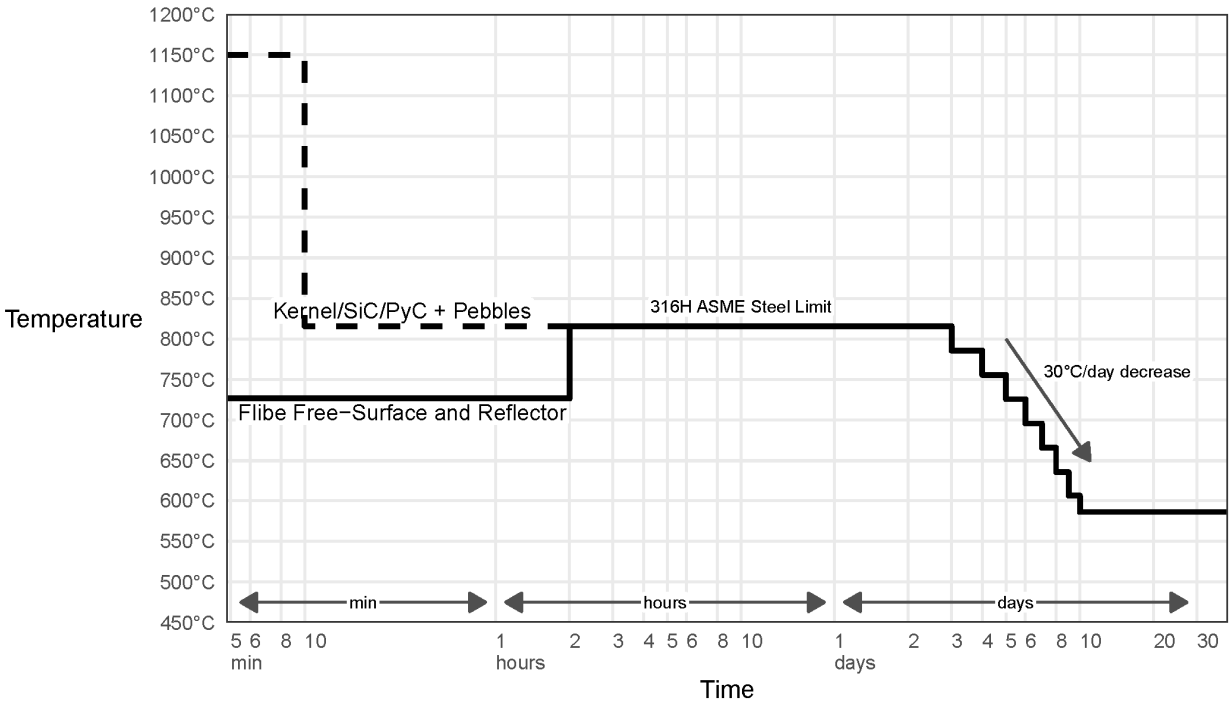

# 3 REQUIREMENTS FOR SAFETY ANALYSIS METHODOLOGY

## 3.1 PURPOSE AND TRANSIENT CLASS

The safety analysis methodology presented in this report can be used to analyze transients for a KP-FHR test reactor facility (consistent with the design description in Section 1.1) to ensure that the resulting dose consequences remain below the 10 CFR 100.11 dose limits described in Section 1.2.

Consistent with NUREG 1537, the MHA described in Section 2 bounds the consequences of other events that are postulated for the test reactor facility. These events are not binned by frequency of occurrence and belong to one transient class called “postulated events.” The postulated events are grouped into categories according to similar characteristics.

The safety analysis methodology in this report is applicable to the following postulated event categories:

- Increase in heat removal
- Decrease in heat removal
- Loss of forced circulation
- Reactivity-initiated event
- Salt spills
- Pebble handling and storage system malfunction
- Radioactive release from a subsystem or component

## 3.2 POSTULATED EVENT DESCRIPTIONS

This section provides a description of each postulated event category that the methods in this report are applicable to. Postulated event groups that are not listed in this section will require additional methods to ensure that events in those groups result in acceptable dose consequences. As described in Limitation 1 (see Section 6.2), the methodology for other postulated event groups will be included in a future licensing submittal.

### 3.2.1 Increase in Heat Removal

Increase in heat removal event scenarios are associated with malfunctions that result in an increase in heat removal from the primary heat transport system (PHTS). Increase in heat removal scenarios can be initiated by a heat rejection blower overspeed that results in excessive cooling of the primary salt in the PHTS, or a primary salt pump overspeed that can lead to enhanced heat transfer. Heat rejection blower overspeed events result in the largest increase in heat removal because the associated increase in airflow causes the following:

- Reduces the heat transfer resistance between the heat rejection radiator tube and the air, and
- Increases the net energy carried away by the heat rejection subsystem.

The resultant overcooling causes relatively cool salt to return to the reactor, which increases the reactivity in the reactor and causes reactor power to increase. This increase in reactor power continues until it is either arrested by inherent feedback (e.g., Doppler feedback from an increase in fuel temperature) or the RPS is actuated on either a high power or high power rate setpoint. In cases where the event is arrested by inherent reactor feedback, the reactor power stabilizes at a higher power but remains below a level that requires RPS actuation to protect against safety limits. The methodology in

this report addresses the short-term power increase associated with the increase in heat removal and does not include the analysis of Flibe freezing conditions or the limiting conditions that are most challenging to freezing, as described in Limitation 2 (see Section 6.2). Cases where the reactor is tripped and the system cools down to levels that indicate the onset of Flibe freezing conditions will be addressed in a future licensing submittal.

### 3.2.2 Decrease in Heat Removal

Decrease in heat removal event scenarios include malfunctions in the heat rejection subsystem that result in a decrease in heat removal from the PHTS. Decrease in heat removal scenarios can be initiated by a loss of electrical power or a heat rejection radiator blower trip which leads to loss of the normal heat sink, or a control malfunction that reduces the heat rejection radiator blower speed and associated airflow. The heat rejection radiator blower trip without a loss of electrical power has the largest decrease in heat removal because the reactor continues to produce energy, which increases the energy in the reactor system and the normal heat sink is not available to remove heat. Following the heat rejection radiator blower trip, temperatures in the reactor and PHTS increase as the power generation exceeds the heat removal via the heat rejection radiator. The reactor power decreases as the reactor heats up (due to inherent negative temperature feedback), but eventually the coolant reaches a high temperature setpoint, which actuates the RPS. The resulting insertion of the shutdown elements and primary salt pump trip associated with the reactor protection actuation arrests the fission reaction and transitions the reactor to natural circulation. Initially, the decay heat exceeds the heat removal through the decay heat removal system (DHRS), which results in a continued heat up of the reactor system. This slow heat up continues until the heat removal via the DHRS exceeds decay heat generation and the reactor system transitions to a monotonic cooldown. The methodology in this report does not include the analysis of Flibe freezing conditions, as described in Limitation 2. Therefore, cases where the reactor is tripped and the system cools down to levels that indicate the onset of Flibe freezing conditions will be addressed in a future licensing submittal.

### 3.2.3 Loss of Forced Circulation

Loss of forced circulation event scenarios are associated with malfunctions that result in a decrease in coolant flow in the reactor system. Loss of forced circulation scenarios can be initiated by a primary salt pump malfunction (e.g., spurious trip, motor failure, shaft seizure), loss of electrical power, plant control system malfunction, or a PHTS flow blockage. The locked rotor (i.e., shaft seizure) event results in the most rapid reduction in PHTS flow. The dedicated (always available) natural circulation path allows for a quick transition to natural circulation, which reduces the sensitivity of the system response to the rate of PHTS flow reduction. The reduction in coolant flow causes temperatures in the reactor to initially increase. The reactor power decreases as the reactor heats up due to inherent negative temperature feedback. For relatively small reductions in flow, reactor power reaches an equilibrium lower power without actuating the RPS. For large reductions in flow, the reactor eventually reaches a high temperature setpoint which actuates the RPS. The resulting insertion of the shutdown elements arrests the fission reaction. Initially, the decay heat exceeds the heat removal through the DHRS, which results in a continued heat up of the reactor system. This slow heat up continues until the heat removal via the DHRS exceeds decay heat generation and the reactor system transitions to a monotonic cooldown. The methodology in this report does not include the analysis of Flibe freezing conditions, as described in Limitation 2 (see Section 6.2). Therefore, cases where the reactor is tripped and the system cools down to levels that indicate the onset of Flibe freezing conditions will be addressed in a future licensing submittal.

### 3.2.4 Reactivity-Initiated Event

Reactivity-initiated event scenarios are associated with malfunctions that initiate an insertion of reactivity (positive or negative) into the reactor. Reactivity-initiated event scenarios can be initiated by malfunctions causing a control element withdrawal, a control or shutdown element insertion or drop, erroneous addition of fuel or moderator pebbles into the core, venting of gas bubbles in the salt coolant, change in pebble bed packing fraction, and changes in reactivity due to shifting of reflector blocks. Very large, rapid reactivity insertions, similar to rod ejection in light water reactors, are not considered because such events are precluded in the test reactor design. Reactivity effects associated with changing Flibe temperature are considered in Increase in Heat Removal events (Section 3.2.1) and Decrease in Heat Removal events (Section 3.2.2). Malfunctions resulting in control element withdrawal have the potential to insert the largest amount of reactivity over a range of operating conditions. The increase in reactivity is arrested by the RPS which is actuated on either a high power or high power rate. A reactivity insertion initiated from high power can result in a power increase (Note: rate of power increase is dependent on the rate and amount of the reactivity insertion). The power increase is arrested by the RPS sufficiently early, such that significant increases in fuel and structural temperatures are precluded. Accordingly, inherent feedback due to Doppler and other feedback mechanisms is limited during these relatively rapid events. A reactivity insertion initiated from low power has the potential to experience a higher power rate due to starting from a power level well below the overpower trip. For reactivity insertions of sufficient small magnitude such that RPS actuation does not occur, the reactor reaches a new equilibrium power where the inherent feedback mechanisms account for the reactivity perturbation. For reactivity insertions that result in a RPS actuation, the resulting insertion of the shutdown elements arrests the fission reaction. Initially, the decay heat exceeds the heat removal through the DHRS, which results in a continued heat up of the reactor system. This slow heat up continues until the heat removal via the DHRS exceeds decay heat generation and the reactor system transitions to a monotonic cooldown. The methodology in this report does not include the analysis of Flibe freezing conditions, as described in Limitation 2. Therefore, cases where the reactor is tripped and the system cools down to levels that indicate the onset of Flibe freezing conditions will be addressed in a future licensing submittal.

### 3.2.5 Salt Spills

Salt spill event scenarios are associated with leaks in Flibe-carrying lines that connect to the reactor vessel and results in a reduction of salt coolant inventory in the PHTS. Leaks that occur in the HRR are outside the scope of this methodology. Salt spill events can be initiated by spurious draining and smaller leaks in the PHTS, a leak from other Flibe-containing systems and components (e.g., inventory management system), leaks that vary in size up to a hypothetical double-ended guillotine break in the PHTS piping, and leaks in Flibe-containing structures connected to the reactor vessel. The hypothetical double-ended guillotine break in the PHTS piping during normal operation results in the largest amount of Flibe to spill from the PHTS. The break in the PHTS piping also causes a loss of the normal heat sink leading to a heat up of the system. The salt spill event is detected by the RPS through the low level or high coolant temperature actuation signals. Reactor protection system actuation results in the insertion of the shutdown elements, which arrests the fission reaction. The RPS actuation also trips the primary salt pump, which along with the anti-siphon features of the reactor vessel system limit the amount of spilled Flibe. Initially, the decay heat exceeds the heat removal through the DHRS, which results in a continued heat up of the reactor system. This slow heat up continues until the heat removal via the DHRS exceeds decay heat generation and the reactor system transitions to a monotonic cooldown. The methodology in this report does not include the analysis of Flibe freezing conditions in the vessel, as described in Limitation 2 (see Section 6.2). Therefore, cases where the reactor is tripped and the system

cools down to levels that indicate the onset of Flibe freezing conditions will be addressed in a future licensing submittal.

In the reactor, air that enters the reactor system from the break reacts with Flibe to form volatile products and oxidizes unsubmerged structural graphite and pebble carbon matrix of unsubmerged pebbles. The methodology in this report does not address the potential for generation of flammable gas due to graphite oxidation in the reactor vessel following an air ingress scenario, as described in Limitation 4 (see Section 6.2). Therefore, cases where air ingress could potentially result in the generation of flammable gas will be addressed in a future licensing submittal.

A fraction of the radionuclides that are normally circulating in the Flibe are released into the facility air when aerosols are generated from the salt that exits the pipe. Spilled Flibe forms a pool, and radionuclide release continues until the pool solidifies.

### 3.2.6 Pebble Handling and Storage Malfunction

Pebble handling and storage malfunction event scenarios are associated with postulated faults of the pebble handling and storage system (PHSS), which transports pebbles into and out of the reactor vessel during normal operations and provides for pebble inspection and storage. These faults include a break of a PHSS transfer line, loss of PHSS cooling, and mechanical damage (i.e., grinding) to a pebble in the PHSS. Mechanical damage and loss of PHSS cooling scenarios that could result in a release of MAR are assumed to be mitigated or precluded by design. Therefore, the methodology in this report covers PHSS malfunctions that occur due to a postulated transfer line break. A transfer line break results in air ingress to the PHSS, which causes the pebble matrix material of high temperature pebbles to oxidize. The transfer line break event is detected by the RPS through the low pressure in the PHSS actuation signal. Reactor protection system actuation results in the insertion of the shutdown elements, which arrests the fission reaction. The RPS actuation also trips the PHSS to stop pebble movement. Initially, the decay heat exceeds the heat removal through the DHRS which results in a continued heat up of the reactor system. This slow heat up continues until the heat removal via the DHRS exceeds decay heat generation and the reactor system transitions to a monotonic cooldown. The methodology in this report does not include the analysis of Flibe freezing conditions in the vessel, as described in Limitation 2. Therefore, cases where the reactor is tripped and the system cools down to levels that indicate the onset of Flibe freezing conditions will be addressed in a future licensing submittal.

Additionally, the methodology in this report does not address the potential for generation of flammable gas due to graphite oxidation in the reactor vessel following an air ingress scenario, as described in Limitation 4 (see Section 6.2). Therefore, cases where air ingress could potentially result in the generation of flammable gas will be addressed in a future licensing submittal.

For pebbles that spill outside of the reactor, the reactivity control function is fulfilled by limiting the number and configuration of pebbles that can spill out of the break, while heat transfer mechanisms within the room fulfill the heat removal function. The structural integrity of the pebbles maintains the confinement function. For pebbles remaining in the PHSS, the reactivity control, heat removal, and confinement functions continue to be fulfilled by the system design for lower temperature pebbles outside of the pebble extraction machine (PEM) and pebble insertion line (PIL) regions. Higher temperature pebbles in these regions are assumed to oxidize, and either release their MAR directly to the gas space or drop MAR into the Flibe, where it is subsequently released.

### 3.2.7 Radioactive Release from Subsystem or Component

A radioactive release from a subsystem or component occurs when the failure of a subsystem or component containing radioactive material that is outside of the functional containment (i.e., Flibe

coolant and TRISO fuel) results in a release of radionuclides. Releases in this event group can involve individual subsystem or component failures, or combined failures of multiple subsystems and/or components that could result from internal or external hazards. The material at risk for release in one or multiple subsystems or components is fully released at the start of the event.

## 3.3 FIGURES OF MERIT

Regulatory Guide 1.203 (Reference 5) defines figures of merit as quantitative standards of acceptance that are used to define acceptable answers for a safety analysis. The principal design criteria provide a general set of requirements for the facility design, but the figures of merit in the safety analysis are generally synonymous with criteria directly associated with the regulations. In the case of a non-power reactor, those regulations are the siting dose criteria described in Section 1.2.

The MHA is used to demonstrate that the siting dose criteria are satisfied. Each postulated event is subsequently shown to be bound by the MHA. The figures of merit are evaluated for the postulated events to (1) confirm that release pathways that are not considered in the dose consequence analysis do not occur and (2) demonstrate that the dose consequences of postulated events are below those of the MHA.

The postulated events that each figure of merit is evaluated for are summarized in Table 3-4.

### 3.3.1 Peak TRISO SiC Temperature

The fuel design includes multiple barriers within the TRISO fuel particles to retain radionuclides during postulated events. Failure of these barriers could increase dose, which would challenge the regulatory dose limits. The peak temperature that a TRISO particle experiences during a postulated event is tracked as a figure of merit to ensure that these failures do not occur in transient conditions. This figure of merit is evaluated using KP-BISON (Reference 22), which takes inputs from KP-SAM as described in Section 4.2.4.

The acceptance criterion for this figure of merit is set at 1600 °C to ensure that the transient failure fraction does not significantly deviate from the steady state particle failure fractions.. This peak TRISO SiC temperature provides assurance that the fuel remains within the qualification envelope described in topical report KP-TR-011-P-A, “Fuel Qualification Methodology for the Kairos Power Fluoride Salt-Cooled High Temperature Reactor (KP-FHR)” (Reference 38).

### 3.3.2 Energy Deposition Pulse Width

Similar to the fuel figure of merit described above, energy deposition has the potential to induce stresses that could lead to fuel failures and challenge regulatory dose limits. Therefore, the energy deposition pulse width is tracked as a figure of merit for reactivity-initiated events to ensure that fuel failures not considered in the MHA do not occur due to energy deposition. The transient response time during KP-SAM reactivity-initiated event simulations (i.e., time from t = 0 to maximum power) is used to confirm that this figure of merit does not exceed the acceptance criterion.

The acceptance criterion for this figure of merit is set to greater than 1 s. The TRISO fuel time constant is sufficiently small such that energy depositions over a longer time period result in a small maximum temperature difference across the TRISO particle, that is independent of the initial energy deposited

(Reference 42). This criterion provides assurance that fuel degradation mechanisms not considered in the MHA are precluded.

### 3.3.3 Fuel Failure Fraction

Manufacturing defects and in-service failures determine the particle configuration fractions of the fuel. The particle configuration fractions and the transient fuel time-temperature history are used to determine the radionuclide releases from the fuel. The fuel failure fraction is a figure of merit that ensures that fuel releases that exceed those assumed for the MHA do not occur in transient conditions. This figure of merit is evaluated by first calculating the peak pebble power and the peak pebble surface temperature through the application of a hot pebble factor methodology using KP-SAM outputs. These conditions are then used for evaluation with KP-BISON in accordance with Reference 22 to determine the transient failure fractions.

The acceptance criterion for this figure of merit is set by the steady state particle configuration fractions used in the dose consequence analysis to ensure that transient failure fractions do not significantly deviate from the steady state particle configuration fractions. This criterion, when evaluated for individual events, provides assurance that fuel performance is consistent with that assumed in the dose consequence analysis.

### 3.3.4 Peak Vessel Temperature

The minimum Flibe level during postulated events must be kept above the active core to maintain a coolable geometry. The reactor vessel maintains the minimum Flibe level above the active core, so the peak vessel temperature is tracked as a figure of merit to ensure that vessel failures do not occur in transient conditions. The transient peak vessel temperature is determined using KP-SAM as described in Section 4.2.4. The surrogate for peak vessel temperature is conservatively set to the coolant temperature at the natural circulation pathway outlet. This surrogate figure of merit is also conservatively used to track the maximum temperature of other metallics outside of the pebble bed core (e.g., core barrel and hold-down structures). The method for evaluating metallics inside of the pebble bed (i.e., shutdown elements) will be provided in a future licensing submittal (see Limitation 6).

The acceptance criterion for this figure of merit is set at 750 °C, which is consistent with the material qualification for the KP-FHR test reactor. This peak vessel temperature, when evaluated in individual events, provides assurance that a coolable geometry is maintained and the assumptions of the MHA are valid.

### 3.3.5 Peak Structural Graphite Temperature

The structural graphite refers to the graphite reflector structures surrounding the reactor core. This graphite must maintain its structural integrity in postulated events for shutdown element insertion and maintaining a natural circulation flow path. Without adequate shutdown reactivity or natural circulation flow, the dose limits could be challenged. The peak structural graphite temperature is tracked as a figure of merit to ensure that graphite failures do not occur in transient conditions. The transient peak reflector temperature is determined using KP-SAM as described in Section 4.2.4.

The acceptance criterion for this figure of merit is set at 950 °C, which is consistent with the material qualification for the KP-FHR test reactor. This peak structural graphite temperature, when evaluated in individual events, provides assurance that a coolable geometry is maintained and the assumptions of the MHA are valid.

### 3.3.6 Dose Figures of Merit

There are multiple dose limits and targets that are applicable to the test reactor. 10 CFR 100.11 defines dose targets for the first two hours at the EAB and the duration of the plume at the LPZ in terms of whole body and thyroid from radioiodine doses. KP-FHR PDC 19 defines dose limits to control room operators in terms of total effective dose equivalent (TEDE) dose for the duration of the accident. Each of these dose limits and targets are explicitly demonstrated to be met by the MHA. Postulated event dose pathways are demonstrated to be bound by the MHA using 30-day TEDE dose at the EAB. This is appropriate because TEDE is an aggregated dose figure of merit that includes the impacts from whole body, thyroid, and other organ doses.

For completeness, the dose consequence analysis for each postulated event group also includes evaluation of the first two hour and duration of the plume whole body and thyroid from radioiodine doses at the EAB and LPZ, respectively.

The acceptance criterion for this figure of merit is the MHA 30-day TEDE dose at the EAB.

#### 3.3.6.1 Primary System Postulated Events

Radiological consequences for primary system releases ($D_{\mathrm{PS\,PE}}^{\mathrm{TEDE}}$ in Equation 3.1) are postulated using a specified set of bounding time-temperature and time-flowrate curves to drive hypothetical radionuclide releases from the intact primary systems using the same release pathways as the MHA. These postulated releases allow the postulated event dose consequences for limiting events to be compared to the MHA. The bounding parameter curves selected for the primary system source term are the following:

- Flibe-cover gas interface time-temperature
- Maximum reflector time-temperature
- Maximum pebble surface time-temperature
- Core mass flowrate-time
- Bypass mass flowrate-time
- Maximum kernel and TRISO layer time-temperature (the kernel temperature is conservatively used for the TRISO layer temperature)

The bounding nature of the specified parameter curves are confirmed using the nominal maximum parameter values from KP-SAM transient simulations without the hot pebble factor and peak reflector and vessel temperature surrogates described in Section 4.2.4. The nominal maximum values are sufficiently conservative to model bulk release of MAR.

The nominal maximum parameter values are significantly higher than the average parameter values during peak transient temperatures for the limiting event(s) when radionuclide transfer rates are the highest. Due to the power to flow mismatch, high system temperatures are generally associated with both high core heat generation rates and high heat removal rates from the decay heat removal system. The axial vessel temperature spread generally shrinks as the vessel cools due to lower core heat generation rates and associated lower heat removal rates from the decay heat removal system. Thus, lower axial temperature spreads are associated with lower temperature states in the vessel where bulk movement of radionuclides is minimized compared to the higher temperature regimes. Therefore, the nominal maximum parameter values provide a sufficiently conservative system response for the dose analysis.

The maximum parameter values from KP-SAM are selected as a function of time for the reflector and pebble components. The Flibe-cover gas interfacial temperature is taken as the Flibe temperature in the

upper plenum (see Section 4.3.7). The maximum pebble surface temperature (without application of the HPF methodology) and the pebble power (without peaking factors) from KP-SAM are input to KP-BISON to determine the maximum kernel temperature.

The specified parameter curves are confirmed to bound the limiting system response from each of the following postulated event groups:

- Increase in heat removal
- Decrease in heat removal
- Loss of forced circulation
- Reactivity-initiated event
- Salt spill

The limiting event(s) for each group are defined as the sequence(s) that are most challenging with respect to the temperature-related figures of merit (i.e., peak TRISO SiC temperature, peak vessel temperature, and peak structural graphite temperature), evaluated using the hot pebble factor and peak reflector and vessel temperature surrogates described in Section 4.2.4.

The acceptance criteria for the 30-day TEDE primary system postulated event dose is the 30-day TEDE MHA dose at the EAB.

$$D_{\mathrm{PS\,PE}}^{\mathrm{TEDE}} < D_{\mathrm{MHA}}^{\mathrm{TEDE}} \tag{3.1}$$

where:

- $D_{\mathrm{PS\,PE}}^{\mathrm{TEDE}}$ is the combined bounding sequence primary system postulated event 30-day TEDE dose at the EAB that combines release from all MHA release pathways
- $D_{\mathrm{MHA}}^{\mathrm{TEDE}}$ is the MHA 30-day TEDE dose at the EAB

#### 3.3.6.2 Non-Intact Postulated Events

For postulated events that impact power and flow in the reactor vessel where the system does not remain intact (i.e., salt spills and PHSS malfunctions), the total 30-day TEDE dose at the EAB for the event includes doses from both the intact portion of the primary system and the non-intact portion of the system. The 30-day TEDE dose at the EAB from the bounding primary system postulated events (Section 3.3.6.1) is used to account for the dose from the intact portion of the primary system. This is added to the 30-day TEDE dose at the EAB from non-MHA release pathways for a given non-intact postulated event to determine the total event dose (Equation 3.2).

The acceptance criteria for the 30-day TEDE non-intact system postulated event dose is the 30-day TEDE MHA dose at the EAB.

$$D_{\mathrm{PS\,PE}}^{\mathrm{TEDE}} + \sum D_{i,\,\mathrm{NI\,PE}}^{TEDE} < D_{\mathrm{MHA}}^{\mathrm{TEDE}} \tag{3.2}$$

where:

- $D_{\mathrm{PS\,PE}}^{\mathrm{TEDE}}$ is the combined bounding sequence primary system postulated event 30-day TEDE dose at the EAB that combines release from all MHA release pathways

- $\sum D_{i,\,\mathrm{NI\ PE}}^{\mathrm{TEDE}}$ is the sum of the 30-day TEDE doses at the EAB for all non-MHA release pathways included in the bounding sequence for the non-intact postulated event
- $D_{\mathrm{MHA}}^{\mathrm{TEDE}}$ is the MHA 30-day TEDE dose at the EAB

#### 3.3.6.3 Release from Subsystem or Component Postulated Event

For postulated events that do not impact the primary system (e.g., release from certain subsystems or components), the additional release pathways from that postulated event are directly compared to the MHA 30-day TEDE dose at the EAB.

$$D_{\mathrm{SC\ PE}}^{\mathrm{TEDE}} < D_{\mathrm{MHA}}^{\mathrm{TEDE}} \tag{3.3}$$

Where:

- $D_{\mathrm{SC\ PE}}^{\mathrm{TEDE}}$ is the release from the bounding sequence from the subsystem or component postulated event 30-day TEDE dose at the EAB
- $D_{\mathrm{MHA}}^{\mathrm{TEDE}}$ is the MHA 30-day TEDE dose at the EAB

## 3.4 SYSTEMS, COMPONENTS, PHASES, GEOMETRIES, FIELDS, AND PROCESSES

Systems/Subsystems/Modules

The systems and hardware relevant to the postulated event categories described in Section 3.1 are described in Section 1.1.3.

Constituents

Relevant systems are composed of TRISO fuel, carbon moderator pebbles, Flibe coolant, SS316H, and ET-10 structural graphite. Additionally, the test reactor uses argon as the cover gas and air as the secondary side coolant in the heat rejection system (HRS). Neutron absorbers (control and shutdown elements) are not explicitly modeled - only the impact of reactivity via point kinetics is captured in the evaluation model. For source term analyses, specific models are used to address tritium, Ar-41, and graphite dust. Radionuclide transport in Flibe is performed by grouping relevant elements into representative groups.

Phases

Phases that need to be modeled for intact events include single-phase Flibe, argon, and air. Salt spill analyses include two-phase Flibe/argon and air.

Geometrical Configurations (phase topology or flow regime)

The fluid flow during intact postulated events is single-phase flow. A significant portion of the fluid flow occurs within a pebble bed that is composed of fuel and moderator pebbles. Reynolds numbers for flow through the pebble bed vary (in terms of order of magnitude), from ~1 under conditions of natural circulation to ~100 under conditions of forced circulation. Reynolds numbers for flow in the downcomer range (in terms of order of magnitude) from ~10 under conditions of natural circulation to ~1,000 under conditions of forced circulation. Flow in the PHTS piping varies from static following a PSP trip (Re = 0) to ~10,000 under conditions of forced circulation. For salt spill events, two-phase modeling is limited to jet break-up and no regime-dependent two-phase flow models are applied.

Fields

Relevant fields that are transported include mass, momentum, and energy of the Flibe salt, and energy conduction within the graphite and steel structures. Additionally, heat removal via the DHRS is dominated by radiative heat transfer. To address fuel performance, the methodology captures the multi-scale heat transfer associated with TRISO fuel (i.e., micro-scale within the TRISO particle, meso-scale within the fuel pebble, and macro-scale within the pebble bed).

Transport Processes

The test reactor design relies on the conduction, convection, and radiation heat transfer processes to transport heat from the reactor fuel to the ultimate heat sink under conditions of natural circulation during postulated events. Specifically, heat that is generated in the TRISO fuel conducts through the fuel pebble and is transferred to the Flibe salt via convection. The Flibe coolant transports this heat to the downcomer where the heat is transferred via convection to the reactor vessel wall. The heat then conducts through the reactor vessel wall and radiates to the DHRS where the heat boils water that is ultimately discharged to the atmosphere.

Dominant transport processes remain constant throughout the transition from forced circulation to long term circulation and long-term cooling. Accordingly, the evaluation models for intact events are not broken up into characteristic periods where different processes and phenomena are dominant (e.g., loss of coolant accidents in light water reactors are generally characterized by distinct phases [blowdown, refill, and reflood] that have different dominant mechanisms to be addressed in each phase).

For source term evaluations, transport of radionuclides occurs via diffusion, convection with moving fluid, evaporation from open pools, and mechanical aerosolization from breaks.

## 3.5 PIRT SUMMARY

The Phenomena Identification and Ranking Table (PIRT) process relies on expert judgment to identify and rank key phenomena for a specific system undergoing a specific time phase of a specific transient. The PIRT process generates a prioritized list of key phenomena that need to be characterized and modeled to predict response to specific transients. It also ranks the knowledge level for each key phenomenon, thus identifying critical gaps in the understanding of specific phenomena.

Kairos Power has performed a series of PIRTs for KP-FHRs. The list of PIRTs relevant to the development of the safety analysis methodology, which leverage different sets of panel experts, include:

- Thermal fluids PIRT
- Reactivity insertion event PIRT
- Radiological source term PIRT (Summary provided in Reference 1)
- Fuel element PIRT (Summary provided in Reference 22)
- Neutronics PIRT (Summary provided in Reference 23)
- High-temperature structural materials PIRT (Summary provided in Reference 24)

The thermal fluids PIRT and the reactivity insertion event PIRT were performed to support the development of evaluation methodologies by identifying and assessing the knowledge level of phenomena relevant to postulated event scenarios. The thermal fluids PIRT addresses thermal fluids phenomena that are relevant to all postulated event groups described in Section 3.2, except for the radioactive release from subsystem or component event group, which does not evaluate a transient in the reactor system.

The reactivity insertion PIRT addresses event scenarios where reactivity is inserted into the reactor (i.e., reactivity-initiated events and increase in heat removal events). The PIRT identifies which phenomena have a controlling impact on the relevant figures of merit and identifies where additional testing is necessary to provide assurance in the evaluation model (EM) capability. Ultimately, the PIRT is a tool that helps inform the safety analysis methodology development and assessment of overall evaluation model adequacy.

Key phenomena relevant to each postulated event group that were identified as having a high or medium importance to safety and the associated treatment in the EM are summarized in Table 3-1 and Table 3-2.

The radiological source term PIRT summarized in Reference 1 was initially performed generically for the KP-FHR technology in 2019. The PIRT was revisited in 2021 specifically considering the preliminary design of a test reactor, and an updated state of knowledge gained through the continued development of the KP-FHR technology. New phenomena identified as having high or medium importance, as well as any phenomena originally identified as having low importance, but which were subsequently found to have a high or medium importance, are summarized in Table 3-3.

Some phenomena identified in the neutronics, fuel element, and high-temperature structural materials PIRTs have impacted the safety analysis methods. Specifically:

- Phenomena identified in the neutronics PIRT impact certain nuclear parameters (e.g., reactivity coefficients, delayed neutron precursor, etc.) that are used as inputs in the event-specific methods. These phenomena are discussed in the topical report KP-TR-024-P, “KP-FHR Core Design and Analysis Methodology” (Reference 23).
- Phenomena identified in the fuel element PIRT impact the fuel performance methods (i.e., KP-BISON) that are used as inputs for source term analyses and to assess the fuel figures of merit. These phenomena are discussed in the topical report KP-TR-010-P-A, “KP-FHR Fuel Performance Methodology” (Reference 22).
- Phenomena identified in the structural materials PIRT impact the acceptance criteria for the structural material (i.e., reactor vessel) figure of merit. These phenomena are discussed in the topical report KP-TR-013-P-A, “Metallic Materials Qualification for the Kairos Power Fluoride Salt-Cooled High-Temperature Reactor” (Reference 24).

**Table 3-1: Thermal Fluids PIRT Summary (High and Medium Importance Phenomena)**

[[

]]

[[

]]

[[

]]

[[

]]

[[

]]

[[

]]

**Table 3-2: Reactivity- PIRT Summary (High and Medium Importance Phenomena)**

[[

]]

[[

]]

**Table 3-3: Source Term PIRT Summary (High and Medium Importance Phenomena)[1]**

[[

]]

[[

]]

[[

]]

[[

]]

[1]Note: This table only presents new phenomena (i.e., not previously summarized in Reference 1) identified as having high or medium importance, as well as any phenomena originally identified as having low importance, but which were subsequently found to have a high or medium importance.

**Table 3-4: Postulated Event Figures of Merit**

| Figure of Merit | Applicable Postulated Events |
|---|---|
| Peak TRISO SiC temperature<br>(Section 3.3.1) | Increase in Heat Removal, Decrease in Heat Removal, Loss of Forced Circulation, Reactivity-Initiated Event, Salt Spill |
| Energy deposition pulse width<br>(Section 3.3.2) | Reactivity-Initiated Event |
| Fuel failure fraction<br>(Section 3.3.3) | Increase in Heat Removal, Decrease in Heat Removal, Loss of Forced Circulation, Reactivity-Initiated Event, Salt Spill |
| Peak vessel temperature<br>(Section 3.3.4) | Increase in Heat Removal, Decrease in Heat Removal, Loss of Forced Circulation, Reactivity-Initiated Event, Salt Spill |
| Peak structural graphite temperature<br>(Section 3.3.5) | Increase in Heat Removal, Decrease in Heat Removal, Loss of Forced Circulation, Reactivity-Initiated Event, Salt Spill |
| 30-day TEDE dose at the EAB<br>(Section 3.3.6) | Increase in Heat Removal, Decrease in Heat Removal, Loss of Forced Circulation, Reactivity-Initiated Event, Salt Spill, Pebble Handling and Storage System Malfunction, Radioactive Release from Subsystem or Component |

# 4 SYSTEMS ANALYSIS

## 4.1 KP-SAM CODE DESCRIPTION

The System Analysis Module code, also known as SAM, was developed by the U.S. Department of Energy and Argonne National Laboratory (References 25 and 26) as a generic system-level safety analysis tool for advanced non-LWRs. The code solves tightly coupled physical phenomena including fission reaction, heat transfer, and fluid dynamics in reactor structures, systems, and components.

Kairos Power has developed and maintained a KP-FHR specific code based on SAM called KP-SAM (References 27 and 28).

SAM is directly built on the Multiphysics Object Oriented Simulation Environment (MOOSE) framework, which handles most of the numerical methods, output processing, and most of the input processing. MOOSE and its base packages, such as LibMesh and PETSc, are open-source software, and thus the major development from SAM to KP-SAM includes a description of the physics and system component behaviors, specific numerical methods such as continuous Finite Element Method stabilizing methods, and the addition of specific functions for the systems code.

KP-SAM, like SAM, uses simplified thermal hydraulic models to represent the major physical components and describe major physical processes such as fluid flow and heat transfer. The main types of components in SAM are listed below.

- Basic geometric components describing individual 1-D/2-D fluid or solid domains
- 0-D components for setting boundary conditions for 1-D fluid domains
- 0-D components for connecting 1-D components
- Assembly components that are constituted by combining different basic geometric components or 0-D connecting components
- Non-geometric components for physics integration, control and trip systems, or special 0-D models such as the point kinetic model

### 4.1.1 Physical Models and Equations

KP-SAM, like SAM has two types of physics models: field equations and closure models. Field equations are solved to determine the transport of the quantities of interest in 0-D, 1-D, or 2-D domains. The single-phase flow field equations in KP-SAM shown in Equation 4.1 include 1-D mass, momentum, and energy conservations along the flow direction.

$$\begin{gathered}\frac{\partial \rho}{\partial t}+\frac{\partial(\rho u)}{\partial s}=0 \\ \rho \frac{\partial u}{\partial t}+\rho u \frac{\partial u}{\partial s}=-\frac{\partial p}{\partial s}+\rho g_s-\frac{f}{D_e} \frac{\rho u|u|}{2} \\ \rho c_p \frac{\partial T}{\partial t}+\rho c_p u \frac{\partial T}{\partial s}=\frac{q_s'' P_h}{A_c} \\ \rho=\rho(p, T)\end{gathered} \tag{4.1}$$

where:

$\rho$ = coolant density

$u$ = velocity

$T$ = coolant temperature

$t$ = time

$s$ = the axial coordinate in flow direction

$p$ = pressure

$g_s = g \bullet \cos\theta$

$\theta$ = angle between the flow direction and gravity vector

$g$ = the gravity constant

$f$ = friction coefficient

$D_e$= equivalent hydraulic diameter

$c_p$ = the specific heat

$q_s''$ = the convection heat flux from solid surface

$P_h$ and $A_c$ = heated perimeter and cross-sectional area of the coolant channel respectively.

The primary variables for the single-phase flow model in KP-SAM are pressure, velocity, and temperature.

Heat structures model the heat conduction inside the solids and permit the modeling of heat transfer at the interfaces between solid and fluid components. Heat structures are represented by 1-D or 2-D heat conduction in Cartesian or cylindrical coordinates. A one-dimensional spherical heat conduction model is also developed for pebble bed simulation. Temperature-dependent thermal conductivities and volumetric heat capacities can be provided in tabular or functional form from user-supplied data, or directly provided by the code and accessed through given material names. The modeling capabilities of heat structures can be used to calculate the heat flux conditions for fluid components, as well as to predict the temperature distributions in solid components such as fuel pins or plates, heat exchanger tubes, and pipe and vessel walls. The thermal conduction inside the solid structures is governed by the heat conduction equation.

KP-SAM includes a TRISO particle average temperature model associated with a pebble bed core channel component model. The fuel pebble of KP-FHR design has a fuel annulus layer between the central low-density core and outer fuel-free shell. The TRISO model in KP-SAM simulates temperatures of the fuel kernel, buffer, and cover (the IPyC, SiC, and OPyC lumped together). It also simulates the average temperature in the fuel annulus, which is modeled by the heat structure model.

Special 0-D models can be taken as 0-D field equations. The 3-D field equations are integrated over the domain and the partial differential equations become ordinary differential equations. The spatial integration process needs special spatial profile assumptions. The special 0-D models in KP-SAM include the volume branch, valve, pump, tank, point kinetic models, thermal radiation, and gap conductance models.

The widely used point kinetics equations model for multiple groups of delayed neutron precursors was implemented in SAM with fully implicit time scheme options available up to 5th order accuracy. The decay heat power can be calculated from the user-provided decay curve. For the predictive decay heat model, the fissile material fission fractions include U-235, U-238, Pu-239, and Pu-241, and are provided by the reactor core design calculation. The fission ratios of fissile materials are provided for various stages of operation (build up). A sensitivity factor can also be applied to the decay heat fraction in order to conservatively account for uncertainties in decay heat.

Closure relations are correlations and equations that help to model the terms in the field equations by providing code capability to model and scale particular processes. Typical closure models include wall friction factor and form loss models for different flow geometries, convective heat transfer correlations for different heat transfer surfaces, and pump performance curves. Fluid and solid properties, including equations of state, are also needed to close the field equations. The fluids to be simulated include Flibe, water, simulant oil, air, and argon gas.

### 4.1.2 Control System Description

The SAM control system is used to perform the evaluation of algebraic and simple ordinary differential equations; the trip system is used to perform the evaluation of logical statements. The fundamental approximation made in the design of the control/trip system is that the execution of the control/trip system is de-coupled from the other parts of the hydraulic systems. The main execution of individual control/trip units is set at the end of each time step.

### 4.1.3 Numerical Methods

SAM uses a continuous finite element methods formulation for the spatial discretization of the 1-D or 2-D field equations. The detailed discretization for both time and space is managed by MOOSE, with the code formulated such that the numerical method orders are controlled through user inputs. For fluid models, a spatial stabilization method is required to suppress checkerboard-type spatial oscillations that manifest when using continuous finite element methods to solve advection dominated problems. The Stream Line-Upwind/Petrov-Galerkin and the Pressure-Stabilizing/Petrov-Galerkin schemes are implemented in SAM to resolve the numerical instability issues (Reference 29).

The physics in SAM is integrated into a single fully coupled nonlinear equation system. The discretized nonlinear equation system is solved using a pre-conditioned Jacobian Free Newton Krylov method. The combination of the Jacobian Free Newton Krylov nonlinear solver and high order numerical methods for both time and space enables the capability to minimize numerical errors.

### 4.1.4 Quality Assurance and Configuration Control

The code description and supporting documentation (References 27 and 28) for the methodology described in this topical report are consistent with KP-SAM version [[ ]] . KP-SAM version [[ ]] is based on the SAM code developed by Argonne National Laboratory (ANL). The SAM code was evaluated as appropriate for use as the basis for KP-SAM version [[ ]] through commercial grade dedication in accordance with the Kairos Power software quality assurance program. The software and computer codes used in the methodology described in this topical report, including the base model described in Section 4.3, are maintained under the Kairos Power software quality assurance program. The activities managed under the program include change management, error reporting, and corrective action.

## 4.2 KP-SAM VERIFICATION AND VALIDATION

The KP-SAM verification process confirms that the software functions as designed and checks the order of convergence for field equations for both time and space. This process includes software verification using fast regression tests, and numerical verification using tests for the fluid models, heat conduction, numerical methods, component models (e.g., pebble bed core channel, reactor power, tank, and heat structure components), and reactor core physics (e.g., decay heat and point kinetics models).

The KP-SAM validation process compares simulation results against experimental data to assess the adequacy of the code to model high-ranked phenomena identified by the PIRT (Section 3.5). Unit test validation covers simple test data and is used to verify the implementation of simple models for fluid and solid properties, and heat transfer and wall friction correlations. Separate effects test (SET) validation covers the important thermal-hydraulic phenomena relevant during accident conditions, as identified by the PIRT. Integrated effects test (IET) validation covers scaled integral tests at the system level or plant level. Reactor tests provide more direct evidence that the systems code can accurately simulate transient responses.

The following sections summarize the numerical verification, SET and IET assessments that will be conducted for validation of KP-SAM, and an overall applicability assessment of KP-SAM for the test reactor. The design and assessment of tests is consistent with the approved scaling methodology topical report (Reference 30). This information is provided for context on how testing will be used to support modeling of specific phenomena identified by the PIRT. However, as described in Limitation 3 (see Section 6.2), validation and code assessment results will be provided in a future licensing submittal.

### 4.2.1 Numerical Verification of KP-SAM Models

The development of KP-SAM includes numerical verification to confirm that the equations are correctly solved by the code. The verification of model solution accuracy is generally performed by comparing KP-SAM solutions with known analytical solutions if available. If not, the Richardson extrapolation method is used, in which small mesh sizes and time steps are used to obtain benchmark solutions as the “correct” results for convergence order calculation of coarse mesh or larger time step cases (Reference 31). Models included in the KP-SAM numerical verification that are relevant to the evaluation model for postulated events include:

- One-dimensional and two-dimensional heat conduction
- Pebble bed core channel component heat transfer
- Reactor Power component for energy deposition
- Volume branch component mass, momentum, and energy transport
- Tank component mass and energy transport
- Decay heat generation
- Point kinetics with reactivity insertion and feedback
- TRISO fuel heat transfer

### 4.2.2 Separate Effects Testing for Validation of High-Importance Ranked Phenomena

This section describes the separate effects tests that will be conducted to validate the modeling of high-importance ranked phenomena in KP-SAM.

#### 4.2.2.1 Downcomer Heat Transfer SET

[[

]] . The [[
]] through separate effects testing, which is scaled in accordance with KP-TR-006 (Reference 30).

[[

]]

Separate effects testing will be performed to validate the [[

]] Resulting test reports will confirm the range of applicability of the heat transfer correlations to ensure applicability to the test reactor.

#### 4.2.2.2 Pebble Bed Pressure Loss SET

[[

]]

Separate effects testing will be performed to [[

]] The test will provide sufficient coverage to address pressure loss ranging from losses associated with flow under conditions of natural circulation and decay heat power levels, to those associated with full power forced flow conditions.
[[

]]

#### 4.2.2.3 Pebble Bed Heat Transfer SET

Separate effects testing will be performed to [[

]]

[[

]] The testing, performed in accordance with KP-TR-006 (Reference 30), and associated assessment are being performed over the ranges provided in Table 4-1 to ensure applicability and scalability to the test reactor.

### 4.2.3 In-Vessel IET

Integral effects testing will be performed to validate [[

]] These integral effects tests will include top-down and bottom-up scaling analyses completed in accordance with KP-TR-006 (Reference 30) to ensure applicability to the Kairos Power test reactor.

### 4.2.4 Limitations of the KP-SAM Modeling

The KP-SAM numerical model, described in Section 4.1, is capable of modeling single-phase one-dimensional flow and two-dimensional heat conduction, but has limited capability to model three-dimensional temperature distributions. Additionally, KP-SAM does not have models to capture gamma and neutron heating of in-vessel heat structures (e.g., reflector and metallics). Instead, it is assumed that all energy deposition from gamma and neutron heating is done in the fuel pebbles, which then transfers this energy to the coolant. The limitations of the KP-SAM modeling are summarized in Table 4-4.

The following methods are applied to further address the limitations of KP-SAM:

- A hot pebble factor is applied to conservatively address the three-dimensional effects of the power distribution on individual pebble temperatures. The hot pebble factor applies this conservative treatment by placing the peak power pebble in the hottest location within the component. Additionally, the hot pebble factor accounts for the uncertainty in the heat transfer closure

correlation used to model heat transfer in the pebble bed. The hot pebble factor is described further in Section 4.2.4.1.

- A peak vessel temperature surrogate, the natural circulation path (NCP) outlet Flibe temperature, is used to address uncertainties due to asymmetric temperature distributions and multi-dimensional flow paths in the reactor vessel. The basis for the method is described further in Section 4.2.4.2.
- A peak reflector temperature surrogate is used to account for non-uniform temperature distributions in the reflector. The peak reflector temperature surrogate is described further in Section 4.2.4.3.

#### 4.2.4.1 Hot Pebble Factor

The hot pebble factor (HPF) methodology is used to process KP-SAM output to provide a bounding pebble surface temperature as input to KP-BISON. The time-dependent pebble surface temperature is used as a boundary condition by KP-BISON for a conservative estimate of the maximum SiC temperature and confirmation of negligible transient fuel failure fractions. The HPF methodology uses the transient KP-SAM inlet temperature, coolant temperature rise, and the maximum pebble film temperature rise, and adds spatial information and uncertainties not available in KP-SAM (e.g., radial/azimuthal peaking factors, and local flow variations). The HPF methodology also addresses the film heat transfer correlation uncertainty. The input to and output from the HPF methodology are shown in Figure 4-3. Core design analysis inputs to the HPF methodology are summarized in Table 5-1.

The factors and uncertainties considered by the HPF methodology are provided in Table 4-5. These factors and uncertainties are combined using a vertical semi-statistical method (Reference 39) to determine multipliers for coolant and film temperature rise (Equation 4.6), which are applied to the KP-SAM transient values. Direct subfactors address KP-SAM model limitations while statistical factors address random uncertainties. The vertical semi-statistical method first calculates the cumulative HPF for each $\Delta T$ section $m$ ($F_m$) by combining subfactors as shown in Equation 4.6. Then, the maximum $\Delta T$ for each $\Delta T$ section $m$ ($\Delta T_{m,\,HPF}$) is independently calculated by multiplying HPF and nominal temperature rise ($F_m \cdot \Delta T_{m,\,nom}$). Finally, the maximum core and pebble surface temperatures are determined using Equations 4.7 and 4.8, respectively. Note that $\Delta T_1$ is the coolant temperature rise and $\Delta T_2$ is the film temperature rise (see Figure 4-4).

$$F_m = F_m^D F_m^S = \left( \prod_{j=1}^{l} f_{j,m}^D \right) \cdot \left( 1 + \sqrt{\sum_{j=1}^{n} \left( f_{j,m}^S - 1 \right)^2} \right) \tag{4.6}$$

$$T_{1(core),HPF} = F_1 \cdot \Delta T_{1,nom} + T_{in} \tag{4.7}$$

$$T_{2(surface),HPF} = F_2 \cdot \Delta T_{2,nom} + F_1 \cdot \Delta T_{1,nom} + T_{in} \tag{4.8}$$

where $F_m$ is the cumulative HPF for each $\Delta T$ section $m$, $F_m^D$ is the direct HPF, $F_m^S$ is the statistical HPF, $f_{j,m}^D$ are the direct subfactors, and $f_{j,m}^S$ are the statistical subfactors by each uncertainty j for each $\Delta T$ section m.

The nominal core temperature rise $\Delta T_{1,\,nom}$ is a direct output by KP-SAM and $\Delta T_{2,\,nom}$ is given by Equation 4.9.

$$\Delta T_{2,nom} = max\left(\frac{\dot{q}}{A \cdot h}\right) \tag{4.9}$$

where $\dot{q}$ is the average pebble power in a KP-SAM axial element, $A$ is the nominal pebble area, and $h$ is given by Equation 4.10.

$$h = \frac{\left(Nu \cdot k_f\right)}{D_P} \tag{4.10}$$

where $k_f$ is the fluid thermal conductivity and $D_P$ is a pebble diameter. $\Delta T_{2,\,nom}$ is calculated for each KP-SAM axial element with the maximum value selected. The Nusselt number (Nu) in Equation 4.10 is calculated using the Wakao correlation, as given by Equation 17.4 in Reference 27.

The subfactors $f_{j,\,m}$ in Equation 4.6 are determined for the parameters in Table 4-5 (except for the [[ ]] ) using a first order numerical approximation shown by Equation 4.11.

$$f_{j,y} = \frac{y\left(x_0, \ldots, x_j + \Delta x_j, \ldots, x_m\right)}{y^0\left(x_0, \ldots, x_j, \ldots, x_m\right)} \tag{4.11}$$

where $f_{j,\,y}$ is the subfactor on target parameter y by $j^{th}$ variable, $y$ and $y^0$ is perturbed and nominal target parameter value, $x$ is each variable value, and $\Delta x_j$ is the perturbed uncertainty of $j^{th}$ variable.

Since KP-SAM has a 1-D core model, the effect on the core temperature rise due to the radial and azimuthal power distribution is not captured, so a direct subfactor is used to determine the multiplier $F_1$. This subfactor includes the upper bound radial and azimuthal peaking factors. For events with global core power changes, such as the increase in heat removal and loss of forced circulation postulated events, the radial peaking factor is not expected to change significantly from the initial, steady-state peaking factor. As such, the maximum of either the All Element Out (AEO) or the control element inserted steady-state radial peaking factor as a function of core power is used. It is acceptable to use only a radial peaking factor for these events as there is no transient induced azimuthal power variation. The radial peaking factor is obtained from 2-D static core design analysis. For events with transient-induced radial and azimuthal power distribution changes (such as a single control element withdrawal), an event-specific radial and azimuthal peaking factor is needed, which is obtained from 3-D static core design analysis.

There are two direct and two statistical subfactors for the pebble film temperature rise. The pebble peaking factor upper bound tolerance is analogous to the radial and azimuthal peaking factor discussed in the coolant rise subfactors. The pebble peaking factor is defined as peak pebble power relative to average pebble power, which includes axial power peaking factor, radial peaking factor, and pebble-to-pebble variance per fuel pass. As discussed for the coolant temperature rise subfactor, the postulated events are grouped by transients with global power distribution changes and those which need event-specific peaking factors. For events with global core power changes, the maximum of either the AEO or the control element inserted pebble peaking factor as a function of core power is used. No azimuthal power variation occurs during these events, therefore using only the pebble peaking factor is acceptable (obtained from 2-D static core design analysis). For events with transient-induced radial and azimuthal power distribution changes, such as a single control element withdrawal, an event-specific pebble peaking factor is needed, which is obtained from 3-D static core design analysis.

The use of peaking factors from static core design calculations are bounding compared to using time dependent (spatial kinetics) calculated values. Using static peaking factors is conservative as spatial kinetics methods solve the flux distribution, including the effects of thermal feedback, at each time step. Because the thermal feedback is updated during each time step, using spatial kinetics (dynamic) results in a flatter flux distribution and hence lower peaking factors compared with static calculated values.

The pebble surface temperature determination includes a second direct subfactor to account for potential flow distribution and mixing heterogeneity. A bounding local flow penalty is also applied. The local flow subfactor is derived using the relationship of film $\Delta T$ given by Equations 4.9, 4.10, and the Wakao correlation, and the generalized form of a subfactor given by Equation 4.11. Thus, the film $\Delta T$ for local flow variations is given by Equation 4.12.

$$f_v = \frac{(v_{norm} + \Delta v)^{-0.6}}{(v_{norm})^{-0.6}} = \left(1 + \frac{\Delta v}{v_{norm}}\right)^{-0.6} \tag{4.12}$$

where $v$ is the fluid velocity.

The flow penalty subfactor will be determined using the [[

]] This subfactor will be determined by selecting a bounding flow penalty factor over a range of core flow rates and resultant Reynolds numbers. [[

]] Known [[ ]] uncertainties will be included, and discretionary conservatism will be applied to account for reliance on calculations conducted for [[ ]]

Two statistical subfactors are considered when determining the HPF pebble surface temperature - the variation in pebble diameter and the [[ ]]. The variation in film $\Delta T$ due to variations in pebble diameter can be determined by Equations 4.9, 4.10, and the Wakao correlation, and the generalized form of a subfactor given by Equation 4.11. The film $\Delta T$ subfactor is given by Equation 4.13.

$$f_{D_P} = \frac{\left(D_{P,norm} + \Delta D_P\right)^{-1.6}}{\left(D_{P,norm}\right)^{-1.6}} = \left(1 + \frac{\Delta D_P}{D_{P,norm}}\right)^{-1.6} \tag{4.13}$$

The allowed variation in pebble diameter is determined based on the pebble diameter specification.

The second statistical factor is the impact of [[ ]] on the film $\Delta T$. This subfactor is determined by [[

]]. The subfactor is determined when a 2-sigma confidence level is obtained.

The pebble film factor $F_2$ is determined using Equation 4.6 and the maximum time dependent pebble surface temperature is determined by Equation 4.8. These HPF pebble surface temperatures are passed to KP-BISON to determine the maximum TRISO SiC temperature and transient fuel failure fractions.

The hot pebble factor methodology addresses/bounds the identified KP-SAM limitations in Table 4-4 through the following:

- Limitation 1: Addressed through the heat transfer correlation uncertainty subfactor.
- Limitation 2 and 4: Addressed through the flow distribution and mixing conservatism subfactor.
- Limitation 3: Addressed through the radial/azimuthal and pebble peaking subfactors.
- Energy deposition in the coolant is maximized due to Limitations 5 and 6. This results in a conservatively high estimation of the pebble surface temperature through the HPF and thus bounds their impact.

Note that KP-SAM Limitations 1-4 apply to coupled phenomena such that each subfactor in the HPF is not solely applicable in treating only single or subset limitations. Instead, the bulleted list above is intended to enumerate which limitations are most directly treated by specific subfactors. The definition of the hot pebble residing at the outlet of the core channel subsumes the impact of unresolved two- and three-dimensional distributions by applying the integral energy addition to the hot pebble in conjunction with the relevant coolant subfactors.

#### 4.2.4.2 Peak Vessel Temperature Surrogate

Since KP-SAM cannot fully resolve hot spots due to radial and azimuthal power and flow variations caused by asymmetric events (such as a single control element withdrawal), the natural circulation path (NCP) outlet Flibe temperature is used as a surrogate for the peak vessel temperature. This is the maximum Flibe temperature within the system. Using the NCP outlet temperature as a surrogate eliminates any in-core temperature asymmetries due to core power distribution or flow because the Flibe in the hot well, which is the source of fluid flow in the NCP, is well-mixed. It also neglects the cooling due to DHRS heat removal on the vessel exterior wall and heat transfer of the fluid in the NCP. Using Flibe temperature as a surrogate also effectively assumes perfect heat transfer to the metallic structures.

Finally, by neglecting all thermal radiation effects that would enhance energy transport to the system boundary and depositing all fission power in the fuel instead of further afield through gamma and neutron heating, the energy uptake in the coolant flowing into the NCP is conservatively maximized.

Due to the above considerations, this approach bounds KP-SAM Limitations 1-6, as defined in Table 4-4.

#### 4.2.4.3 Peak Reflector Temperature Surrogate

As with the peak vessel temperature, the maximum Flibe fluid temperature is used as a surrogate for the peak reflector temperature, but with penalty factors to account for within-core power and flow distributions. To conservatively bound local reflector temperatures, radial power peaking and flow factors are used. As discussed in the HPF methodology, the events are grouped into events with global (uniform) power and flow distributions and those with asymmetric distributions, such as the single control element withdrawal. Both uniform and asymmetric events apply radial peaking and flow reduction penalties, but with differing values. The maximum reflector temperature is calculated using Equation 4.14. This equation effectively aligns the location of radial peak power and local flow reduction along the entire core length, generating a hot Flibe channel that perfectly transfers energy to the reflector.

$$T_{maxg} = T_{inlet} + (T_{max} - T_{inlet}) \left( \frac{RPF_{max}}{1 - FF} \right) \quad (4.14)$$

where $T_{inlet}$ and $T_{max}$ are from KP-SAM.

The $RPF_{max}$ is the maximum uniform steady-state AEO or control element inserted upper bound radial peaking factor as a function of power for events with uniform transient power distribution changes, and $FF$ is the uniform local flow reduction penalty. As described for the hot pebble flow subfactor, a single flow penalty (FF) based on [[ ]] is used for all events, since an asymmetric power distribution does not affect the pebble bed flow distribution.

For asymmetric (i.e., non-uniform) events, the $RPF_{max}$ is the upper bound radial peaking factor from a fully withdrawn control element. Core design inputs to the peak reflector temperature surrogate are summarized in Table 5-1.

Since this approach leverages the peak vessel temperature surrogate and includes additional penalty factors it bounds KP-SAM Limitations 1-6, as defined in Table 4-4.

### 4.2.5 KP-SAM Applicability Assessment

KP-SAM is developed based on the Argonne National Laboratory code SAM and includes models developed to ensure applicability to the KP-FHR test reactor design. Model verification studies have been completed as described in Section 4.2.1 and assessment against scaled SETs and IETs will be performed (see Limitation 3 in Section 6.2). These SETs and IETs are scaled in accordance with Reference 30 and tests are performed over a sufficient range to provide assurance of (1) applicability and scalability of correlations obtained from SETs to the evaluation of the KP-FHR test reactor, and (2) capability of the IETs to assess system/component interactions and demonstrate global capability of the KP-SAM code to evaluate the KP-FHR test reactor. Assurance of applicability to the KP-FHR test reactor is provided through the completion of assessments against SETs and IETs as described in Section 4.2.2 and 4.2.3.

## 4.3 KP-SAM BASE MODEL

The KP-SAM base model is a best estimate simulation of a KP-FHR test reactor that is developed for postulated event analysis. The biases that need to be applied to this base model to perform conservative safety analysis are discussed in Section 5. The base model is developed using the KP-SAM Theory Manual (Reference 27) and the KP-SAM User Guide (Reference 28). The base model simulates the behavior of the reactor (including the fuel and reflector), PHTS (including the primary salt pump and heat rejection radiator), and the downcomer. DHRS performance is modeled as a boundary condition. Control functions include shutdown reactivity insertion, primary salt pump control, and heat rejection radiator control. The analytical limits provide setpoints for tripping these controls to simulate the RPS.

The vessel portion of the KP-SAM base model is axisymmetric around the axial, i.e., z-axis. This assumption is valid for the test reactor conditions because relevant flow and heat transfer phenomena are expected to be axisymmetric, and radial power distribution asymmetries are captured by the hot pebble factor methodology (Section 4.2.4). The vessel top and bottom head outer boundaries are adiabatic (Neumann) boundary conditions. This treatment is conservative for the methodology figures of merit as it neglects potential heat removal pathways.

The bypass flow fraction is set to a conservative value on an event-specific basis (as described in Section 5) during pumped, normal operating conditions. During the transients where the PSP trips, the bypass flow fraction evolves dynamically according to the system pressure distribution following the trip.

### 4.3.1 Nodalization

Nodalization is performed with sufficient resolution to ensure the following:

- Global mass and energy balances are appropriately maintained for all calculations
- Spatial gradients in the solution variables are appropriately captured

The number of elements used in a component is generally selected to obtain an element size of approximately 10 cm. In some cases, further refinement is needed for maintaining appropriate global mass and energy balance and capturing spatial gradients in the solution variables. Coarser discretization may be used for parts of the system without steep temperature gradients, such as the adiabatic primary heat transport system hot and cold legs The KP-SAM User's Guide (Reference 28) provides guidance on the minimum number of elements that should be used for certain components.

The adequacy of the model nodalization scheme is assessed as part of the overall evaluation model assessment described in Section 4.2. This includes dedicated mesh sensitivity studies to confirm independence of the simulation solutions from spatial discretization. These evaluations extend to ensuring that temperature inputs for the HPF are not dependent on the chosen discretization level.

The base model for a typical KP-FHR test reactor is nodalized as shown in Figure 4-1 and Figure 4-2. The components identified in Figures 4-1 and 4-2 are described in Table 4-2.

### 4.3.2 Reactor

The reactor is modeled using the components described in Figures 4-1 and 4-2, and Table 4-2.

The reactor power and associated reactor kinetics are simulated using the ReactorPower component in KP-SAM with an associated PointKinetics component. The point kinetics inputs for the base model, include the reactivity components from fuel (Doppler), moderator pebbles, coolant, reflector, and shutdown elements. Reactivity contributions from other sources (e.g., control element movement) are addressed in the event-specific methodology in Section 5.

Shutdown reactivity insertion control logic is used to simulate the reactivity shutdown system.

The modeling of fuel pebble heat structures in the reactor (Section 2.4 of Reference 28) includes the following:

- Fuel pebbles — modeled as a three region heat structure consisting of the pebble core, the fueled region, and the pebble shell
- Moderator pebbles — modeled as single-region pebbles
- TRISO fuel particles — modeled using the KP-SAM TRISO particle model

Material properties for the fuel and moderator pebbles are provided in Section 15 of Reference 27.

The following options, identified in Table 4-3 are selected to capture the closure models for flow and heat transfer in the pebble bed region, as described in Section 4.2:

- WF_user_option = KTA is selected to apply the KTA pressure loss correlation, which is assessed by Kairos Power for the evaluation of pressure drop in the reactor, for flow through the pebble bed reactor (see Section 4.2.1 of Reference 28).

- HTC_geometry_type = KPPebbleBed is selected to apply the heat transfer correlations that are assessed for the evaluation of heat transfer within an FHR pebble bed (see Section 4.1.1 of Reference 28).

The reflector is modeled using heat structures that are coupled to the pebble bed. The following option, identified in Table 4-3, is selected to capture the closure models for heat transfer in the reflector region, as described in Section 4.2:

- HTC_geometry_type_left = KPPebbleBedWall is selected to apply the heat transfer correlations that are assessed by Kairos Power for the evaluation of heat transfer between an FHR pebble bed and an attached structure (see Section 4.1.2 of Reference 28).

The Diverging and Converging regions are truncated cones that are modeled as cylinders in KP-SAM. Truncated cones are converted into cylinders by calculating an effective radius that preserves the volume of the truncated cone. This assumption does not introduce bias into the model because it preserves the mass of material and associated stored energy. To preserve the heat transfer surface area, a separate heated perimeter is calculated and used to obtain the heat transfer surface area.

Power deposition in each axial PebbleBedCoreChannel component that makes up the reactor core is calculated as the product of the overall core power calculated by the point kinetics model and a statically defined power fraction based on the integral of the normalized axial power shape function for the axial length over which each PebbleBedCoreChannel is defined. The axial power shape function is then applied piecewise to each PebbleBedCoreChannel to resolve the axial power for each node. This calculated power is then applied to the fuel matrix layer of the spherical heat structures that represent the pebble bed at each axial node.

### 4.3.3 Primary Heat Transport System

The PHTS is modeled using the components described in Figure 4-1 and Table 4-2 to simulate flow through the primary salt pump, PHTS piping, and heat rejection radiator.

The primary salt pump is the primary driving force for coolant circulation, and the component control logic includes an RPS trip, coastdown curve, and proportional-integral control controller. For the PHTS piping outer wall boundary conditions, the pipe walls are not modeled, which effectively results in adiabatic boundary conditions. A heat structure is used to model the heat rejection radiator heat transfer with air. The heat rejection is modeled through a control logic driven heat flux boundary condition on the secondary (air) side of the HRR heat structure to simulate the heat rejection radiator energy removal function. During the steady state phase, a proportional-integral control function is used to modify the heat flux magnitude within a preset range to establish the correct HRR outlet temperature. Upon RPS initiation, the control logic is replaced by a conservatively short linear coastdown function that drives the HRR heat flux from the required steady state value to zero, thus resulting in an adiabatic condition for the entirety of the PHTS.

### 4.3.4 Downcomer

Flow through the downcomer (between the core barrel and the vessel wall) is modeled using the components described in Figure 4-1, 4-2, and Table 4-2. The following option, identified in Table 4-3, is selected to capture the closure models for flow in the downcomer region, as described in Section 4.2:

- WF_geometry_type = ParallelPlate is selected to apply parallel plate pressure loss correlation for flow through regions that have parallel plate geometry (see Section 4.2.2 of Reference 28).

Heat structures model the downcomer heat transfer between the core barrel, coolant, and vessel wall. The following option, identified in Table 4-3, is selected to capture the closure models for heat transfer in the downcomer region, as described in Section 4.2:

- HTC_geometry_type = Vertical-ParallelPlate is selected to apply the heat transfer correlations for the evaluation of heat transfer in vertical, parallel-plate geometry (see Section 4.1.3 of Reference 28).

### 4.3.5 Decay Heat Removal System

The DHRS is modeled in KP-SAM using heat flux boundary conditions that are tuned to match a specified DHRS performance curve. The DHRS heat transfer performance curve can be set to provide best-estimate, minimum, or maximum heat removal to bound the DHRS heat transfer rates. Required DHRS performance will be verified through testing. Additionally, surveillance of the DHRS will be performed to provide assurance of adequate DHRS performance.

### 4.3.6 Material Properties

The materials for the base model are identified in Table 4-2. The properties for these materials are inputs to KP-SAM as described in Reference 27 and should be consistent with the material properties specified by the KP-FHR test reactor design. There is no bias applied to material properties in the base model, except for the thermal conductivity of ET-10 graphite. Justification for the use of unbiased material properties will be provided in the final safety analysis.

Thermal conductivity for ET-10 graphite is lower against the grain, decreases with increasing irradiation temperature, and decreases with increasing fluence. Accordingly, ET-10 graphite thermal conductivity is calculated using against-grain properties, a conservatively low irradiation temperature, and a bounding maximum value for fluence in the reflector. This results in a conservatively low estimate of thermal conductivity, which maximizes the stored energy retained in the reflector.

Geometrical uncertainties and the impact of tolerances arising from the manufacturing process for the steel and graphite structures in the reactor are neglected. The volumetric heat capacities of both the Flibe and graphite, which constitute the bulk of the thermal mass of the system, are large. Thus, minor differences in the volumes of either constituent, as well as the remainder of the system volume composed of steel, are not expected to significantly impact the overall thermal mass of the system. Tolerances will be controlled sufficiently to enable the assembly of the system and thus the magnitude of geometrical uncertainty is not expected to be significant.

### 4.3.7 Upper Plenum

The upper plenum is modeled using the Tank component, as described in Table 4-2 and shown in Figure 4-1. The Tank component resolves the Flibe free surface and cover gas space inside the vessel. The cover gas is coupled to the Flibe free surface through convective heat transfer using a constant convective heat transfer coefficient which is calculated using the [[
]] . The Flibe in the upper plenum is coupled to the upper section of the vessel wall.

No radiative couplings are included in the Tank component. Instead, the upper surface of the reflector is coupled through a radiative coupling to the inner surface of the vessel top head to facilitate energy transfer to this heat structure.

### 4.3.8 Reflector Bypass

The graphite reflector is composed of multiple stacked blocks that are mechanically constrained to limit the excessive relative motion induced by flow and buoyancy effects. This arrangement leads to the formation of a series of interstitial gaps between the reflector blocks during reactor operation. Potential gaps include horizontally oriented radial gaps between the axially stacked blocks, vertically oriented radial gaps that form between the azimuthal block extents, and the rim gap that results from the reflector outer radius being smaller than the core barrel for the purposes of accommodating differential thermal expansion between structural materials. The reflector blocks also feature engineered axial and radial flow channels to accommodate instrumentation and control equipment.

The flow paths through the gaps in the reflector and associated frictional and form-loss closures are not modeled in KP-SAM due to the uncertainty associated with the detailed geometry. However, there is not expected to be a significant amount of flow within the reflector gaps. Thus, the reflector is modeled as a solid structure. Two parallel, axial flow channels are modeled within the core barrel — the flow channel through the pebble bed (including inlet and outlet flow channels) and the annular rim gap. The impact of neglecting flow through other reflector gaps is bound by the event-specific sensitivity analyses (see Section 5).

The modeled flow channels take in flow from the lower plenum flow components. The desired bypass flow fraction during nominal steady state conditions, (i.e., the fraction of flow bypassing the core through the rim gap and NCP), is set by perturbing the rim gap width in the sealing layer region of the reflector. These perturbations remain in place once postulated event transients are initiated. Event-specific sensitivity analyses will be performed to evaluate the impact of bypass flow fraction on the figures of merit (see Section 5).

Flow through the rim gap (between the reflector and the core barrel inner wall) is modeled using the components described in Figures 4-1 and 4-2, and Table 4-2. The following option, identified in Table 4-3, is selected to capture the closure models for flow in the rim gap region, as described in Section 4.2:

- WF_geometry_type = ParallelPlate is selected to apply parallel plate pressure loss correlation for flow through regions that have parallel plate geometry (see Section 4.2.2 of Reference 28).

Heat structures model the rim gap heat transfer between the reflector, coolant, and core barrel inner wall. The following option, identified in Table 4-3, is selected to capture the closure models for heat transfer in the rim gap region, as described in Section 4.2:

- HTC_geometry_type = Vertical-ParallelPlate is selected to apply the heat transfer correlations for the evaluation of heat transfer in vertical, parallel-plate geometry (see Section 4.1.3 of Reference 28).

### 4.3.9 Metallic Structures

Resolved metallic structures in the model include the vessel top and bottom heads, vessel wall, and the core barrel. Metallic structures that are not included in the model are the reflector hold down plate and shutdown and control elements. The neglected structures do not substantially impact thermal response of the system due to their low thermal mass relative to the remainder of the system constituents.

### 4.3.10 Modifications for Salt Spill Analysis

The base model is modified with components to model characteristics specific to salt spill postulated event analysis. For the salt spill event analysis, valve components are used to model the anti-siphon

features on the PSP and the cold leg of the PHTS (described in Section 1.1.3), as well as the pipe break on the PHTS.

To model the PSP anti-siphon, a valve component is added directly below the PSP component. When the Flibe level in the upper plenum is below the axial location of the PSP anti-siphon level, the valve closes and stops the flow into the PSP.

To model the cold leg anti-siphon, a valve component is added on the cold leg component, so when the Flibe level in the upper plenum is below the axial location of the cold leg anti-siphon level, the valve closes and stops the flow into the cold leg.

The pipe break in the PHTS piping is modeled using three additional valves. One valve, which is in line with the PHTS piping, is used to impose a binary option of either a guillotine break or a smaller, non-severed break.

For the guillotine break scenario, the first valve is closed at the beginning of the transient to model the complete severing of the two sections of PHTS piping where the break occurs. The other two valves are attached to either side of the first valve to enable flow from either end of the severed pipe.

For the smaller break scenario, the first valve remains open to model the continued flow path through the PHTS. The combined area of the other two valves represents the overall break size since the flow around the PHTS loop is maintained. These valves are defined to connect the PHTS to an atmospheric boundary condition, which represents the pathway for the loss of Flibe from the system.

**Table 4-1: Parameter Ranges to Address Heat Transfer in KP-FHR Test Reactor Pebble Bed**

| Parameter | Test Reactor |
|---|---|
| Re | [[ ]] |
| Pr | [[ ]] |

**Table 4-2: Component Types and Associated Materials in KP-SAM Base Model**

| Acronym | Component | KP-SAM Component Type | Material Composition |
|---|---|---|---|
| CBRL | Core Barrel | PBCoupledHeatStructure | SS316H |
| CL | Cold Leg | PBOneDFluidComponent | Flibe |
| CON | Converging Region | PebbleBedCoreChannel | Flibe, Fuel Pebbles, Moderator Pebbles |
| CYL | Cylinder Region | PebbleBedCoreChannel | Flibe, Fuel Pebbles, Moderator Pebbles |
| DEF | Defueling Region | PebbleBedCoreChannel | Flibe, Fuel Pebbles, Moderator Pebbles |
| DFC | Defueling Flow Channel | PBOneDFluidComponent | Flibe |
| DIV | Diverging Region | PebbleBedCoreChannel | Flibe, Fuel Pebbles, Moderator Pebbles |
| DWN | Downcomer | PBOneDFluidComponent | Flibe |
| FUR | Fueling Region | PBOneDFluidComponent<br><br>PebbleBedCoreChannel | Flibe<br><br>Flibe, Fuel Pebbles, Moderator Pebbles |
| HL | Hot Leg | PBOneDFluidComponent | Flibe |
| HRR | Heat Rejection Radiator | PBCoupledHeatStructure | SS316H |
| HRR_P | Heat Rejection Radiator (Primary Side) | PBOneDFluidComponent | Flibe |
| HWL | Hot Well | PBOneDFluidComponent | Flibe |
| IFC | Inlet Flow Channel | PBOneDFluidComponent | Flibe |
| IFD | Inlet Flow Distributor | PBVolumeBranch | Flibe |
| LPN | Lower Plenum | PBOneDFluidComponent | Flibe |
| NCP | Natural Circulation Path | PBOneDFluidComponent | Flibe |

| Acronym | Component | KP-SAM Component Type | Material Composition |
|---|---|---|---|
| OFC | Outlet Flow Channel | PBOneDFluidComponent | Flibe |
| PEM | Pebble Extraction Machine | PebbleBedCoreChannel | Flibe, Fuel Pebbles, Moderator Pebbles |
| PSP | Primary Salt Pump | PBOneDFluidComponent, PBPump | Flibe |
| PWL | Pump Well | PBOneDFluidComponent | Flibe |
| REF | Reflector | PBCoupledHeatStructure | ET-10 |
| RIM | Rim Gap | PBOneDFluidComponent | Flibe |
| UP | Upper Plenum | Tank | Flibe, Argon |
| VSLB | Vessel Bottom | PBCoupledHeatStructure | SS316H |
| VSLH | Vessel Head | PBCoupledHeatStructure | SS316H |
| VSLW | Vessel Wall | PBCoupledHeatStructure | SS316H |

**Table 4-3: Required KP-SAM User Options to Ensure Consistency with Code Assessment**

| Component | Component Specific User-Options |
|---|---|
| Reactor Pebble Bed components | WF_user_option = KTA<br>HTC_geometry_type = KPPebbleBed |
| Reflector components attached to Pebble Bed | HTC_geometry_type_left = KPPebbleBedWall |
| Downcomer components | WF_geometry_type = ParallelPlate<br>HTC_geometry_type = Vertical-ParallelPlate |
| Heat structures attached to Downcomer (Core Barrel and Vessel Wall) | HTC_geometry_type = Vertical-ParallelPlate |

**Table 4-4: Limitations of KP-SAM Modeling**

| Index | Limitation |
|---|---|
| 1 | 2-D and 3-D temperature distribution |
| 2 | 2-D and 3-D flow distribution |
| 3 | 2-D and 3-D power distribution |
| 4 | Non-uniform porosity |
| 5 | Radiative heat transfer |
| 6 | Gamma and neutron heating of in-vessel heat structures |

**Table 4-5: Subfactors for the Hot Pebble Factor**

| Description | Coolant $\Delta T$ | Film $\Delta T$ |
|---|---|---|
| *Direct Subfactors* | | |
| Flow distribution and mixing conservatism | | X |
| Radial/azimuthal peaking factor upper bound tolerance | X | |
| Pebble peaking factor upper bound tolerance | | X |
| *Statistical Subfactors* | | |
| Pebble diameter variation | | X |
| [[ ]] | | X |

**Figure 4-1: KP-SAM Base Model Nodalization**

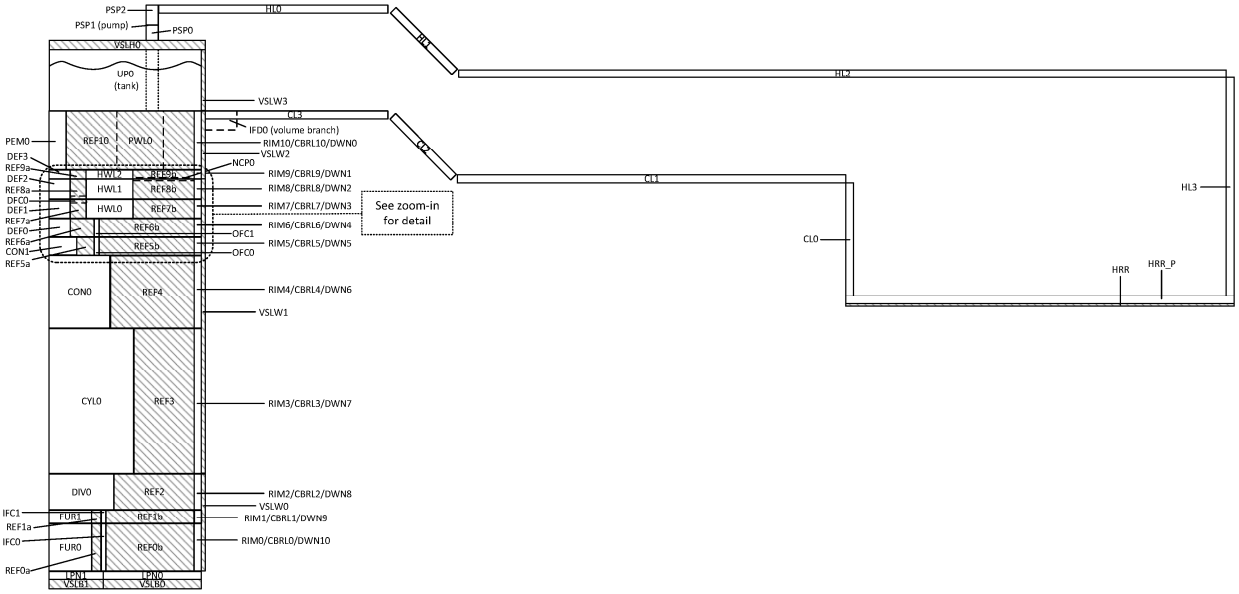

**Figure 4-2: Enlarged Segment from Figure 4-1**

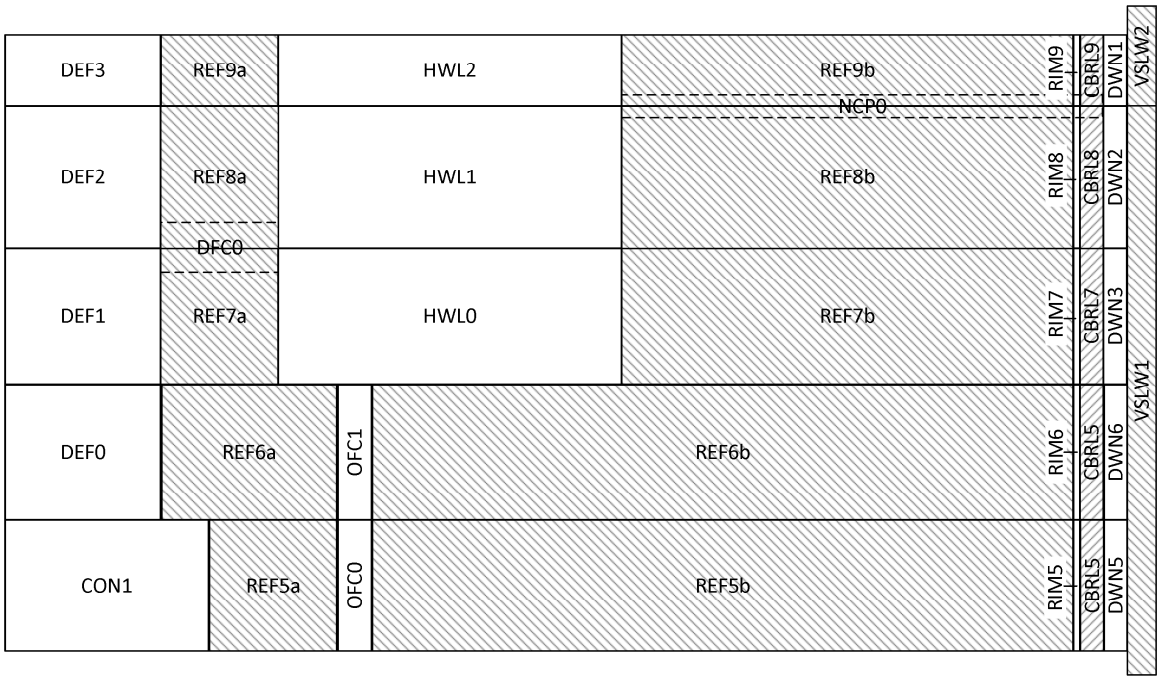

**Figure 4-3: Hot Pebble Factor Overview**

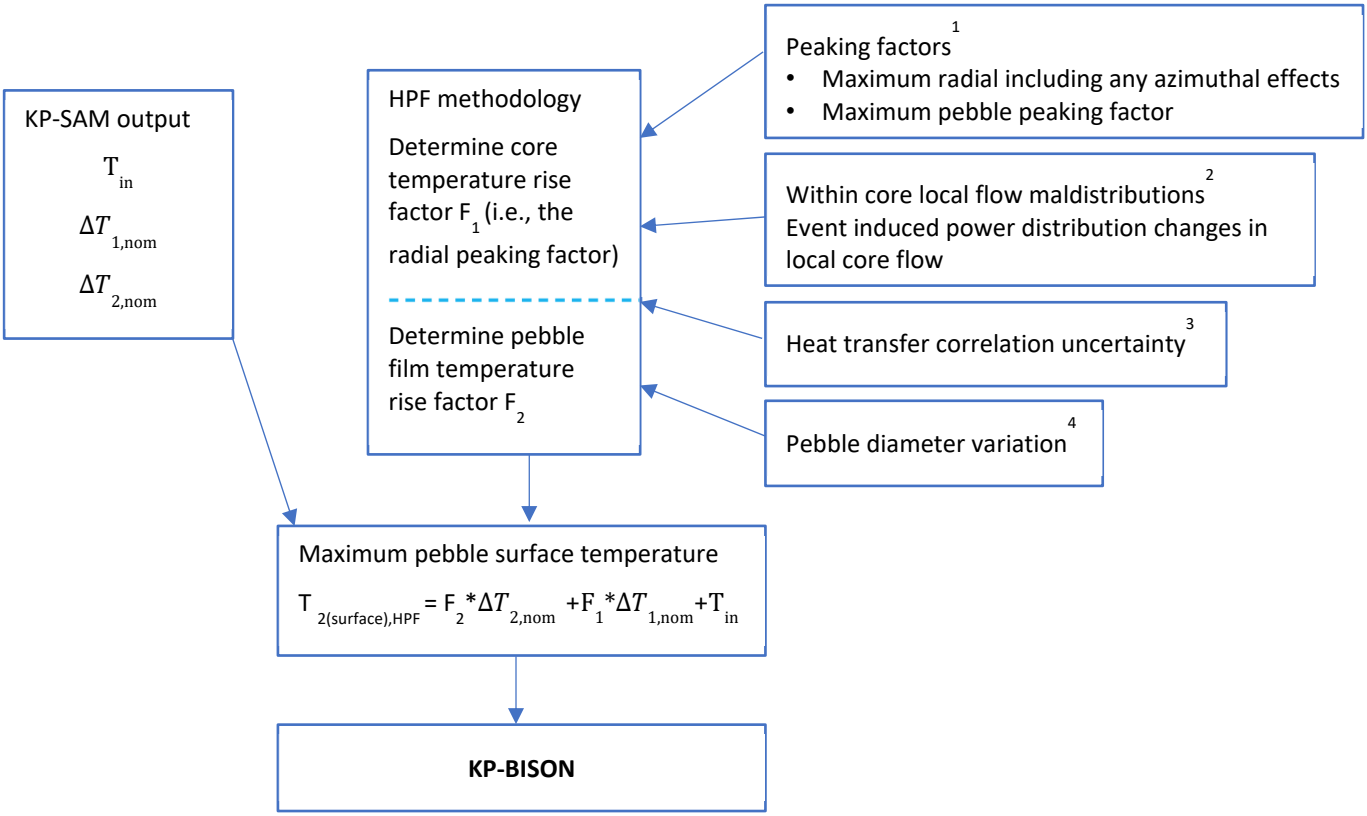


1. From core design, 2-D for symmetric events; 3-D for asymmetrical events
2. From [[ ]] analysis
3. Subfactor determined by bounding experimental data
4. Based on pebble diameter specification lower limit

**Figure 4-4: KP-SAM 1-D Pebble Bed Core Channel Model for HPF**

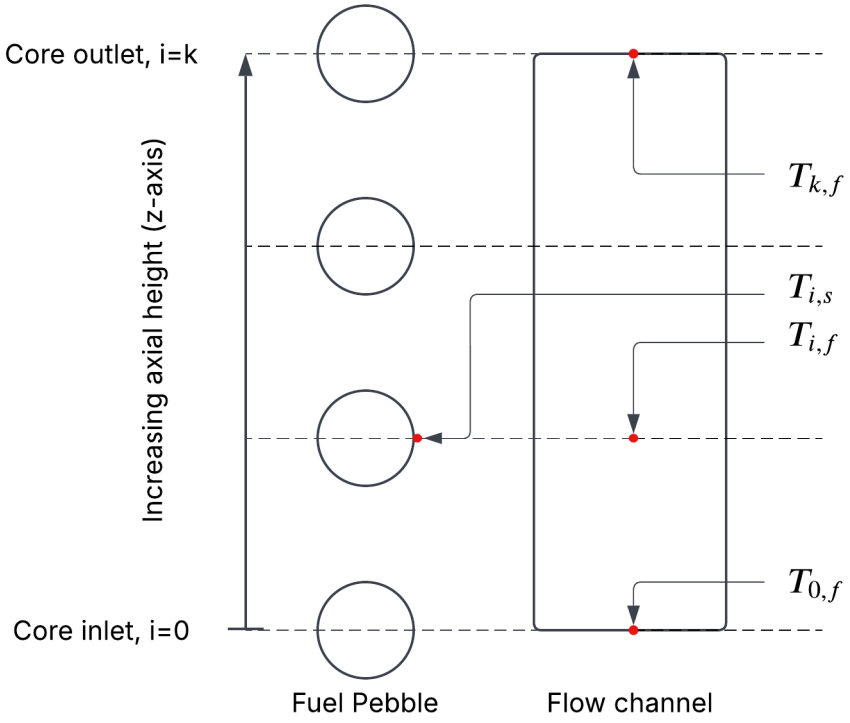


$$\Delta T_{1,nom} = T_{k,f} - T_{0,f}$$

$$\Delta T_{2,nom} = \max\left(T_{i,s} - T_{i,f}\right) \equiv \max\left(\frac{\dot{q}_i}{A \cdot h_i}\right); i \in [0, k]$$

Schematic representation of the KP-SAM 1-D pebble bed core channel model with an axial flow channel and coupled pebble at each axial node (dotted lines). The subscript *f* refers to fluid and *s* to surface. $\Delta T_{1,nom}$ represents the axial core temperature rise, while $\Delta T_{2,nom}$ is defined as the maximum of the differences between pebble surface and coolant temperatures for all axial nodes in the core channel.

# 5 EVENT-SPECIFIC METHODS

This section provides the event-specific methods that use the evaluation models with conservative inputs to analyze the transients discussed in Section 3.2. Sample results are provided in Appendix A to illustrate a generic system response for selected transients. Considerations that apply to event specific methods include the following:

- Analytical limits – Analytical limits for the RPS are set to ensure that the acceptance criteria described in Section 3.3 are met, consistent with the methodology described in Reference 32.
- Core Design Inputs – Reactor physics parameters (Table 5-1) are calculated using the methodology in Reference 23 and applied to the evaluation of postulated events with conservative bias. This conservative bias considers the best-estimate parameter and associated Nuclear Reliability Factor (NRF) in accordance with Reference 23.
- Reactor Physics Parameters - Sufficient bias is applied to bound the associated reactor physics parameter (Table 5-1) for both startup and equilibrium cores. The direction of conservative bias is determined on an event-specific basis and described in the subsections below.
- Fuel Performance Evaluations – Fuel performance calculations are outside of the scope of this report. However, outputs from the safety analysis are used in fuel performance calculations. Specifically, peak pebble power and surface temperatures (as calculated by KP-SAM) are inputs to the KP-BISON code to assess fuel radionuclide release rates. The peak pebble power and surface temperatures account for uncertainty through the application of a hot pebble factor.
- Coolant Properties – Flibe coolant thermophysical properties are biased on an event-specific basis to accommodate uncertainties in accordance with Reference 4. The direction of conservative bias is determined on an event-specific basis and described in the subsections below.
- Peak Reactor Vessel and Reflector Temperatures – Peak temperature surrogates are used for the reactor vessel and reflector. These surrogates account for modeling uncertainties and for factors not explicitly captured in the KP-SAM model (e.g., gamma/neutron heating in the reflector and asymmetric temperature distribution).
- Single Failure Considerations – The event-specific methods include the consideration of single-failures associated with safety-related SSCs on an event-specific basis. This consideration of single-failure is discussed in the subsections below. Examples of single-failure considerations:
    - If a single active failure can degrade heat removal, that degraded heat removal performance would be evaluated to determine if it has an effect on the figures of merit.
    - If the RPS is designed with sufficient redundancy and diversity to preclude a single failure from affecting the safety function of the system, then the RPS will actuate in postulated events.
    - Single failure of an ex-vessel detector during a spurious single-element withdrawal scenario has the potential to result in the measured power being below the actual power. The potential for this single-failure is addressed through the application of an ex-vessel detector penalty.
- Non-Safety-Related Plant Control System – The non-safety-related plant control system is not assumed to be available to mitigate the consequences of postulated events. Event-specific methods consider the potential for non-safety-related plant control systems to exacerbate the effects of the postulated event.
- Electrical Power – Electrical power is not assumed to be available to mitigate the consequences of postulated events.

- Operator Actions – No operator actions are assumed to mitigate the consequences of postulated events.

## 5.1 INCREASE IN HEAT REMOVAL

The increase in heat removal postulated event group is described in Section 3.2.1. The figures of merit evaluated for this event are described in Section 3.3. The KP-SAM base model is used with conservative biases to analyze various increase in heat removal scenarios to identify the limiting event or events for this group. The limiting event(s) are defined as the scenario(s) that result in the least amount of margin to the acceptance criteria for the figures of merit. Specifically, the limiting event(s) represent the following:

- Maximum pebble film and coolant temperatures used as input to the hot pebble factor (HPF), to maximize temperature inputs to KP-BISON (Section 4.2.4.1)
    - Minimizes margin to acceptance criteria for peak TRISO SiC temperature and fuel failure fraction figures of merit (Section 3.3.1 and 3.3.3)
- Maximum pebble power calculated from KP-SAM to maximize power input to KP-BISON
    - Minimizes margin to acceptance criteria for peak TRISO SiC temperature and fuel failure fraction figure of merit (Section 3.3.1 and 3.3.3)
- Maximum coolant temperature at the natural circulation pathway outlet used for the peak reflector and vessel temperature surrogates (Section 4.2.4.2 and 4.2.4.3)
    - Minimizes margin to acceptance criteria for peak vessel temperature figure of merit (Section 3.3.4)
    - Minimizes margin to acceptance criteria for peak structural graphite temperature figure of merit (Section 3.3.5)

### 5.1.1 Bias Application

The KP-SAM base model, described in Section 4.3, is used to analyze the increase in heat removal scenarios with conservative biases described below:

- Reactor Initial Power – The cases initiating from full power conditions are biased high at a value that accounts for the uncertainty in power measurement.
- Reactivity Parameters
    - Reactivity Coefficients - Reactivity coefficients are biased downwards for core constituents that cool down and biased upwards for constituents that heat up.
        - Doppler reactivity coefficient is biased to be most positive (least negative) to limit the negative feedback associated with the power increase.
        - Moderator reactivity coefficient is biased to be most positive (least negative) to limit the negative feedback associated with the power increase.
        - Coolant reactivity coefficient is biased to be most negative to maximize the reactivity insertion associated with the coolant temperature change.
        - Reflector reactivity is biased to be the least positive (most negative) to limit the negative feedback associated with the decrease in temperature.
    - Reactor Kinetics Parameters – The power increase is maximized for a given reactivity insertion, associated with the decrease in coolant temperature, by minimizing the neutron mean generation time and effective neutron fractions and maximizing the delayed neutron precursor decay constants.

  - Power Distribution – A top peaked power distribution is applied to result in a high thermal center for the reactor core, minimizing the coolant flow under natural circulation conditions. A bottom peaked power distribution is applied to calculate the shutdown element worth curve, which pushes the shutdown worth maximum to a lower location in the reactor core. A hot pebble factor, which conservatively treats the power shape and associated uncertainties, is applied to calculate the highest temperature fuel pebble.
  - Shutdown Margin – The shutdown worth applied assumes the highest worth shutdown element is fully withdrawn from the reactor core to ensure that shutdown margin is minimized in the analysis.
  - Shutdown Element Insertion Time – Insertion time is biased high to slow shutdown and maximize temperatures.
- System Pressure – The system pressure does not have an effect on the transient conditions, so nominal values for system pressure are used with no bias.
- Heat Generation and Removal Parameters
  - Heat rejection blower – The heat rejection radiator heat removal is maximized to maximize the resulting increase in reactor power. The heat rejection blower overspeed, which is captured by a ramp from steady-state removal rate up to the maximum heat rejection blower capacity at the maximum ramp rate, is the bounding initiator.
  - DHRS Capacity – Minimum DHRS performance including single-failure considerations is applied. Minimizing DHRS performance permits larger transient changes in core inlet temperature to occur, which induces larger increases in power.
  - Decay Heat – Decay heat is maximized to provide a conservative estimate of the heat-up following reactor trip.
- Instrumentation and Control Parameters
  - Reactor Protection System Actuation Delay – The delay in RPS actuations include instrument response time and actuation delays.

### 5.1.2 Sensitivities

An increase in heat removal event could be postulated to occur from the various initiators described in Section 3.2.1. These initiators (as well as varied initial plant conditions and properties) are analyzed by executing sensitivity studies to identify a limiting event for this group. The biases described in Section 5.1.1 are applied to the KP-SAM base model (which is described in Section 4.3) to perform safety analyses with sensitivities on the following parameters:

- Reactor Initial Power – varied from low to full power.
- Reactor Coolant Average Temperature – coolant inlet temperature and mass flow rate varied over a sufficient range to cover potential operating states and measurement uncertainty.
- Material Properties – coolant properties should be biased to maximize the induced overpower. However, there are competing effects that inform which biasing direction achieves the conservative result. Accordingly, a sensitivity study that covers the thermophysical property uncertainties is performed.
- Heat Rejection Radiator (Flibe) Outlet Temperature – sensitivities are performed to account for the range of site-specific minimum to maximum ambient temperatures at the HRR (air) inlet.
- Plant Control Systems – sensitivities are performed on reactivity control and primary salt pump control.
- Bypass Flow Fraction – Sensitivities are performed on the defined flow fraction to cover a sufficient range of bypass flow conditions for the design.

When a limiting postulated Increase in Heat Removal Event scenario(s) is identified, the peak pebble power and surface temperature are provided as input to a KP-BISON calculation to ensure that the fuel figures of merit are met.

## 5.2 DECREASE IN HEAT REMOVAL

The decrease in heat removal postulated event group is described in Section 3.2.2. The figures of merit evaluated for this event are described in Section 3.3. The KP-SAM base model is used with conservative biases to analyze various decrease in heat removal scenarios to identify the limiting event or events for this group. The limiting event(s) are defined as the scenario(s) that result in the least amount of margin to the acceptance criteria for the figures of merit. Specifically, the limiting event(s) represent the following:

- Maximum pebble film and coolant temperatures used as input to the hot pebble factor (HPF), to maximize temperature inputs to KP-BISON (Section 4.2.4.1)
    - Minimizes margin to acceptance criteria for peak TRISO SiC temperature and fuel failure fraction figures of merit (Section 3.3.1 and 3.3.3)
- Maximum pebble power calculated from KP-SAM to maximize power input to KP-BISON
    - Minimizes margin to acceptance criteria for peak TRISO SiC temperature and fuel failure fraction figure of merit (Section 3.3.1 and 3.3.3)
- Maximum coolant temperature at the natural circulation pathway outlet used for the peak reflector and vessel temperature surrogates (Section 4.2.4.2 and 4.2.4.3)
    - Minimizes margin to acceptance criteria for peak vessel temperature figure of merit (Section 3.3.4)
    - Minimizes margin to acceptance criteria for peak structural graphite temperature figure of merit (Section 3.3.5)

### 5.2.1 Bias Application

The KP-SAM base model, described in Section 4.3, is used to analyze the decrease in heat removal scenarios with conservative biases described below:

- Reactor Initial Power – The cases initiating from full power conditions will be biased high at a value that accounts for the uncertainty in power measurement.
- Reactivity Parameters
    - Reactivity Coefficients - Reactivity coefficients are biased to be the most positive (least negative) to minimize the inherent feedback that would reduce the power during the event.
    - Power Distribution – A top peaked power distribution is applied to result in a high thermal center for the reactor core, minimizing the coolant flow under natural circulation conditions. A bottom peaked power distribution is applied to calculate the shutdown element worth curve, which pushes the shutdown worth maximum to a lower location in the reactor core. A hot pebble factor, which conservatively treats the power shape and associated uncertainties, is applied to calculate the highest temperature fuel pebble.
    - Shutdown Margin – The shutdown worth applied assumes that the highest worth shutdown element is fully withdrawn from the reactor core to ensure that shutdown margin is minimized in the analysis.
    - Shutdown Element Insertion Time – Insertion time is biased high to slow shutdown and maximize temperatures.

- Reactor Coolant Thermophysical Properties – Coolant properties are biased to maximize the temperature increase by maximizing viscous flow resistance (minimizing flow) and minimizing heat transfer and heat capacity.
- System Pressure – The system pressure does not have an effect on the transient conditions, so nominal values for system pressure are used with no bias.
- Heat Generation and Removal Parameters
    - Heat Rejection Blower – The heat rejection radiator heat removal is minimized to limit heat removal by assuming a rapid coastdown time for the heat rejection blower.
    - DHRS Capacity – Minimum DHRS performance, including single-failure considerations, is applied. Minimizing DHRS performance ensures that the heat up is maximized.
    - Decay Heat – Decay heat is maximized to ensure that the heat up is maximized.
    - Material Properties – Biased to maximize the temperature increase by increasing stored energy in the reflector and biasing the coolant properties to increase flow resistance and minimize heat transfer.
- Instrumentation and Control Parameters
    - Reactor Protection System Actuation Delay – The delay in RPS actuations includes instrument response time and actuation delays.

### 5.2.2 Sensitivities

A decrease in heat removal event could be postulated to occur from the various initiators described in Section 3.2.2. These initiators (as well as varied initial plant conditions and properties) are analyzed by executing sensitivity studies to identify a limiting event for this group. The biases described in Section 5.2.1 are applied to the KP-SAM base model (which is described in Section 4.3) to perform safety analyses with sensitivities on the following parameters:

- Reactor Initial Power – In addition to the full power case, a reduced power case should be performed to verify expected sensitivity results (that the full power case is limiting).
- Reactor Coolant Average Temperature – Coolant inlet temperature and mass flow rate varied over a sufficient range to cover potential operating states and measurement uncertainty.
- Plant Control Systems – Sensitivities are performed on reactivity control and primary salt pump control.
- Bypass Flow Fraction – Sensitivities are performed on the defined flow fraction to cover a sufficient range of bypass flow conditions for the design.

When a limiting postulated decrease in heat removal event scenario(s) is identified, the peak pebble power and surface temperature are provided as input to a KP-BISON calculation to ensure that the fuel figures of merit are met.

## 5.3 LOSS OF FORCED CIRCULATION

The loss of forced circulation postulated event group is described in Section 3.2.3. The figures of merit evaluated for this event are described in Section 3.3. The KP-SAM base model is used with conservative biases to analyze various loss of forced circulation scenarios to identify the limiting event or events for this group. The limiting event(s) are defined as the scenario(s) that result in the least amount of margin to the acceptance criteria for the figures of merit. Specifically, the limiting event(s) represent the following:

- Maximum pebble film and coolant temperatures used as input to the hot pebble factor (HPF), to maximize temperature inputs to KP-BISON (Section 4.2.4.1)
    - Minimizes margin to acceptance criteria for peak TRISO SiC temperature and fuel failure fraction figures of merit (Section 3.3.1 and 3.3.3)
- Maximum pebble power calculated from KP-SAM to maximize power input to KP-BISON
    - Minimizes margin to acceptance criteria for peak TRISO SiC temperature and fuel failure fraction figure of merit (Section 3.3.1 and 3.3.3)
- Maximum coolant temperature at the natural circulation pathway outlet used for the peak reflector and vessel temperature surrogates (Section 4.2.4.2 and 4.2.4.3)
    - Minimizes margin to acceptance criteria for peak vessel temperature figure of merit (Section 3.3.4)
    - Minimizes margin to acceptance criteria for peak structural graphite temperature figure of merit (Section 3.3.5)

### 5.3.1 Bias Application

The KP-SAM base model, described in Section 4.3, is used to analyze the loss of forced circulation scenarios with conservative biases described below:

- Reactor Initial Power – The cases initiating from full power conditions will be biased high at a value that accounts for the uncertainty in power measurement.
- Reactivity Parameters
    - Reactivity Coefficients – Coefficients are biased to be the most positive (least negative) to minimize the inherent feedback that would reduce the power during the event.
    - Power Distribution – A top peaked power distribution is applied to result in a high thermal center for the reactor core, minimizing the coolant flow under natural circulation conditions. A bottom peaked power distribution is applied to calculate the shutdown element worth curve pushing the shutdown worth maximum to a lower location in the reactor core. A hot pebble factor, which conservatively treats the power shape and associated uncertainties, is applied to calculate the highest temperature fuel pebble.
    - Shutdown Margin – The shutdown worth applied assumes the highest worth shutdown element is fully withdrawn from the reactor core to ensure that shutdown margin is minimized in the analysis.
    - Shutdown Element Insertion Time – Insertion time is biased high to slow shutdown and maximize temperatures.
- Reactor Coolant Thermophysical Properties – Coolant properties are biased to maximize the temperature increase by maximizing viscous flow resistance (minimizing flow) and minimizing heat transfer and heat capacity.
- System Pressure – The system pressure does not have an effect on the transient conditions, so nominal values for system pressure are used with no bias.
- Heat Generation and Removal Parameters
    - DHRS Capacity – Minimum DHRS performance including single-failure considerations is applied. Minimizing DHRS performance ensures that the heat up is maximized.
    - Decay Heat – Decay heat is maximized to ensure that the heat up is maximized.
    - Material Properties – Biased to maximize the temperature increase by increasing stored energy in the reflector and biasing the coolant properties to increase flow resistance and minimize heat transfer.
- Instrumentation and Control Parameters

- Reactor Protection System Actuation Delay – The delay in RPS actuations includes instrument response time and actuation delays.

### 5.3.2 Sensitivities

A loss of forced circulation event could be postulated to occur from the various initiators described in Section 3.2.3. These initiators, as well as varied initial plant conditions and properties, are analyzed by executing sensitivity studies to identify a limiting event for this group. The biases described in Section 5.3.1 are applied to the KP-SAM base model (which is described in Section 4.3) to perform safety analyses with sensitivities on the following parameters:

- Reactor Initial Power – In addition to the full power case, a reduced power case should be performed to verify expected sensitivity results (that the full power case is limiting).
- Reactor Coolant Average Temperature – Coolant inlet temperature and mass flow rate varied over a sufficient range to cover potential operating states and measurement uncertainty.
- Primary Salt Pump – Although the thermal inertia of the system results in little sensitivity to pump coast down time, two cases are analyzed to provide conservative initiators – nominal coast down and near-instantaneous (simulating shaft seizure). For the shaft seizure/locked rotor cases, a conservatively large flow resistance is applied to the primary salt pump.
- Plant Control Systems – Sensitivities are performed on reactivity control and heat rejection blower control.
- Bypass Flow Fraction – Sensitivities are performed on the defined flow fraction to cover a sufficient range of bypass flow conditions for the design.

When a limiting postulated loss of forced circulation event scenario(s) is identified, the peak pebble power and surface temperature are provided as input to a KP-BISON calculation to ensure that the fuel figures of merit are met.

## 5.4 REACTIVITY-INITIATED EVENT

The reactivity-initiated postulated event group is described in Section 3.2.4. The figures of merit evaluated for this event are described in Section 3.3. The KP-SAM base model is used with conservative biases to analyze various reactivity-initiated scenarios to identify the limiting event or events for this group. The limiting event(s) are defined as the scenario(s) that result in the least amount of margin to the acceptance criteria for the figures of merit. Specifically, the limiting event(s) represent the following:

- Maximum pebble film and coolant temperatures used as input to the hot pebble factor (HPF), to maximize temperature inputs to KP-BISON (Section 4.2.4.1)
  - Minimizes margin to acceptance criteria for peak TRISO SiC temperature and fuel failure fraction figures of merit (Section 3.3.1 and 3.3.3)
- Maximum pebble power calculated from KP-SAM to maximize power input to KP-BISON
  - Minimizes margin to acceptance criteria for peak TRISO SiC temperature and fuel failure fraction figure of merit (Section 3.3.1 and 3.3.3)
- Maximum coolant temperature at the natural circulation pathway outlet used for the peak reflector and vessel temperature surrogates (Section 4.2.4.2 and 4.2.4.3)
  - Minimizes margin to acceptance criteria for peak vessel temperature figure of merit (Section 3.3.4)
  - Minimizes margin to acceptance criteria for peak structural graphite temperature figure of merit (Section 3.3.5)

- Minimum transient response time (i.e., time from t = 0 to maximum power)
    - Minimizes margin to acceptance criteria for energy deposition pulse width figure of merit (Section 3.3.2)

### 5.4.1 Bias Application

The KP-SAM base model, described in Section 4.3, is used to analyze the reactivity-initiated scenarios with conservative biases described below:

- Reactor Initial Power – The cases initiating from full power conditions will be biased high at a value that accounts for the uncertainty in power measurement.
- Reactivity Parameters
    - Reactivity Coefficients – Coefficients are biased to be the most positive (least negative) to minimize the inherent feedback that would reduce the power during the event.
    - Reactor Kinetics Parameters – Minimizing the neutron mean generation time and effective neutron fractions, and maximizing the delayed neutron precursor decay constants maximizes the power increase for a given reactivity insertion.
    - Power Distribution – A top peaked power distribution is applied to result in a high thermal center for the reactor core, minimizing the coolant flow under natural circulation conditions. A bottom peaked power distribution is applied to calculate the shutdown element worth curve pushing the shutdown worth maximum to a lower location in the reactor core. For the withdrawal of all control elements, the event-specific pebble peaking factor accounts for a potential shift in the power shape to the upper portion of the reactor with an associated increase in axial peaking factor. An event-specific radial peaking factor is not applied because the withdrawal of all control elements results in a symmetric reactivity insertion. Event-specific radial and pebble peaking factors are applied for the single element withdrawal events to account for axial and radial changes in the power shape during the reactivity-initiated event. A hot pebble factor, which conservatively treats the power shape and associated uncertainties, is applied to calculate the highest temperature fuel pebble.
    - Shutdown Margin – The applied shutdown worth assumes the highest worth shutdown element is fully withdrawn from the reactor core to ensure that shutdown margin is minimized in the analysis.
    - Shutdown Element Insertion Time – Insertion time is biased high to slow shutdown and maximize temperatures.
- Reactor Coolant Thermophysical Properties – Coolant properties are biased to maximize the temperature increase by maximizing viscous flow resistance (minimizing flow) and minimizing heat transfer and heat capacity.
- System Pressure – The system pressure does not have an effect on the transient conditions, so nominal values for system pressure are used with no bias.
- Heat Generation and Removal Parameters
    - Heat Rejection Blower – The heat rejection radiator heat removal is maximized to maximize the resulting increase in reactor power. The heat rejection blower overspeed, which results in a ramp from steady-state air speed up to the maximum heat rejection blower capacity at the maximum ramp rate, is the bounding initiator.
    - DHRS Capacity – Minimum DHRS performance (including single-failure considerations) is applied. Minimizing DHRS performance ensures that the heat up is maximized. For scenarios that are initiated below the DHRS activation threshold, heat removal is through parasitic heat losses.

  - Decay Heat – Decay heat is maximized to ensure that the resulting heat up is maximized following reactor trip.
- Instrumentation and Control Parameters
  - Reactor Protection System Actuation Delay – The delay in RPS actuations includes instrument response time and actuation delays.

### 5.4.2 Sensitivities

A reactivity-initiated event could be postulated to occur from the various initiators described in Section 3.2.4. These initiators, as well as varied initial plant conditions and properties, are analyzed by executing sensitivity studies to identify a limiting event for this group. The biases described in Section 5.4.1 are applied to the KP-SAM base model, described in Section 4.3, to perform safety analyses with sensitivities on the following parameters:

- Reactor Initial Power – Varied from low to full power.
- Reactor Coolant Average Temperature – Coolant inlet temperature and mass flow rate varied over a sufficient range to cover potential operating states and measurement uncertainty.
- Plant Control Systems – Sensitivities are performed on primary salt pump and heat rejection blower control.
- Reactivity Insertion – Sensitivities on the magnitude of reactivity insertion are performed to simulate the range of control element withdrawals.
- Bypass Flow Fraction – Sensitivities are performed on the defined flow fraction to cover a sufficient range of bypass flow conditions for the design.

When a limiting postulated reactivity-initiated event scenario(s) is identified, the peak pebble power and surface temperature are provided as input to a KP-BISON calculation to ensure that the fuel figures of merit are met.

## 5.5 SALT SPILL

The salt spill event category is described in Section 3.2.5. As described in Section 3.3, the acceptance criteria for release pathways not included in the MHA is the dose figure of merit, to ensure that total releases from the event are bounded by the MHA. The method for determining the dose contribution from release pathways included in the MHA is also described in Section 3.3. The KP-SAM base model (as modified in Section 4.3.10) is used with conservative biases to analyze various salt spill scenarios to identify the limiting event for evaluating the dose contribution from release pathways included in the MHA.

For release pathways not included in the MHA, the limiting event is conservatively modeled as a combination of the most limiting break conditions, as described in Section 5.5.2. For release pathways that are included in the MHA, the limiting event(s) are defined as the scenario(s) that result in the least amount of margin to the acceptance criteria for the figures of merit. Specifically, the limiting event(s) represent the following:

- Maximum pebble film and coolant temperatures used as input to the hot pebble factor (HPF), to maximize temperature inputs to KP-BISON (Section 4.2.4.1)
  - Minimizes margin to acceptance criteria for peak TRISO SiC temperature and fuel failure fraction figures of merit (Section 3.3.1 and 3.3.3)
- Maximum pebble power calculated from KP-SAM to maximize power input to KP-BISON

    - Minimizes margin to acceptance criteria for peak TRISO SiC temperature and fuel failure fraction figure of merit (Section 3.3.1 and 3.3.3)
- Maximum coolant temperature at the natural circulation pathway outlet used for the peak reflector and vessel temperature surrogates (Section 4.2.4.2 and 4.2.4.3)
    - Minimizes margin to acceptance criteria for peak vessel temperature figure of merit (Section 3.3.4)
    - Minimizes margin to acceptance criteria for peak structural graphite temperature figure of merit (Section 3.3.5)

The following event-specific release pathways, which are not included in the MHA analysis, must be considered for this event:

- Single-phase and two-phase mechanical aerosol generation through the break
- Splashing of Flibe onto the catch pan
- Release of radionuclides from the spilled Flibe pool via evaporation
- Tritium and argon-41 releases from oxidized graphite in the reflector

The evaluation model uses the approved methods in Reference 1 to evaluate both single-phase mechanical aerosol generation through the break and aerosols generated due to splashing of Flibe onto the catch pan.

### 5.5.1 Bias Application

The following assumptions and the application of conservative biases are used to analyze the event-specific release pathways for salt spill postulated events:

- The initial conditions for the amount and distribution of MAR are identified and quantified so that transient releases of MAR can be calculated. The only MAR subject to release from non-MHA release pathways is the MAR in the Flibe in the primary system. The Flibe MAR bounds expected circulating activity that originates from the following sources:
    - Irradiation of actinide impurities in the coolant (i.e., fission and transmutation of naturally enriched uranium and thorium).
    - Accumulation of heavy metal contaminants and fission products from fuel pebbles (i.e., fission and transmutation of enriched uranium).
    - Activation products in the coolant (e.g., sulfur, sodium, fluorine).
- Correlations for temperature dependent Flibe properties (e.g., density, viscosity, and surface tension) are specified. Cover gas (argon) properties are specified based on the ideal gas law. The cover gas temperature is conservatively assumed to be the same as the Flibe temperature.
- The initial amount of MAR is biased high by assuming the reactor has operated at full power for long enough for the fuel to contain fission products at equilibrium conditions. This assumption also results in the maximum amount of decay heat being available at the start of the event.
- Pressure loss in the PHTS is conservatively ignored to maximize differential pressure at the break.
- Volatile product formation from Flibe chemical reaction with water, concrete, and structural materials (e.g., insulation and steel) is assumed to be negligible. Flibe-water and Flibe-concrete interactions are assumed to be prevented by design. Volatile product formation from Flibe chemical reaction with steel is negligible. It is assumed that the design will use insulation whose chemical reaction with Flibe releases a *de minimis* fraction of radionuclides compared to mechanical aerosolization such that the dose impact by Flibe-insulation interaction is negligible.

- The Flibe in the PHTS is conservatively assumed to be in a horizontal pipe of the same diameter as the cold leg (i.e., the variation of PHTS piping elevations is neglected), which maximizes the amount of Flibe that can interact with the cover gas to form aerosols during a two-phase discharge.
- Cover gas is supplied to the reactor vessel by a supply tank. The supply tank valve, which connects the supply tank to the reactor vessel upper head is not credited with closing during the reactor trip. Therefore, the gases in the tank are conservatively assumed to release during the salt spill.
- Hold-down structures in the reactor vessel (described in Section 1.1.3) keep the graphite reflector sufficiently submerged to ensure that the structural integrity of the reflector is not challenged due to oxidation resulting from air ingress following a break.

The KP-SAM base model, described in Section 4.3 (as modified in Section 4.3.10), is used to analyze the salt spill scenarios with conservative biases described below:

- Reactor Initial Power – The cases initiating from full power conditions will be biased high at a value that accounts for the uncertainty in power measurement.
- Reactivity Parameters
    - Reactivity Coefficients – Coefficients are biased to be the most positive (least negative) to minimize the inherent feedback that would reduce the power during the event.
    - Power Distribution – A top peaked power distribution is applied to result in a high thermal center for the reactor core, which minimizes the coolant flow under natural circulation conditions. A bottom peaked power distribution is applied to calculate the shutdown element worth curve pushing the shutdown worth maximum to a lower location in the reactor core. A hot pebble factor, which conservatively treats the power shape and associated uncertainties, is applied to calculate the highest temperature fuel pebble.
    - Shutdown Margin – The shutdown worth applied assumes the highest worth shutdown element is fully withdrawn from the reactor core to ensure that shutdown margin is minimized in the analysis.
    - Shutdown Element Insertion Time – Insertion time is biased high to slow shutdown and maximize temperatures.
- Reactor Coolant Thermophysical Properties – Coolant properties are biased to maximize the temperature increase by maximizing viscous flow resistance (minimizing flow) and minimizing heat transfer and heat capacity.
- Coolant Average Temperature – Temperatures are biased high to maximize the initial amount of stored energy in the system.
- System Pressure – The system pressure is biased high, which results in higher mass flow rates from the break.
- Heat Generation and Removal Parameters
    - DHRS Capacity – Minimum DHRS performance including single-failure considerations is applied. Minimizing DHRS performance ensures that the heat up is maximized.
    - Decay Heat – Decay heat is maximized to ensure that the heat up is maximized.
    - Material Properties – Biased to maximize the temperature increase by increasing stored energy in the reflector and biasing the coolant properties to increase flow resistance and minimize heat transfer.
- Instrumentation and Control Parameters
    - Reactor Protection System Actuation Delay – The delay in RPS actuations includes instrument response time and actuation delays.
- Anti-Siphon Activation Level – Biased low to delay the onset of natural circulation cooling. The bias includes the uncertainty in the initial Flibe level.

- Inventory Management System Recirculation Flow and Flibe Volume – Biased high to delay the actuation of the RPS level trip.

### 5.5.2 Sensitivities

The entire spectrum of break sizes and locations must be considered to identify the limiting conditions for each release pathway. The limiting event is conservatively modeled as a combination of the most limiting break conditions rather than a single break scenario. The jet breakup conditions assume a break that maximizes aerosol generation, while the spilled pool conditions assume a break that maximizes the volume of Flibe in the pool (i.e., Flibe is instantly discharged at the event initiation). For the release pathways that are included in the MHA, the biases described in Section 5.5.1 are applied to the KP-SAM base model, described in Section 4.3, to perform safety analyses with sensitivities on the following parameters:

- Plant Control Systems – Sensitivities are performed to assess impact of PCS manipulation.
- Bypass Flow Fraction - Sensitivities are performed on the defined flow fraction to cover a sufficient range of bypass flow conditions for the design.

For the limiting postulated salt spill event scenario(s), the peak pebble power and surface temperature are provided as input to a KP-BISON calculation to ensure that the fuel figures of merit are met.

### 5.5.3 Source Term Methods

The grouping structure used to model transport of radionuclides from Flibe is the same as defined for the MHA, including the specified vapor pressures for representative elements (Section 2.2).

A range of break sizes must be evaluated to determine the limiting break size for releases due to mechanical aerosolization and splashing. The limiting break size is determined by using weighted release fractions based on release fractions, breathing rates defined in Reference 33, and a series of $\chi/Q$ values that define the atmospheric release to the EAB, as shown in Equation 5.1.

$$\text{Total RF}_w = \frac{\int_{t=0}^{t_1} \frac{d(RF)}{dt} \times \frac{\chi}{Q} \times B \, dt}{\int_{t=0}^{t_1} \frac{\chi}{Q} \times B \, dt} \tag{5.1}$$

where:

- Total $\text{RF}_w$ is a total integrated weighted release fraction over time (-),
- $t_1$ is 3 days for the weighted RF calculation,
- $\frac{d(RF)}{dt}$ is release fraction rate as time (1/s),
- $\frac{\chi}{Q}$ is dispersion over source value for the EAB that varies with time ($s/m^3$), and
- $B$ is the breathing rate ($m^3/s$) as a function of time at the EAB (Reference 33).

The $\chi/Q$ and breathing rate values are defined independent of the break size, therefore only the release fraction varies for different break sizes and release pathways. The break size with a maximum total weighted release fraction is selected as the limiting break size for each pathway. Therefore, the limiting break size for mechanical aerosol generation and splashing could be different. A small break generally

results in limiting results for both mechanical aerosolization and splashing release pathways, which discharges the Flibe slowly over the duration of the transient. However, the spilled Flibe evaporation pathway still conservatively assumes that Flibe is instantly discharged to the catch pan, resulting in the limiting case for each release pathway.

Releases from mechanical aerosols

Initial Flibe release through a break is modeled as single-phase flow while the Flibe-cover gas interface level is above the siphon break point. Above this point, gas pressure is not enough to overcome the Flibe hydrostatic pressure, which prevents gas flow through the break. There are two siphon break points – the PSP siphon break point for the hot leg side, and the reactor vessel siphon break point for the cold leg side. The PSP anti-siphon allows the cover gas to enter the pump when the salt level reaches the anti-siphon elevation to prevent the Flibe mass from being lost from the hot leg side. The pump quickly de-primes as the cover gas enters the pump. Once the Flibe-cover gas interface level is below the reactor vessel siphon break point, the reactor vessel siphon device creates a passage from the upper plenum to the upper downcomer, which allows cover gas to reach the cold leg and prevents Flibe flow from the reactor vessel to the PHTS.

The PSP anti-siphon is located at a higher elevation than the reactor vessel siphon break point. For a break in the hot leg, the two-phase flow discharge begins when the interface elevation is below the PSP siphon break point. For a break in the cold leg, the two-phase flow discharge begins when the interface elevation is below the reactor vessel siphon break point. The cold leg break is more limiting due to a lower discharge elevation than the hot leg break, which results in a larger amount of total Flibe spilled. Once the interface elevation reaches the reactor vessel siphon break point, no additional Flibe enters the PHTS, and Flibe remaining in the PHTS is then modeled as two-phase discharge. The airborne release fraction is not sensitive to the precise timing of the transition from single phase flow to two-phase flow, because the jet breakup by high void fraction two-phase flow is the dominating factor for the jet breakup airborne release fraction.

The salt spill evaluation model uses the aerosol release models for single-phase jet breakup from Reference 1.

The model for mechanical aerosol generation from two-phase flow uses the empirical correlation for a side break of a pressurized tank from Reference 34 to calculate the mass flow rate of liquid and gas, and the corresponding quality of the two-phase flow. Two-phase flow occurs when the liquid level is between two critical levels: $h_{BGE}$ and $h_{BLE}$ as shown in Figure 5-1.

- $h_{BGE}$ is the height of the liquid level above the mid-elevation of the break where gas entrainment starts
    - If $h_{BGE}$ is less than half of the break diameter, two-phase flow would not begin, even though the break area is exposed to gas. To prevent this nonphysical scenario, $h_{BGE}$ is set to at least half of the break diameter
- $h_{BLE}$ is the height of the liquid level below the mid-elevation of the break where liquid entrainment starts.

Correlations for $h_{BGE}$ and $h_{BLE}$ are shown in Equations 5.2 through 5.5:

$$h_{BGE} = 0.57d(FR_{BGE})^{0.4} \quad (5.2)$$

$$h_{BLE} = -0.87d(FR_{BLE})^{0.31} \quad (5.3)$$

$$FR_{BGE} = \frac{\dot{m}_{l,BGE}}{A\left(gd\rho_l(\rho_l - \rho_g)\right)^{0.5}} \tag{5.4}$$

$$FR_{BLE} = \frac{\dot{m}_{g,BLE}}{A\left(gd\rho_g(\rho_l - \rho_g)\right)^{0.5}} \tag{5.5}$$

where:

- $\rho_l$ is the fluid density (e.g., Flibe) (kg/m$^3$),
- $\rho_g$ is the gas density (i.e., argon) (kg/m$^3$),
- d is characteristic length (i.e., break diameter) (m),
- $\dot{m}_{l,BGE}$ is the single-phase fluid mass flow rate before start gas entrainments (kg/s),
- $\dot{m}_{g,BLE}$ is the single-phase gas mass flow rate after liquid entrainments (kg/s),
- g is acceleration of gravity (9.8 m/s$^2$), and
- A is break flow area (m$^2$).

Correlations for quality and two-phase flow rate are shown in Equations 5.6 through 5.10:

$$x = 0.2\exp\left[\frac{6H(1-11.67H)}{1-H}\right] + 0.8(1-H^2)^{1.3}\left[-0.0122 + \frac{0.42}{1+\left(\frac{\rho_l}{\rho_g}\right)^{0.5}}\right]^H \tag{5.6}$$

$$M = H^2\exp[-1.84H^2(1-H^2)^{1.318}] \tag{5.7}$$

$$H = \frac{h - h_{BLE}}{h_{BGE} - h_{BLE}} \tag{5.8}$$

$$M = \frac{\dot{m}_{2p} - \dot{m}_{g,BLE}}{\dot{m}_{l,BGE} - \dot{m}_{g,BLE}} \tag{5.9}$$

$$\dot{m}_{2p} = M\left(\dot{m}_{l,BGE} - \dot{m}_{g,BLE}\right) + \dot{m}_{g,BLE} \tag{5.10}$$

where:

- $\dot{m}_{2p}$ is the two-phase mass flow rate (kg/s).

The term $\left[-0.0122 + \frac{0.42}{1+\left(\frac{\rho_l}{\rho_g}\right)^{0.5}}\right]$ in Equation 5.6 is a correction for the density ratio dependence on gas entrainment. A higher density ratio means lower gas entrainment resulting in lower quality as expressed

in this term. The liquid versus gas density ratio for Flibe and argon is lower than that of water and air in Reference 34, so the density-dependent term and predicted quality of the Flibe-argon two-phase flow should be smaller than that of water and air. Since this term is empirically fit, it can produce a non-physical negative value for Flibe and argon at high temperatures.

To develop a conservative approximation for the empirical correction factor, the impact of density ratio on quality was evaluated. Four different gas pressures (316 kPa, 378 kPa, 448 kPa, and 517 kPa) were used as boundary conditions in Reference 34 and the resulting quality and density ratios from these conditions were used to derive the correlation. The density-dependent terms from these density ratios range from 0.012 to 0.0185. A higher density ratio term yields higher quality, which is more conservative for aerosol generation. Considering these relations between density ratio and quality, use of the densities of water and air instead of the densities of Flibe and argon is a conservative approach. This is because the Flibe-argon density ratio is lower than water and air. A value of 0.02, is conservatively used for the $\left[-0.0122+\frac{0.42}{1+\left(\frac{\rho_l}{\rho_g}\right)^{0.5}}\right]$ term to bound the test conditions. Additional justification for the use of this approximation is its small impact. Reference 34 shows small deviations between different air pressure test data sets especially at low dimensionless H (i.e., at high quality). Since most aerosol generation during the jet breakup occurs under high quality and void fraction, the impact of the density-dependent term on the overall two-phase jet breakup model is small.

Equation 5.6 is simplified to Equation 5.11:

$$x = 0.2\exp\left[\frac{6H(1-11.67H)}{1-H}\right] + 0.8(1-H^2)^{1.3}[0.02]^H \tag{5.11}$$

$\dot{m}_{l,BGE}$ is calculated using the single-phase release model from Reference 1. $\dot{m}_{g,BLE}$ is calculated using Equation 5.12:

$$\dot{m}_{g,BLE} = (AC_d)\left[2\left(\frac{\gamma}{\gamma-1}\right)P_g\rho_g r^{\frac{2}{\gamma}}\left(1-r^{\frac{\gamma-1}{\gamma}}\right)\right]^{0.5} \tag{5.12}$$

where:

- $\gamma$ is the specific heat ratio, dimensionless,
- r is a pressure ratio, dimensionless (i.e., (enclosure pressure) / (reactor vessel pressure)),
- $P_g$ is a gas pressure (Pa),
- $C_d$ is the orifice coefficient or drag coefficient, dimensionless.

Equation 5.12 is consistent with the gas flow model in Section 5.3.1 of Reference 25.

Two-phase mass flow rate of each phase is calculated using Equations 5.13 and 5.14.

$$\dot{m}_{l,2p} = (1-x)\dot{m}_{2p} \tag{5.13}$$

$$\dot{m}_{g,2p} = x\dot{m}_{2p} \tag{5.14}$$

To derive the Sauter Mean Diameter (SMD) for two-phase flow, the study for a liquid jet injected into a parallel flowing high-velocity gas stream from Reference 35 is utilized. The empirical correlation is defined as follows:

$$\text{SMD}_{2p} = 0.48 d_l^{0.6} \left(\frac{\sigma}{\rho_g (u_r)^2}\right)^{0.4} \left(1 + \frac{\dot{m}_{l,2p}}{\dot{m}_{g,2p}}\right)^{0.4} + 0.15 d_l^{0.5} \left(\frac{\mu_l^2}{\sigma \rho_l}\right)^{0.5} \left(1 + \frac{\dot{m}_{l,2p}}{\dot{m}_{g,2p}}\right) \tag{5.15}$$

Where:

$$d_l = d_0 (1-\alpha)^{0.5}, u_r = u_g - u_l \tag{5.16}$$

$$u_g = \frac{\dot{m}_{g,2p}}{\rho_g A \alpha}, u_l = \frac{\dot{m}_{l,2p}}{\rho_l A (1-\alpha)} \tag{5.17}$$

[[

]] For simplicity, it is assumed that $u_r \sim u_g$, which is conservative as it results in a smaller SMD. From the relation between $u_l$, $u_g$, and $\alpha$ in Equation 5.17, $\alpha$ is derived as shown in Equation 5.18. Accurate estimation of $\alpha$ is difficult since relative velocities between two phases are unknown. Assuming a no-slip condition between liquid and gas, the void fraction ($\alpha$) and no-slip void fraction ($\bar{\alpha}$) are expressed in Equation 5.18:

$$\alpha = \frac{\frac{\dot{m}_{g,2p}}{\rho_g}}{\frac{\dot{m}_{g,2p}}{\rho_g} + \frac{\dot{m}_{l,2p}}{\rho_l}\frac{u_g}{u_l}}, \bar{\alpha} = \frac{\frac{\dot{m}_{g,2p}}{\rho_g}}{\frac{\dot{m}_{g,2p}}{\rho_g} + \frac{\dot{m}_{l,2p}}{\rho_l}} \tag{5.18}$$

The resulting no-slip condition SMD is shown in Equation 5.19:

$$\text{SMD}_{2p} = 0.48 \bar{d}_l^{0.6} \left(\frac{\sigma}{\rho_g \left(\bar{u}_g\right)^2}\right)^{0.4} \left(1 + \frac{\dot{m}_{l,2p}}{\dot{m}_{g,2p}}\right)^{0.4} + 0.15 \bar{d}_l^{0.5} \left(\frac{\mu_l^2}{\sigma \rho_l}\right)^{0.5} \left(1 + \frac{\dot{m}_{l,2p}}{\dot{m}_{g,2p}}\right) \tag{5.19}$$

where:

$$\bar{d}_l = d_0 (1-\bar{\alpha})^{0.5}, \bar{u}_g = \frac{\dot{m}_{g,2p}}{\rho_g A \bar{\alpha}} \tag{5.20}$$

Since $u_g > u_l$, $\alpha < \overline{\alpha}$. Higher $\alpha$ decreases $d_l$, so the second term in Equation 5.19 is lower than the second term in Equation 5.15. It can be proven mathematically that the first term is also lower than the same term in Equation 5.15 for large void fraction, which is the dominant condition of the aerosol generation. Therefore, the simplifications made in Equation 5.19 are indeed conservative because they lead to a smaller SMD.

This two-phase flow SMD is compared with the single phase SMD from Reference 1, and the smaller SMD between the two of them is used in the two-phase flow model.

Once the SMD is calculated, the Rosin and Rammler formula (Reference 36) is utilized to derive the airborne release fraction from the two-phase flow jet break.

The cover gas in the upper plenum is connected to the supply tank, where the pressure and volume of gas is much greater than the upper plenum to maintain cover gas pressure. As gas is discharged through the break, the supply tank pressure gradually decreases until the tank pressure is equal to the upper plenum pressure, at which point the reactor vessel pressure begins decreasing. This depressurization is simulated in the model based on gas mass change.

The salt spill evaluation model uses the aerosol release models for splashing-induced gas entrainment from Reference 1.

Evaporative releases from spilled Flibe

The same evaporation model used for in-vessel releases in the MHA is used to calculate evaporative releases from the spilled Flibe pool. The MHA temperature curve is replaced with a surface temperature curve obtained from the pool cooling model in KP-SAM (Section 14 of Reference 25).

Although spilled Flibe could react with oxygen in the air and potentially form more volatile compounds than those formed by the in-vessel MAR, the application of the Flibe grouping structure (Table 2-1) and evaporative release model, which ignores liquid-side resistance (described in Section 2.2.4), is conservative for the salt spill evaporative releases. While not modeled, at the initiation of a salt spill a monolayer of Flibe will develop at the liquid-vapor interface with a de minimis quantity of radionuclides due to their low concentrations. For oxygen in the air to influence the chemistry of radionuclides in the Flibe, the bulk of the radionuclides must diffuse to the surface to react with the oxygen (i.e., liquid-side mass transfer resistance resistance). This dynamic is slightly different for shallow and deep pools of spilled Flibe:

- For shallow pools of spilled Flibe, a solidified film, or crust, forms rapidly at the liquid-vapor interface. At this point, evaporative mass transport effectively ceases and is therefore de minimis because the cold crust encapsulates the Flibe and the accompanying RNs.
- For deeper pools of spilled Flibe, potential radionuclide reactions with oxygen are de minimis due to the small relative size of the liquid-vapor interface compared to the bulk of the spilled Flibe. Further, the reduced temperature of the cooling spilled Flibe slows down reactions and lowers both equilibrium vapor pressures and liquid side mass transport that drive release as the Flibe transfers heat to the surrounding structures and air.

Because the liquid side mass transport is diffusion kinetics limited, it is conservative to use the Flibe grouping structure in Table 2-1 and evaporative release model without liquid-side resistance as described in Section 2.2.4 to model releases from a Flibe pool.

Releases from spilled Flibe to the gas space are modeled as evaporative releases driven by high-temperature conditions. Radionuclides may migrate from the Flibe to the gas space via either

vaporization or off-gassing as described in Section 2.2.4., with the exception that the number and duration of release intervals are determined by balancing the desire for a relatively few number of release intervals with the need to reduce numerical error associated with the use of constant release rate intervals necessitated by RADTRAD. However, if releases from radionuclides in the salt-soluble fluoride (SSF) group are screened per the isotopic screening methodology described in Section 2.2.5, then evaporative releases from spilled Flibe are not evaluated as a non-MHA release pathway and thus a RADTRAD calculation is not performed. The MHA includes the Flibe inventory in the reactor vessel and PHTS, so the volume of spilled Flibe is accounted for in the MHA's Flibe inventory. Since the SSF group is the only radionuclide group whose transport is impacted by the surface area of the Flibe, the spilled Flibe releases are bound by the MHA if this group is screened from the dose analysis.

Tritium and argon-41 releases from oxidized graphite in the reflector

The salt spill uses the same methods as the MHA to determine tritium and argon-41 inventories in the graphite reflector material pre-transient. The portion of the reflector that could be exposed and is at risk of oxidation during a salt spill is expected to experience low Flibe flow rates, which would preclude significant tritium accumulation. A full and instantaneous release of MAR from the reflector is conservatively assumed.

Gas space transport

Radionuclides released through mechanical aerosol generation, splashing, and spilled Flibe evaporation transport as an aerosol into the gas space, unless the radionuclide decays into a gas during the transient, in which case the decayed fraction of that radionuclide transports as a gas. Off-gassing of noble gases are conservatively modeled as a "puff" release into the gas space. The gases released from the Flibe transport as gases unless they decay into an aerosol during the transient.

The gas space transport is modeled using the same methods as described for the MHA from Reference 1 (See Section 2). The building volume specified for the salt spill is the volume of the reactor cell instead of the reactor cavity volume used for the MHA, due to the location of the spilled Flibe.

## 5.6 PEBBLE HANDLING AND STORAGE SYSTEM MALFUNCTION

The PHSS malfunction event group is described in Section 3.2.6. The PHSS malfunction event is characterized as a transfer line break, which results in an air ingress of the pebble extraction machine (PEM) and the pebble insertion line (PIL). The following event-specific release pathways, which are not included in the MHA analysis, must be considered for this event:

- Fuel kernels of TRISO particles with manufacturing defects or in-service failures resulting in a failed SiC layer are exposed due to pebble oxidation
    - Radionuclides are released as a function of temperature via diffusion models
- TRISO particles with intact SiC layer are dislodged from oxidized fuel pebbles and fall into the Flibe pool via gravity, where the SiC layer is assumed to fail, and the kernels instantly dissolve
    - Radionuclides release via the same Flibe transport groups described in the MHA (see Section 2)
- Graphite dust accumulated in the pebble insertion line during normal operations is resuspended
    - Radionuclides are assumed to "puff" release at the start of the transient
- Tritium and argon-41 releases from oxidized graphite in the reflector and pebble matrix material
- Pebbles that spill outside of the PEM and PIL

As described in Section 3.3.6, the acceptance criteria for release pathways not included in the MHA is the dose figure of merit, to ensure that total releases from the event are bounded by the MHA. The method for determining the dose contribution from release pathways included in the MHA is described in Section 3.3.6. The evaluation model uses the approved methods in Reference 1 to evaluate radionuclide release via diffusion from exposed fuel kernels and releases from dissolved fuel in Flibe. The methods for evaluating releases from graphite dust resuspension, tritium and argon-41 releases from oxidized graphite in the reflector and pebble matrix materials, and for screening releases from other potential dose pathways are described in the following sections.

### 5.6.1 Bias Application

The following assumptions are used to analyze a PHSS transfer line break event:

- Damage to TRISO particles due to mechanical stress (e.g., grinding or ex-vessel drop height) in excess of the fuel qualification envelope is not included in the methods.
- Only MAR from the TRISO particles in fuel pebbles in the PEM and PIL is considered for release. No Flibe MAR is assumed to be held up in fuel or moderator pebble matrix material as Flibe infiltration into pebbles is assumed to be precluded.
- Pebbles in the PEM and PIL are above the Flibe free-surface. These pebbles are at nominal temperatures greater than 400°C and therefore are subject to oxidation. Other pebbles in the PHSS have nominal temperatures below 400°C and are not expected to experience significant oxidation.
- Pebbles in the PEM and PIL are conservatively assumed to oxidize instantaneously to bound oxidation behavior of the pebble carbon matrix material.
- TRISO particles with intact SiC layers that are dislodged from oxidized fuel pebbles fall into the Flibe pool via gravity, where the SiC layer is assumed to fail (if intact at the beginning of the transient), and the kernels instantly dissolve.
- PyC layers are assumed to fail upon oxidation and thus are not credited as a barrier to release.
- The oxidation process is conservatively assumed to cause the pebble temperature to increase 100°C above the nominal PEM/PIL temperature. Due to the low decay heat level of pebbles above the Flibe free-surface, pebbles would only rise above the cover gas temperature due to exothermic oxidation. These pebbles would also be cooled by the incoming cold air, limiting any expected pebble temperature increases.
- Full resuspension of graphite dust accumulated in the pebble transfer line is conservatively assumed to occur, resulting in an effective puff release of the graphite dust MAR.
- Hold-down structures in the reactor vessel (described in Section 1.1.3) keep the graphite reflector sufficiently submerged to ensure that the structural integrity of the reflector is not challenged due to oxidation resulting from air ingress following a break.

The initial conditions of the event are biased to ensure that the maximum amount of MAR is released. The MAR in different barriers (regions) at the start of the transient are identified and quantified so that transient releases of MAR can be evaluated.

Fuel in the PEM and PIL

The MAR in the TRISO particle is retained by the fuel kernel and the three TRISO layers (IPyC, SiC, and OPyC). Each of these layers have varying levels of expected manufacturing defects and predicted in-service failure fractions that impact their radionuclide retention functions pre-transient. All configurations of TRISO particles are assumed to retain their radionuclide inventory during normal operation regardless of the particles expected radionuclide release behavior. This conservatively maximizes the fuel inventory available for release during the transient. Additionally, because the initial

Flibe inventory is modeled with a bounding inventory that accounts for radionuclides that could diffuse from TRISO particles during operations, these releases are effectively double counted.

Fission is neglected in the PEM chamber and screw region due to low flux rates.

The number of pebbles and pebble residence time within the different regions of the vessel, PEM, and PIL are used to determine the amount of MAR available for release during the transient. Pebble decayed inventories are provided by Serpent 2 (Reference 23), and an averaging scheme is used to calculate a representative decayed inventory within key zones to determine treatment in the transient release models.

$$\overline{I_{\text{PEM}}^{\text{Invessel}}} = \frac{I_{\text{PEM}}^{\text{Free-Surface}} + I_{\text{PEM}}^{\text{Vessel Head}}}{2} \tag{5.21}$$

$$\overline{I_{\text{PEM}}^{\text{Exvessel}}} = \frac{I_{\text{PEM}}^{\text{Vessel Head}} + I_{\text{PEM}}^{\text{PEM Exit}}}{2} \tag{5.22}$$

$$\overline{I_{\text{PEM}}^{\text{All}}} = \frac{I_{\text{PEM}}^{\text{Invessel}} \times N_{\text{pebbles}}^{\text{Invessel}} + I_{\text{PEM}}^{\text{Exvessel}} \times N_{\text{pebbles}}^{\text{Exvessel}}}{N_{\text{pebbles}}^{\text{Invessel}} + N_{\text{pebbles}}^{\text{Exvessel}}} \tag{5.23}$$

$$\overline{I_{\text{Oxidized}}^{\text{All}}} = \frac{I_{\text{PEM}}^{\text{All}} \times N_{\text{pebbles}}^{\text{PEM}} + I_{\text{PIL}}^{\text{All}} \times N_{\text{pebbles}}^{\text{PIL}}}{N_{\text{pebbles}}^{\text{PEM}} + N_{\text{pebbles}}^{\text{PIL}}} \tag{5.24}$$

where:

- $I_x^y$ is the inventory at region $x$ and location $y$ and
- $N_{\text{pebbles}}^{\text{z}}$ is the number of pebbles in region $x$.

Graphite Dust Accumulated in the PHSS

The amount of graphite dust accumulated in the PHSS is based on an estimated maximum dust generation rate during normal operation. Pebble activities are weighted over time and number of passes through the core. The graphite dust activity accounts for decay over the operational time in the transfer line. Note that while it is conservative to assume no holdup in the pebble matrix material for other source term analyses, this holdup must be evaluated to determine a conservative activity for the graphite dust.

Activated graphite dust is generated from the outer matrix shell, therefore radionuclides that comprise the graphite dust MAR are grouped and screened based on whether they are considered stable (as defined in Reference 1 or mobile with respect to transport from intact TRISO particles to the outer matrix shell. As with the fuel inventories described above, the graphite dust MAR is determined using the same assumptions for TRISO particle radionuclide retention during normal operations and fission product inventory hold up in pebble matrix material. For the exclusive purpose of calculating graphite dust activities, mobile radionuclides in defective TRISO particles (e.g., manufacturing defects and in-service failures) are conservatively assumed to release completely to the graphite matrix and distribute uniformly in the matrix. This carbon matrix material is assumed to leave the pebble in the form of dust as the pebbles wear while rolling through the PHSS.

The specific activity of graphite dust (in $Bq/g$ of graphite) is obtained through the following equations:

$$\mathrm{SA_{graphite}} = \mathrm{SA_{UCO}} \times \mathrm{f_{Fuel}} \times \frac{\mathrm{V_{UCO}} \times \rho_{\mathrm{UCO}} \times \mathrm{f_{defect}}}{\mathrm{V_{graphite}} \times \rho_{\mathrm{graphite}}} \quad (5.25)$$

$$SA_{\mathrm{graphite}} = \frac{A_{\mathrm{UCO}} \times f_{\mathrm{Fuel}} \times V_{\mathrm{UCO}} \times f_{\mathrm{defect}}}{V_{\mathrm{graphite}} \times \rho_{\mathrm{graphite}}} \quad (5.26)$$

Where:

- $\rho_{\mathrm{UCO}}$ is the density of uranium oxycarbide, expressed in the unit of g/cc.
- $\rho_{\mathrm{graphite}}$ is the density of the graphite pebble, expressed in the unit of g/cc.
- $V_{\mathrm{UCO}}$ is the volume of uranium oxycarbide, expressed in the unit of cc.
- $V_{\mathrm{graphite}}$ is the volume of the graphite pebble, expressed in the unit of cc.
- $A_{\mathrm{UCO}}$ is the activity per unit volume of uranium oxycarbide, expressed in the unit of Bq/cc.
- $f_{\mathrm{defect}}$ is the fraction of the defective particles whose activity is incorporated in the graphite dust activity (i.e., SiC layers, exposed kernels, and heavy metal contamination).
- $f_{\mathrm{Fuel}}$ is the fraction of fueled pebbles.
- $SA_{\mathrm{UCO}}$ is the specific activity of uranium oxycarbide, expressed in the unit of Bq/g of graphite.

### 5.6.2 Source Term Methods

The objective of the analysis of the PHSS break event is to evaluate key figures of merit for the event, so that the dose consequence can be assessed and demonstrated as being bounded by the consequence of the MHA.

As stated in Section 5.6, these methods only account for release pathways that are not accounted for in the MHA analysis. The methodology for analyzing dose consequences from MHA release pathways is described in Section 3.3.6 and is combined with the dose consequences from the non-MHA release pathways to demonstrate that total doses from the PHSS break events remain bounded by the MHA.

Releases from exposed TRISO kernels via diffusion

Exposed kernels are retained in the oxidized pebble matrix above the Flibe free-surface at an assumed pebble extraction machine and pebble insertion line gas-space temperature of 650°C (100°C hotter than the nominal PEM/PIL pebble temperature), rather than dropping into the Flibe.

Due to the small exposed-kernel fraction, the assumption that these particles do not drop into the Flibe does not significantly reduce evaporative releases from Flibe and allows for a diffusion path of radionuclides out of the pebbles. The kernel grouping structure and models for radionuclide transport via diffusion are consistent with Reference 1 and the MHA (Section 2.2.2). If these releases do not screen, then the time-dependent evaporative release fractions are simplified into a series of constant release intervals, where the number and duration of release intervals are determined by balancing the desire for a relatively few number of release intervals with the need to reduce numerical error associated with the use of constant release rate intervals necessitated by RADTRAD.

Releases from dissolved TRISO particles in Flibe via evaporation and off-gassing

TRISO particles that drop into the Flibe from oxidized pebbles in the PEM and PIL are assumed to submerge before dissolving, and the associated radionuclides are assumed to mix homogenously with

the Flibe in the vessel and subsequently transport from the Flibe using the same radionuclide grouping structure as described for the MHA (Table 2.1).

It is conservative to assume that the TRISO particles with intact SiC layers at the start of the transient drop in to the Flibe rather than remain suspended above the Flibe free-surface (and thereby undergoing a temperature-driven diffusion through the kernel and SiC layer). This is due to the assumed instantaneous failure of the SiC layer in contact with the Flibe, which leads to releases of volatile materials and gasses that would otherwise undergo diffusion through the kernel and SiC layer.

Releases from Flibe to the gas space are modeled as evaporative releases due to the prolonged high temperature conditions. The solubility of radionuclides in Flibe is evaluated as described in Section 2.2.4 to confirm a dilute solution. Radionuclides may migrate from the Flibe to the gas space during the transient via either vaporization or off-gassing as described in Section 2.2.4. A time-temperature curve must be specified for the hot well following the break to model evaporative releases. Time-dependent evaporative release fractions are simplified into a series of constant release intervals, where the number and duration of release intervals are determined by balancing the desire for a relatively few number of release intervals with the need to reduce numerical error associated with the use of constant release rate intervals necessitated by RADTRAD.

Releases from graphite dust resuspension

The full radionuclide inventory of the graphite dust accumulated in the pebble transfer line as described in Section 5.6.1 is conservatively assumed to puff release to the gas space at the initiation of the transient.

Tritium and argon-41 releases from oxidized graphite in the reflector and pebble matrix material

The pebble transfer line break event uses the same methods as the MHA to determine tritium and argon-41 inventories in the graphite reflector and pebble matrix material pre-transient. The portion of the reflector that could be exposed and is at risk of oxidation during a pebble transfer line break is expected to experience low Flibe flow rates, which would preclude significant tritium accumulation. A full and instantaneous release of MAR from the reflector and oxidized pebbles is conservatively assumed.

Gas space transport

Gas space transport includes building transport and atmospheric dispersion. The gas space transport is modeled using the same methods as described for the MHA from Reference 1 (See Section 2).

## 5.7 RADIOACTIVE RELEASE FROM SUBSYSTEM OR COMPONENT

A radioactive release could result from the failure of a subsystem or component containing radioactive material that is outside of the functional containment (i.e., Flibe coolant and TRISO fuel). This section describes how releases from these subsystems and components are evaluated. These methods can be used to evaluate releases from individual subsystem or component failures, or combined failures that could result from internal or external hazards. Although internal and external hazard events are outside the scope of this topical report, this section describes how combined failures are evaluated for subsystems and components. The limiting event in this group is expected to be a seismic event, which results in a failure of the subsystems and components not designed to withstand the design basis earthquake (i.e., tritium management system, chemistry control system, radioactive waste handling and storage systems).

The MAR contained in subsystems and components in this event group is assumed to puff release at the transient initiation. As discussed in Section 2.2.5, this approach produces conservative estimates of TEDE doses at the EAB compared to the expected RADTRAD result because it ignores two-hour building holdup and associated radioactive decay, and it ignores delayed releases of radionuclides (i.e., all radionuclides are released at the beginning of the transient).

Therefore, the evaluation model is composed of the methods for establishing MAR inventories and combining releases from multiple subsystem or component failures, and the gas space transport model from Reference 1, as described in Section 2 for the MHA.

Key isotopes are identified for each source of MAR. In order to facilitate dose calculations, a representative “effective” isotope is designated for each source of MAR. The effective isotope activities represent the amount of that effective isotope that alone would produce the same TEDE dose as the combined activities of the identified key isotopes for each source of MAR.

The acceptance criteria for this group is the dose figure of merit from the sources of MAR for release during the limiting event. Radionuclide inventories of subsystems or components included in this event group are administratively controlled where feasible, or the potential inventory is conservatively bound to ensure that the dose acceptance criteria are not exceeded.

**Table 5-1: Core Design Analysis Inputs to Event-Specific Methods**

| Parameter | Purpose |
|---|---|
| Reactivity coefficients[1] | KP-SAM input |
| Reactor kinetics[1] | KP-SAM input |
| Integral and differential element worth[1] | KP-SAM input |
| Nominal axial power distribution[2] | KP-SAM input for reactivity coefficient weighting |
| Top-skewed power distribution[2] | Used in KP-SAM to reduce natural circulation flow rate |
| Bottom-skewed power distribution[2] | KP-SAM input for determining rate of negative reactivity insertion from shutdown elements |
| Maximum radial power peaking factor<br>- Non-RIE and symmetric withdrawal events (all element out or control element inserted)[1,2]<br>- Asymmetric withdrawal events[1,3] | HPF ($F_1$ subfactor) and reflector temperature surrogate ($RPF_{max}$) |
| Maximum pebble peaking factor<br>- Non-RIE and symmetric withdrawal events[1,2]<br>- Asymmetric withdrawal events[1,3] | HPF (direct $F_2$ subfactor) and KP-BISON input for pebble power |
| Minimum flow factor (all element out)[4] + discretionary conservatism | HPF (direct $F_2$ subfactor) and reflector temperature surrogate (FF) |

1. Includes core design nuclear reliability factors (NRFs) from Reference 23
2. From 2-D static core design analysis
3. From 3-D static core design analysis (includes azimuthal effects)
4. [[ ]]

**Figure 5-1: Representative Side Break Two-Phase Flow Model**

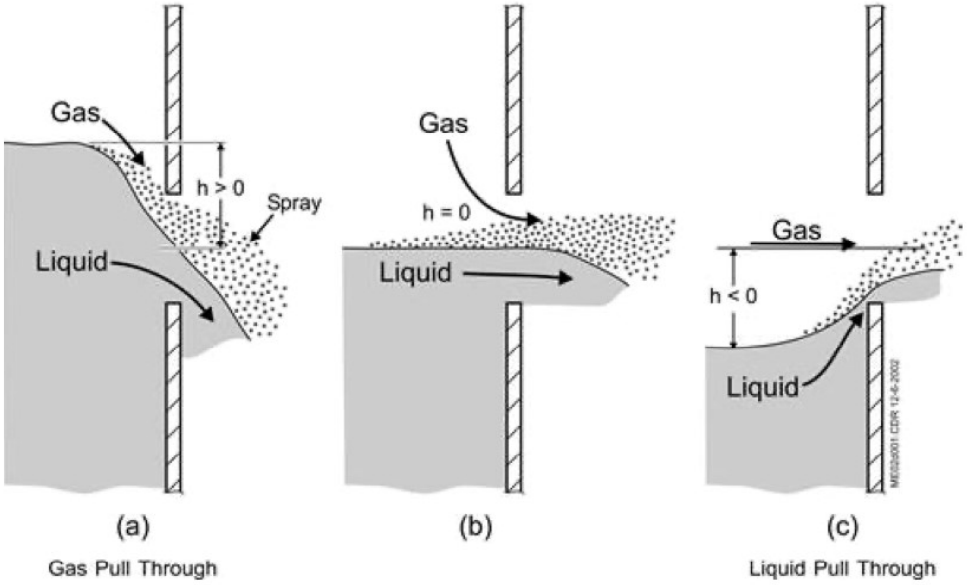

# 6 CONCLUSIONS AND LIMITATIONS

## 6.1 CONCLUSIONS

This report documents a safety analysis methodology to evaluate an MHA and postulated events to ensure that the dose consequences of a KP-FHR test reactor facility remain below acceptable limits. Kairos Power is requesting NRC approval of this methodology (subject to the limitations in Section 6.2 below) for use by licensing applicants of a KP-FHR test reactor as an appropriate means to evaluate such analyses as required by 10 CFR 100.11 (as referenced by 10 CFR 50.34(b)(1)), and KP-FHR PDC 19.

## 6.2 LIMITATIONS

This section describes limitations on the use of the safety analysis methodology presented in this topical report. Each limitation must be addressed in future licensing submittals.

1 The methodologies in this report are applicable to the postulated event groups described in Section 3.2. Methods needed to support evaluation of postulated event groups not listed in Section 3.2 must be provided to complete the safety analysis methodology.
2 The methodologies described in the report do not address the potential for or consequences of the Flibe coolant freezing within the reactor vessel.
3 Validation and code assessment results must be provided for the phenomena described in Section 4.2. The code assessment will also confirm or update the base model inputs described in Section 4.3.
4 The methodologies described in this report do not address the potential for generation of flammable gas due to graphite oxidation in the reactor vessel following an air ingress scenario.
5 The methodology presented in this topical report is based on design features of a KP-FHR provided in Section 1.1. Deviations from these design features will be justified by an applicant using these methods in other licensing submittals.
6 The methodologies described in this report do not address evaluation of peak temperatures for metallic materials inside of the pebble bed (i.e., shutdown elements).

# 7 REFERENCES

1. Kairos Power LLC, *KP-FHR Mechanistic Source Term Methodology*. KP-TR-012-P-A. May 2022.
2. University of California Berkeley Nuclear Engineering. 2015. *Fluoride Salt Cooled High Temperature Reactor*. [ONLINE] Available at: http://fhr.nuc.berkeley.edu. (Accessed April 23, 2024).
3. Kairos Power LLC, *Design Overview of Kairos Power Fluoride Salt Cooled, High Temperature Reactor*. KP-TR-001, Revision 1. February 2020.
4. Kairos Power LLC, *Reactor Coolant for the Kairos Power Fluoride Salt-Cooled High Temperature Reactor*, KP-TR-005-P-A. July 2020.
5. U.S. Nuclear Regulatory Commission, "Transient and Accident Analysis Methods," Regulatory Guide 1.203. December 2005.
6. Kairos Power LLC, *Principal Design Criteria for the Kairos Power Fluoride Salt-Cooled, High Temperature Reactor*, KP-TR-003-NP-A. May 2020.
7. G. M. Watson, R. B. E. III, W. R. Grimes, and N. V. Smith, "Solubility of Noble Gases in Molten Fluorides: In Lithium-Beryllium Fluoride," Journal of Chemical and Engineering Data, vol. 7, no. 2, 1962.
8. M.F. Young, "MELCOR Fission Product Release Model for HTGRs," SAND2010-0800C, Sandia National Laboratories, 2010.
9. B. J. Lewis, D. Evens, F. C. Iglesias, and Y. Liu, "Modelling of Short-Lived Fission Product Release Behavior During Annealing Conditions," Journal of Nuclear Materials, vol. 238, pp. 183–188, 1996.
10. "High Temperature Gas Cooled Reactor Fuels and Materials," International Atomic Energy Agency, Vienna, IAEA-TECDOC-1645, 2010.
11. O. Redlich and A. T. Kister, "Algebraic Representation of Thermodynamic Properties and the Classification of Solutions," Industrial and Engineering Chemistry, vol. 40, no. 2, pp. 345-348, 1948, doi: 10.1021/ie50458a036.
12. M. Newton, A. Merwin, J. W. McMurray, and M. Simpson, "Effect of metal chloride impurities on equilibrium potential of iron in molten LiCl-KCl (in review)," Journal of The Electrochemical Society, 2023.
13. NOT USED.
14. L. L. Humphries, V. G. Figueroa, M. F. Young, D. Louie, and J. T. Reynolds, "MELCOR Computer Code Manuals Vol. 1: Primer and Users' Guide," SAND2015-6691, Sandia National Laboratories, 2015.
15. D. R. Lide, CRC Handbook of Chemistry and Physics. CRC press, 1992.
16. M. Chase, "Journal of Physical and Chemical Reference Data, NIST-JANAF Thermochemical Tables," American Chemical Society and American Institute of Physics, Washington DC, 1998.
17. R. C. Reid, J. M. Prausnitz, and B. E. Poling, "The properties of gases and liquids," 1987.
18. N. Saunders and A. P. Miodownik, CALPHAD (calculation of phase diagrams): a comprehensive guide. Elsevier, 1998.
19. B. Sundman, H. Lukas, and S. Fries, *Computational thermodynamics: the Calphad method*. Cambridge University Press, Cambridge, 2007.

20. D. R. Stull, *JANAF Thermochemical Tables*. Clearinghouse, 1965.
21. U.S. Nuclear Regulatory Commission, "Atmospheric Relative Concentrations for Control Room Radiological Habitability Assessments at Nuclear Power Plants," Regulatory Guide 1.194. June 2003.
22. Kairos Power LLC, *KP-FHR Fuel Performance Methodology*. KP-TR-010-P-A. May 2022.
23. Kairos Power LLC, *KP-FHR Core Design and Analysis Methodology*. KP-TR-024-P, Revision 0. April 2024.
24. Kairos Power LLC, *Metallic Materials Qualification for the Kairos Power Fluoride Salt-Cooled High-Temperature Reactor Topical Report*. KP-TR-013-P-A. April 2023.
25. R. Hu, L. Zou, G. Hu, D. Nunez, T. Mui, and T. Fei, "SAM Theory Manual," ANL/NSE-17/4, Revision 1. Argonne National Laboratory, February 2021.
26. R. Hu, L. Zou, G. Hu, "SAM User's Guide," ANL/NSE-19/18. Argonne National Laboratory, August 2019.
27. Kairos Power LLC, *KP-SAM Theory Manual*. KP-RPT-000231, Revision 0. August 2023.
28. Kairos Power LLC, *KP-SAM Users Guide*. KP-RPT-000226, Revision 0. August 2023.
29. L. Cheng, A. Hanson, D. Diamond, J. Xu, J. Carew, D. Rorer, *Physics and Safety Analysis for the NIST Research Reactor*, BNL-NIST-0803, Rev. 1, March 2004.
30. Kairos Power LLC, *Scaling Methodology for the Kairos Power Testing Program*. KP-TR-006-P-A. June 2020.
31. W. Oberkampf and C. Roy, *Verification and Validation in Scientific Computing*, 2010.
32. Kairos Power LLC, *Instrument Setpoint Methodology for the Kairos Power Fluoride Salt-Cooled High-Temperature Reactor*. KP-TR-021-NP-A. April 2024.
33. U.S. Nuclear Regulatory Commission, "Alternative Radiological Source Terms for Evaluating Design Basis Accidents at Nuclear Power Reactors," Regulatory Guide 1.183, Revision 1. October 2023.
34. I. G. Hassan, H. M. Soliman, G.E. Sims, and J. E. Kowalski, "Two-phase flow from a stratified region through a small side branch," Journal of Fluids Engineering, vol. 120, no. 3, pp. 605–612, 1998.
35. N. K. Rizk and A. H. Lefebvre, "Spray characteristics of plain-jet airblast atomizers," Journal of Engineering for Gas Turbines and Power, vol. 106, no. 3, pp. 634–638, 1984.
36. M. Epstein and M. Plys, "Prediction of aerosol source terms for DOE site facility applications," Proc. EFCOG Safety Analysis Working Group, pp. 15, 2006.
37. K. Wagner, "MELCOR Accident Progression and Source Term Demonstration Calculations for a FHR," SAND2022-2751, Sandia National Laboratories, 2022.
38. Kairos Power LLC, Fuel Qualification Methodology for the Kairos Power Fluoride Salt-Cooled High Temperature Reactor (KP-FHR). KP-TR-011-P-A. March 2023.
39. N. Todreas and M. Kazimi, Nuclear Systems II: Elements of Thermal Hydraulic Design. Hemisphere Publishing Corporation, 2001.
40. C. Barton, "SOLUBILITY OF PLUTONIUM TRIFLUORIDE IN FUSED-ALKALI FLUORIDE—BERYLLIUM FLUORIDE MIXTURES," The Journal of Physical Chemistry, vol. 64, no. 3, pp. 306-309, 1960.

41. F. Incropera, D. Dewitt, T. Bergman, and A. Lavine, Fundamentals of Heat and Mass Transfer, 7th ed. Wiley, 2011.

42. U.S. Nuclear Regulatory Commission, Canadian Nuclear Safety Commission, “U.S. NRC-CNSC Memorandum of Cooperation FINAL REPORT concerning Tristructural Isotropic (TRISO) Fuel Qualification,” ML20336A052. 2023.

# APPENDIX A. Example Calculations

The sample calculations included in this appendix do not represent final design information but are provided to illustrate a generic system response for selected transients. Kairos Power is not asking for NRC review and approval of these sample calculations in a safety evaluation report.

## A.1 Loss of Forced Circulation (Locked Rotor)

An example calculation for the locked rotor event is initiated from a high power, high temperature operating condition. A high power of [[ ]] represents full power plus [[ ]] uncertainty. The results of the example calculation are shown for the event initiation (first three minutes) to demonstrate the initial event progression and safety system response, and over a longer term (72 hours) to demonstrate long term heat-up and cool-down behavior.

Event Initiation

Figure A.1-1 shows the event initiated by the loss of head delivered by the PSP and Figure A.1-2 shows the corresponding drop in flow through the PHTS. Figure A-3 demonstrates the rapid flow reversal through the natural circulation path (NCP) to establish natural circulation flow. The loss of forced circulation causes a heat-up shown in Figure A.1-4 through Figure A.1-7. The heat-up leads to negative reactivity feedback and a reduction in reactor power, shown in Figure A.1-8 and Figure A.1-9, respectively. A preliminary high hot well temperature analytical limit of [[ ]] is reached in [[ ]] with a subsequent RPS actuation initiated [[ ]] seconds later (see Figure A.1-10). For these example calculations, preliminary RPS actuation delays of [[ ]] seconds for nuclear instrumentation and [[ ]] seconds for all other instrumentation are used.

[[

]]

**Figure A.1-1: Locked Rotor - PSP Head**

[[

]]

**Figure A.1-2: Locked Rotor – PHTS Flow**

[[

]]

**Figure A.1-3: Locked Rotor – NCP Flow**

[[

]]

**Figure A.1-4: Locked Rotor – Hot Well Temperature**

[[

]]

**Figure A.1-5: Locked Rotor – Hot Leg and Cold Leg Temperatures**

[[

]]

**Figure A.1-6: Locked Rotor – Max TRISO Temperature**

[[

]]

**Figure A.1-7: Locked Rotor – Reflector Temperatures**

[[

]]

**Figure A.1-8: Locked Rotor – Reactivity**

[[

]]

**Figure A.1-9: Locked Rotor – Reactor Power**

[[

]]

**Figure A.1-10: Locked Rotor – RPS Actuation**

Event Initiation

Following the initial phase of the locked rotor event, the reactor experiences a long heat-up period until the heat removed by the DHRS exceeds the decay heat generated by the reactor core. The DHRS model consists of an annular heat structure surrounding the vessel, which uses an outer surface temperature boundary condition of [[ ]] to simulate energy lost to boiling. The inner wall of the DHRS annulus is radiatively coupled to a segment of the outer vessel wall, VSLW1, which extends from the diverging region of the core up to the NCP. Both surfaces are assigned emissivity values of [[ ]] , and the view factor from VSLW1 to the DHRS is artificially tuned to remove [[ ]] % of full reactor power while maintaining the peak vessel temperature below 730°C.

Figure A.1-11 shows that flow stagnates in the PHTS and that flow through the NCP decreases over the first few hours of the event before reaching a stable long term flow rate that decreases with reducing decay heat. Figure A.1-12 shows that all heat removal from the reactor is through the DHRS over the long term and Figure A.1-13 shows the balance between heat generation and heat removal during the event. Figure A.1-13 specifically shows that, with minimum DHRS performance, the heat removal through the DHRS exceeds the decay heat generation approximately [[ ]] hours into the event. Comparing against the Safety Analysis Acceptance Criteria provided in Section 3.3:

- The acceptance criterion from Section 3.3.1 for peak TRISO SiC temperature is met because Figure A.1-15 demonstrates that peak TRISO temperature remains well below 1600°C. Confirmation of this criterion would be provided in downstream KP-BISON analysis.
- The acceptance criterion form Section 3.3.2 for power pulse width is not applicable because no power pulse occurs as shown in Figure A.1-9.

- The acceptance criterion from Section 3.3.3 for fuel release fraction would be addressed through downstream KP-BISON analysis.
- The acceptance criterion from Section 3.3.4 for peak vessel temperature is met because Figure A.1-14 shows that the peak vessel temperature is maintained well below 750°C (max vessel temperature reached is approximately [[ ]] ).
- The acceptance criterion from Section 3.3.5 for peak structure graphite temperature is met because Figure A.1-16 demonstrates that the peak reflector temperature remains well below the transient limit of 950°C.
- The acceptance criterion from Section 3.3.6 for dose consequences would require additional justification. Figure A.1-15 through Figure A.1-17 demonstrate that peak TRISO, peak reflector, and Flibe free-surface temperatures remain below the prescribed MHA temperatures. However, when considering the HPF and peak temperature surrogate for the reflector, TRISO and max reflector temperatures are expected to exceed the prescribed MHA temperature profiles from Figure 2-1. The transient temperatures shown in Figure A.1-15 through A.1-17 are used to inform bounding primary system event temperature profiles which are used to calculate bounding primary system event dose consequences for comparison against the MHA and used in the dose consequence evaluation for spills and leaks.

The full range of parameter sensitivities are to be performed in the calculations that implement this methodology. Additionally, example analyses are limited to KP-SAM calculations. Full application of the methodology involves application of the HPF, fuel performance analysis in KP-BISON, and the application of temperature surrogates for peak vessel and reflector temperatures.

[[

]]

**Figure A.1-11: Locked Rotor – PHTS and NCP Flow (Long Term)**

[[

]]

**Figure A.1-12: Locked Rotor – Heat Removal (Long Term)**

[[

]]

**Figure A.1-13: Locked Rotor – Heat Generation and Removal (Long Term)**

[[

]]

**Figure A.1-14: Locked Rotor – Reactor Vessel Temperature (Long Term)**

[[

]]

**Figure A.1-15: Locked Rotor – Max TRISO Temperature (Long Term)**

[[

]]

**Figure A.1-16: Locked Rotor – Max Reflector Temperature (Long Term)**

[[

]]

**Figure A.1-17: Locked Rotor – Max Flibe Free-Surface Temperature (Long Term)**

## A.2 Reactivity-Initiated Event (Ramp Insertion)

An example calculation for a reactivity-initiated event is performed for a reactor in a startup/low-power condition. A ramp insertion of reactivity that corresponds to the worth of all control elements is inserted linearly over [[ ]] seconds. Figure A.2-1 shows the ramp insertion of reactivity is accurately captured and that the inherent feedback mechanisms (i.e., Doppler, Moderator, Coolant, and Reflector) are not significant because temperatures changes are not significant. The reactor power is shown in Figure A.2-2 and shows that reactivity insertion results in a rapid power increase until an RPS actuation on high flux rate, shown in Figure A.2-3, results in the insertion of RSS elements and shuts down the reactor.

A preliminary rate trip rate trip analytical limit is selected to be [[ ]] per second (this is equivalent to a rate of [[ ]] Decades per Minute [DPM]), which is reached in [[ ]] s with a subsequent RPS actuation initiated at [[ ]] s (power rate shown in Figure A.2-4). The resulting maximum power reached during the event is approximately [[ ]] kW. Temperatures for the fuel, shown in Figure A.2-5, remain relatively unchanged during the event because the power increase is arrested before high levels are reached (this temperature behavior is exhibited for all structures). Accordingly, significant margin is exhibited to the limits for all structures. Additionally, the energy deposition occurs over a time period much longer than 1 s. The preliminary analytical limit demonstrates large margin to the acceptance criteria for the fuel, reflector, and vessel.

[[

]]

**Figure A.2-1: Ramp Reactivity Insertion – Reactivity**

[[

]]

**Figure A.2-2: Ramp Reactivity Insertion – Reactor Power**

[[

]]

**Figure A.2-3: Ramp Reactivity Insertion – RPS Actuation**

[[

]]

**Figure A.2-4: Ramp Reactivity Insertion – Power Rate**

[[

]]

**Figure A.2-5: Ramp Reactivity Insertion – Max TRISO Temperature**

## A.3 Salt Spill

This section provides an example analysis of a salt spill postulated event. In the following subsections:

- MAR is identified,
- Release pathways are identified,
- Inputs and boundary conditions to the jet breakup and splashing release models are defined,
- Thermal-fluid behavior in the system is summarized,
- Release fractions are evaluated for limiting breaks for splashing and jet breakup,
- Inputs and boundary conditions for the spilled Flibe evaporation release pathway are identified,
- Release fractions from spilled Flibe evaporation are evaluated,
- Gas space transport model inputs are defined, and
- Dose consequences are reported.

Identification of MAR for the Salt Spill Event

The MAR evaluated for release in the salt spill event is the entire Flibe inventory in the PHTS and the Flibe inventory in the vessel located above the primary salt pump anti-siphon feature.

Identification of Release Pathways for the Salt Spill Event

The release pathways evaluated for the salt spill are described in Section 5.5, including single- and two-phase jet breakup, splashing of Flibe on surfaces, and evaporation of radionuclides from spilled Flibe. Note that this example analysis includes Flibe releases during the break event but does not include an evaluation of the tritium and argon-41 releases from oxidized reflector graphite.

Each pathway is first evaluated using the isotopic screening methodology described in Section 2.2.5. This evaluation involves first calculating the time-dependent pathway release fractions over the duration of the break and then integrating those release fractions into a cumulative release fraction for use in screening analysis. The screened-in isotopes from pathways that remain then use the time-dependent pathway release fractions to provide the inputs to RADTRAD to calculate 30-day TEDE dose consequences at the EAB for comparison to the MHA.

Inputs to the Jet Breakup and Splashing Release Pathways for the Salt Spill Event

Initial and boundary conditions used in the analysis of jet breakup and splashing release fractions are provided in Table A.3-1. These inputs are required to calculate the time-dependent release fractions for the jet breakup and splashing release pathways.

**Table A.3-1: Initial and Boundary Conditions for Jet Breakup and Splashing**

| Parameter | Value |
|---|---|
| Cover Gas Temperature (°C) | [[ ]] |
| Cover Gas dP (psig) | [[ ]] |
| Gas Tank Pressure (bar) | [[ ]] |
| Gas Tank Volume ($m^3$) | [[ ]] |
| Discharge Coefficient | 0.61[2] |
| Gas Tank Temperature (°C) | [[ ]] |
| Flibe Temperature (°C) | [[ ]] |
| Flibe Volume in PHTS ($m^3$) | [[ ]] |
| PHTS Pipe Diameter (m) | [[ ]] |
| Jet Falling Height (m) | [[ ]] |
| Pump dP (Pa) | [[ ]] |
| Nominal Flibe Level from Top of Vessel (m) | [[ ]] |
| Pump Trip Level from Top of Vessel (m) | [[ ]] |
| Pump Anti-Siphon Level from Top of Vessel (m) | [[ ]] |
| RV Anti-Siphon Level from Top of Vessel | [[ ]] |
| Flibe Volume from Pump Trip to Nominal Level ($m^3$) | [[ ]] |
| Flibe Volume from Pump Anti-Siphon to Trip Level ($m^3$) | [[ ]] |
| Flibe Volume from RV Anti-Siphon to Pump Anti-Siphon Level ($m^3$) | [[ ]] |

[1]Cover gas temperature will be between room temperature and Flibe temperature due to continual gas supply from an uninsulated gas tank and heat transfer with Flibe. Flibe temperature is conservatively used.
[2]Flow loss coefficient is a typical value for circular orifices.
[3]The gas tank is located outside of the reactor cell, and no insulation is credited. However, this parameter has a negligible impact on the results.
[4]Maximum PHTS elevation.

The EAB X/Qs and breathing rates are required to calculate the weighted release fractions using Equation 5.1 (see Table A.3-2). The screening analysis uses the first two-hour values from this table.

**Table A.3-2: EAB (250 m) X/Qs for the Site**

| Time Interval (hrs) | X/Q ($s/m^3$) | Breathing Rate ($m^3/s$) |
|---|---|---|
| 0-2 | 1.5e-04 | 3.5e-04 |
| 2-8 | [[ ]] | 3.5e-04 |
| 8-24 | [[ ]] | 1.8e-04 |
| 24-96 | [[ ]] | 2.3e-04 |
| 96-720 | [[ ]] | 2.3e-04 |

The spill is assumed to occur in the reactor cell with an assumed gas volume of [[ ]] $m^3$.

Evaluation of the Thermal Fluid Response to the Salt Spill

The thermal fluid response of the bounding break size (as determined in the following sections) is provided in Figures A.3-1 and A.3-2 using the inputs and boundary conditions from Table A.3-1. Figure A.3-1 shows the Flibe/cover gas interface level in the upper plenum versus time until the level reaches the reactor vessel anti-siphon level. Figure A.3-2 shows the differential pressure from the PHTS to the enclosure. The pump head is added to the differential pressure before the interface level reaches the pump anti-siphon level. Once the interface level reaches the pump anti-siphon level, the pump is assumed to be de-primed. The differential pressure from this point forward is the cover gas gauge pressure.

[[

]]

**Figure A.3-1: Jet Breakup Limiting Diameter – Flibe Level in Upper Plenum versus Time**

[[

]]

**Figure A.3-2: Jet Breakup Limiting Diameter – Pressure Differential versus Time**

These values are evaluated for a range of break diameters. The break diameter impacts various components of the transient including the rate at which Flibe spills into the reactor cell, the time-dependent two-phase flow conditions, and the Flibe parameters (e.g., density, viscosity, surface tension) which are used to determine the mechanical aerosolization release fractions.

Evaluation of Releases from Splashed Flibe

The time-dependent release fractions from mechanical aerosol generation due to Flibe splashing are calculated as described in Section 5.5.3 using the inputs and boundary conditions from Table A.3-1. This calculation involves determining the exit velocity of the Flibe as a function to time to determine the impact velocity of the Flibe on the pool, per the aerosol release models for splashing-induced gas entrainment from Reference 1.

These time-dependent release fractions are then combined with the values from Table A.3-2 to calculate the weighted release fraction from splashing for various break diameters (up to a hypothetical double-ended guillotine break) using Equation 5.1. The resulting weighted RF is shown in Table A.3-2 for each

break diameter. The limiting break diameter (i.e., highest weighted RF) for splashing from the spectrum of break sizes in Table A.3-3 is shown to be [[ ]] meters in this example.

**Table A.3-3: Calculated Weighted RF from Splashing for Various Break Diameters**

[[

]]

Conservative dose assessments are conducted using the weighted release fraction for the limiting break diameter, and the five highest TEDE dose isotopes are reported in Table A.3-4. Note that the cumulative weighted release fraction over the duration of the transient is hypothetically assumed to be instantly released at transient initiation for the scoping analysis. As shown in Table A.3-4, the top five highest TEDE dose isotopes are below the 0.001 rem screening threshold. Therefore, detailed modeling of these release pathways in RADTRAD is not performed, and the pathway is screened out.

**Table A.3-4: Screening Isotopic Doses for Splashed Flibe**

[[

]]

Releases from mechanical aerosols due to jet breakup

The time-dependent release fractions from mechanical aerosol generation due to jet breakup are calculated as described in Section 5.5.3 using the inputs and boundary conditions from Table A.3-1. These time-dependent release fractions are then combined with the values from Table A.3-2 to calculate the weighted release fraction from jet breakup for various break diameters (up to a hypothetical double-ended guillotine break) using Equation 5.1. The resulting weighted RF is shown in Table A.3-5. The limiting break diameter (i.e., highest weighted RF) for the jet breakup is [[ ]] meters.

**Table A.3-5: Weighted RF for Jet Breakup from Various Break Diameters**

[[

]]

The aerosol mass generation rate and Flibe mass discharge rate are calculated for every break diameter in Table A.3-5 to determine the time-dependent release fractions. Figure A.3-3 shows the aerosol mass generation rate and the Flibe mass discharge rate for the limiting break diameter for jet breakup. Figure A.3-4 shows the cumulative release fraction versus time for this limiting break diameter. There is a single radionuclide group for jet breakup aerosol generation (i.e., all radionuclides are assigned the same release fraction). The jet breakup cumulative release fraction is [[ ]] for the limiting break size, and this RF is applied to all radionuclides. The jet breakup cumulative release fraction equals the cumulative aerosol generation amount divided by the amount of possible spilled Flibe, which is a sum of the Flibe volume in the PHTS and in the upper plenum above RV anti-siphon level. Note that this cumulative release fraction is larger than the weighted release fraction in Table A.3-5 because it does not include the weighting from changing breathing rates and X/Qs with time.

[[

]]

**Figure A.3-3: Jet Breakup Limiting Diameter – Aerosol Mass Generation Rate and Flibe Mass Discharge Rate**

[[

]]

**Figure A.3-4: Jet Breakup Limiting Diameter – Cumulative Release Fraction**

Table A.3-6 shows the screening dose contributions from individual isotopes. The isotopic screening threshold of 0.001 rem is used for determining which isotopes are used in the RADTRAD analysis.

**Table A.3-6: Screening Isotopic Doses for Jet Breakup**

[[

]]

Time-dependent release fractions are simplified into a series of constant release intervals, where the number and duration of release intervals are determined by balancing the desire for a relatively few number of release intervals with the need to reduce numerical error associated with the use of constant release rate intervals necessitated by RADTRAD.

Inputs to the Evaporation from the Flibe Pool Release Pathways for the Salt Spill Event

The initial and boundary conditions used as input to the calculation are provided in Table A.3-7. The evaporation of radionuclides in the spilled Flibe is calculated as a function of spilled Flibe surface temperature. The pool cooling is modeled in KP-SAM and results in the time-temperature curve shown in Figure A.3-5. The release fractions for the RN groups are then calculated as shown in Figure A.3-6.

Note that because the pool cooling evaluation conservatively assesses releases only from a fully formed pool, the initial and boundary conditions in Table A.3-1 (along with the limiting break size), do not impact the evaluation of evaporative releases from a spilled pool.

[[

]]

**Figure A.3-5: Spilled Flibe Temperature versus Time (KP-SAM)**

[[

]]

**Figure A.3-6: Release Fractions from Spilled Flibe Evaporation**

**Table A.3-7: Initial and Boundary Conditions for Spilled Flibe Evaporation**

| Parameter | Value |
|---|---|
| Flibe Initial Temperature (°C) | [[ ]] |
| Building Gas Temperature (°C) | [[ ]] |
| Building Gas Pressure (kPa) | [[ ]] |
| Discharged Flibe Volume ($m^3$) | [[ ]] |
| Catch Pan Area ($m^2$) | [[ ]] |
| Catch Pan Thickness (m) | [[ ]] |
| Catch Pan Density ($kg/m^3$) | [[ ]] |
| Catch Pan Thermal Conductivity (W/m-K) | [[ ]] |
| Catch Pan Heat Capacity (J/kg-K) | [[ ]] |
| Concrete Layer Thickness (m) | [[ ]] |
| Concrete Density ($kg/m^3$) | [[ ]] |
| Concrete Thermal Conductivity (W/m-K) | [[ ]] |
| Concrete Heat Capacity (J/kg-K) | [[ ]] |

Evaporative releases from spilled Flibe

Evaporative releases from spilled Flibe are calculated as described in Section 5.5.3 using the inputs in Table A.3-7.

Although Flibe is discharged over the duration of the event, radionuclides that are released via evaporation from the spilled Flibe pool are conservatively modeled to start evaporating at the event initiation. The time-dependent evaporative release fractions are initially determined and then used to calculate the cumulative release fractions for use in a screening dose assessment. Table A.3-8 shows dose contributions from individual isotopes using a 1E-3 rem cutoff. As shown in Table A.3-8, the dose-driving isotopes (i.e., those that would not be screened out at the 1E-3 rem cutoff for RADTRAD analysis) are As-76, P-32, and S-35, which are all grouped as gases in Table 2.1. All non-gas radionuclides are screened for spilled Flibe evaporation.

Since the Flibe MAR inventory used in the MHA includes all Flibe in the vessel and PHTS, the spilled Flibe MAR inventory is inherently included in the MHA analysis. Spilled Flibe evaporation would be an additional release pathway compared to the MHA, due to the additional surface area of the pool in addition to the in-vessel Flibe surface, however, in both the MHA and postulated event analysis, all gases are puff released.

Therefore, the spilled Flibe release pathway is effectively a pathway modeled by the MHA, and thus is not considered as a non-MHA release pathway. This dose is accounted for in the evaluation of the primary system dose (as described in Section 3.3.6) which is added to the jet breakup dose for comparison to the MHA for the total salt spill postulated event dose. Explicit modeling of the dose due to evaporation from the spilled Flibe is therefore not performed.

**Table A.3-8: Isotopic Doses for Spilled Flibe Evaporation**

[[

]]

Gas space transport

Releases from Flibe to the gas space and subsequent gas space transport are modeled as described in Section 5.5.3. The reactor cell is assumed to be [[ ]] $m^3$.

RADTRAD is used to evaluate the 30-day TEDE dose at the EAB for comparison to the MHA.

Results: Jet Breakup EAB Dose Evaluation

No grouping structure is used for jet breakup mechanical aerosolization, and therefore the same release fraction is applied to all radionuclides (Figure A.3-4). Figure A.3-7 shows the building activity for each isotope as a function of time. The void fraction of the break flow becomes larger as the Flibe level decreases, and mechanical aerosolization is more vigorous at higher void fraction, resulting in higher activities as the transient progresses, until the system ultimately depressurizes. The figure also highlights transitions in the transient such as the primary salt pump trip, initiation of the anti-siphon devices, and the transition from single-phase to two-phase break flow. The 30-day TEDE isotopic dose results at the

EAB are provided in Table A.3-8. The total resulting dose contribution from the jet breakup pathway is [[ ]] TEDE.

[[

]]

**Figure A.3-7: Jet Breakup – Building Activities**

**Table A.3-9: 30-Day TEDE Isotopic Dose Results at the EAB – Jet Breakup**

[[

]]

## A.4 Pebble Handling and Storage System Malfunction (Transfer Line Break)

This section provides an example analysis of a postulated pebble handling and storage system (PHSS) transfer line break event. In the following subsections:

- MAR is identified,
- Release pathways are identified,
- Inputs and boundary conditions are defined,
- Thermal-fluid behavior in the system is summarized,
- Release fractions are evaluated for diffusion from exposed kernels,
- Release fractions are evaluated from Flibe for dissolved TRISO particles,
- Gas space transport model inputs are defined, and
- Dose consequences are reported.

Identification of MAR for the PHSS Malfunction Analysis

The MAR evaluated for release in the PHSS malfunction are the pebbles suspended above the Flibe free-surface in the pebble extraction machine (PEM) and the pebble insertion line (PIL).

Identification of Release Pathways for the PHSS Malfunction Analysis

The release pathways evaluated for the PHSS transfer line break are described in Section 5.6, including diffusion of radionuclides from exposed kernels suspended above the Flibe free-surface and evaporation of TRISO-originating MAR which is dissolved in Flibe. Note that this example analysis addresses fuel releases but does not include an evaluation of the releases from graphite dust resuspension or the tritium and argon-41 releases from oxidized reflector graphite and pebble matrix material.

Each pathway is first evaluated using the isotopic screening methodology described in Section 2.2.5. Release pathways that do not screen are further evaluated for 30-day TEDE dose consequences at the EAB for comparison to the MHA.

Inputs and boundary conditions

The following inputs are used in support of the example PHSS Malfunction Analysis

- There are [[ ]] pebbles in the PEM and [[ ]] in the PIL that are subject to oxidizing temperatures above the Flibe free-surface.
- [[ ]] of these pebbles are fueled pebbles with discharge inventories decayed and averaged consistent with their locations in the PEM per Section 5.6 (between [[ ]] hours after core discharge in the PEM and [[ ]] hours after PEM discharge in the PIL). The remainder of the pebbles are assumed to be moderator pebbles with no appreciable MAR.
- The exposed kernel fraction is assumed to be [[ ]] (due to assumed oxidation-induced failure of the PyC layers), and the kernel temperature is conservatively assumed to be [[ ]] K over [[ ]] days.
- There is [[ ]] $m^3$ of Flibe in the reactor vessel. This volume equates to [[ ]] molecules of Flibe.
- The transfer line break is assumed to occur into the reactor cavity, with an assumed gas volume of [[ ]].
- EAB X/Qs and breathing rates are provided in Table A.3-2.

Releases from exposed TRISO kernels via diffusion

Release fractions for exposed kernels are evaluated using the approach described in Section 2.2.2, with a diffusion temperature of [[ ]] K and a time interval of [[ ]] days. The resulting release fractions for each radionuclide group in the kernel grouping structure are shown in Table A.4-1. The results of the isotopic screening for the kernel diffusive releases are shown in Table A.4-2 for the five highest TEDE dose isotopes. None of the isotopes exceed the 0.001 rem isotopic screening threshold, and therefore this release pathway is screened and not modeled in RADTRAD.

**Table A.4-1: Kernel Release Fractions**

[[

]]

**Table A.4-2: Isotopic Doses for Kernel Diffusive Releases**

[[

]]

Releases from dissolved TRISO particles in Flibe via evaporation and off-gassing

As described in Section 5.6, a release fraction from TRISO to Flibe of 1.0 is assumed for all the MAR contained inside TRISO particles with intact SiC layers that fall into the Flibe once the pebble is oxidized. The released radionuclides are regrouped into the Flibe grouping structure (see Table 2.1), and transported per the evaporation model provided in Section 2.2.4, with the exception that the number and duration of release intervals are modified to better represent the release profile. These are determined by balancing the desire for a relatively few number of release intervals with the need to reduce numerical error associated with the use of constant release rate intervals necessitated by RADTRAD.

[[ ]] pebbles are oxidized above the Flibe free surface during the break. The inventory from the intact SiC particles contained in these pebbles falls into [[ ]] $m^3$ of Flibe in the reactor vessel. This MAR is summarized in Table A.4-3 (truncated at 1E-10 parts per billion [ppb]). Given that these elemental mole fractions are less than 6325 parts per million, these salt-soluble fluorides (SSF) are below the solubility limit and the dilute solution approximation is assumed to apply. The total number of grouped atoms that are transferred into the reactor vessel are presented in Table A.4-4.

**Table A.4-3: Mole Fraction of SSFs from Dissolved Fuel in the Vessel**

[[

]]

**Table A.4-4: Total Atoms in Flibe Radionuclide Groups Transferred from TRISO Dissolved in the Vessel into the Flibe**

[[

]]

Evaporation from the Flibe free surface is calculated as a function of temperature. The post-air ingress hot well temperature transient follows the time-temperature curve shown in Figure A.4-1. Release fractions for the Flibe radionuclide groups are calculated as described in Section 5.6.2 and are shown in Figure A.4-2. The total release fraction for each RN group is shown in Table A.4-5.

[[

]]

**Figure A.4-1: Hot Well Transient Time-Temperature**

[[

]]

**Figure A.4-2: Flibe Release Fractions**

**Table A.4-5: Release Fractions from Flibe in the Vessel**

[[

]]

Gas space transport

Releases from Flibe to the gas space and subsequent gas space transport are modeled as described in Section 5.6.2. The transfer line break is assumed to occur into the reactor cavity, with an assumed volume of [[ ]].

RADTRAD is used to evaluate the 30-day TEDE dose at the EAB for comparison to the MHA.

Results: Evaporative Releases from Oxidized Pebbles Dissolved in Flibe

Releases from MAR that diffuses out of exposed kernels suspended above the Flibe free-surface are screened as discussed above. Therefore, only releases from MAR in particles that are dissolved in the Flibe and subsequently degassed and evaporated are evaluated for 30-day TEDE doses at the EAB. Isotopic dose results are provided in Table A.4-6. The resulting EAB dose is [[ ]] rem TEDE. This dose is added to the primary system dose (as described in Section 3.3.6) for comparison to the MHA.

**Table A.4-6: 30-Day Isotopic Dose Results at the EAB for Intact SiC Particles Dissolved in Flibe**

[[

]]

## A.5 Hot Pebble Factor

This section provides an example calculation of the hot pebble factor, described in Section 4.2.4.1. The inputs for the example calculation are shown in Table A.5-1.

**Table A.5-1: Hot Pebble Factor Inputs**

| Parameter | Value | Description |
|---|---|---|
| $T_{in}$ | [[ ]] | Inlet temperature |
| $\Delta T_{1,nom}$ | [[ ]] | Core temperature rise |
| $\Delta T_{2,nom}$ | [[ ]] | Maximum local temperature rise |
| $F_1$ | [[ ]] | Radial peaking factor |
| $F_2$ Direct | [[ ]] | Pebble peaking factor |
| | [[ ]] | [[ ]] local flow reduction |
| $F_2$ Statistical | [[ ]] | Pebble diameter |
| | [[ ]] | [[ ]] correlation uncertainty |

$F_2$ is calculated as shown below using Equation 4.6.

$$F_2 = [[\quad ]]$$

$F_1$ is [[ ]]. The maximum pebble surface temperature is calculated as shown below using Equation 4.8.

$$T_{2(surface),HPF} = F_2 \times \Delta T_{2,nom} + F_1 \times \Delta T_{1,nom} + T_{in}$$

$$T_{2(surface),HPF} = [[\quad ]]$$